Design Considerations for Thermoelectric Power Generation

Man, Elena Anamaria

DOI (link to publication from Publisher):
10.5278/vbn.phd.engsci.00132

Publication date:
2016

Document Version
Publisher's PDF, also known as Version of record

DESIGN CONSIDERATIONS FOR THERMOELECTRIC POWER GENERATION

BY
ELENA ANAMARIA MAN

DISSERTATION SUBMITTED 2016

AALBORG UNIVERSITY
DENMARK

DESIGN CONSIDERATIONS FOR THERMOELECTRIC POWER GENERATION

by

Elena Anamaria Man

AALBORG UNIVERSITY
DENMARK

Dissertation submitted

.

Thesis submitted:	July 31, 2016
PhD supervisor:	Associate Prof. Erik Schaltz, Aalborg University
Assistant PhD supervisor:	Prof. Lasse Rosendahl, Aalborg University
PhD committee:	Prof. Keith Burnham, University of Wolverhampton Prof. Kai Sun, Tsinghua University Associate Prof. Carsten Bojesen, Aalborg University
PhD Series:	Faculty of Engineering and Science, Aalborg University

ISSN (online) – 2246-1248
ISBN (online) - 978-87-7112-766-9

Published by:
Aalborg University Press
Skjernvej 4A, 2nd floor
DK – 9220 Aalborg Ø
Phone: +45 99407140
aauf@forlag.aau.dk
forlag.aau.dk

Printed in Denmark by Rosendahls, 2016

ENGLISH SUMMARY

Thermoelectricity is a renewable technology with good potential to convert the vast existent amount of waste heat worldwide into electrical energy. Since the 1950s, significant research effort has been made to increase the initial efficiency of the thermoelectric modules from 1.5% – 2% to its present 5% – 10% in the commercial devices and ~20% in research. Moreover, the current research focuses on a multitude of potential thermoelectric (TE) materials to cover all the temperature availabilities from room temperature to >1000°C.

This thesis investigates two types of commercial TE modules: the widespread Bi_2Te_3 with ~5% conversion efficiency but temperature limited to 250°C and calcium-manganese oxide (CMO) with ~0.4% conversion efficiency that can cover a wider temperature range from room temperature to >1000°C. The first part of the work is focused on acquiring the electrical parametric characterization (*I-V* and *P-V* curves) of the oxide module using a commercial apparatus and the typical constant temperature method. Such one-module characterizations are generally used to predict the behaviour of multiple-module TEG integrated into applications.

Depending on the application, research shows that the temperature variations on the hot side of TE modules can reach 5°C/s or higher. It is known that hill-climbing maximum power point tracking (MPPT) algorithms (*e.g.* Perturb&Observe – P&O) have difficulties in accurately tracking the maximum power point (MPP) in rapidly changing conditions. Moreover, without the existence of TEG simulators, it is difficult to accurately quantify the dynamic MPPT efficiency. In this thesis, the static and dynamic MPPT efficiency of typical TEG systems were investigated using a developed TEG emulator. The electrical characterization of the CMO was used to form a 30-module TEG in order to match the *I-V* characteristic to the converter's efficient operating point. The 30-module TEG was modelled using a programmable DC power supply connected through a commercial non-inverting buck-boost converter to a resistive load. The MPPT static and dynamic efficiencies were analysed for different case scenarios related to conditions existent in practical TEG applications.

So far, the theoretical MPP in TEG systems is set according to the *maximum power transfer theorem* and met when the load resistance is matched to that of the TEG. However, this condition is formed from a purely electrical point of view and it does not consider any thermal interactions in the TEG system. This thesis reveals through experimental analysis that the Peltier effect can maximize the power generated by a TEG system resulting in the existence of a *real* MPP higher than the one predicted by the theory. By changing the operating point of the TE device (*i.e.* set voltage higher than half of open circuit voltage), less current flows though the

module. Because of the current change, the Peltier effect is less pronounced and the thermal conductivity of the device is reduced. The heat flux through the module is therefore decreased which leads to an increase in the temperature difference across the device and a higher power output. This concept was first investigated on a one-module test fixture and afterwards on a developed TEG hot gas system using Bi_2Te_3 modules. Results show that the power generated by the TEG system can increase up to 8% by positively manipulating the Peltier effect.

Even though research mostly focuses on developing more efficient TE materials/modules, this work reveals a novel approach to maximize the power generated by a TEG system only by changing the operating point of the TEG. However, the conditions for the TEG to operate at the real MPP vary mainly dependent on the heat flux through the TEG. Nevertheless, the thermal transient of the Peltier effect and its outcome on the TEG system are slow (*i.e.* minutes) and fast MPPT methods (typical response in *ms*) do not allow the system to thermally react to any electrical changes. This means that proper MPPT algorithms need to be designed to be compatible with the real MPP operation of TEG systems and to account for the beneficial but slow Peltier effect.

DANSK RESUME

Thermoelektricitet er en vedvarende teknologi med gode muligheder for at omdanne den eksisterende store mængde spildvarme på verdensplan til elektrisk energi. Siden 1950'erne, er der sket en betydelig forskningsindsats for at øge den oprindelige effektivitet af termoelektriske moduler fra 1,5% – 2% til nuværende 5% – 10% i kommercielle enheder og ca. 20% på laboratorieniveau. Desuden fokuser den nuværende forskning på en lang række potentielle termoelektriske (TE) materialer til at dække alle temperaturer fra stuetemperatur til over 1000°C.

Denne afhandling undersøger to typer af kommercielle TE moduler: den udbredte Bi_2Te_3 med ca. 5% virkningsgrad, men temperaturer begrænset til 250°C og calcium-manganoxid (CMO) med ca. 0,4% virkningsgrad, der kan dække et bredt temperaturområde fra stuetemperatur til over 1000°C. Den første del af arbejdet er fokuseret på at erhverve den elektriske parameter-karakterisering (I-V og P-V kurver) af oxid modulet ved hjælp af et kommercielt apparat, der benytter den typiske konstant-temperatur metode. Sådanne ét-moduls karakteriseringer anvendes generelt til at forudsige opførslen af flere moduler integreret i en TE generator (TEG) applikation.

Afhængig af anvendelsen, viser forskning, at temperaturvariationerne på den varme side af TE-moduler kan komme op på 5°C/s eller højere. Det er kendt, at hill-climping Maximum Power Point Tracker (MPPT) algoritmer (f.eks. Perturb & Observer - P&O) har problemer med præcis sporing af maximum power point (MPP) under hurtigt skiftende forhold. Desuden, uden eksistensen af TEG simulatorer, er det vanskeligt nøjagtigt at kvantificere den dynamiske MPPT effektivitet. I denne afhandling blev den statiske og dynamiske MPPT effektivitet af typiske TEG-systemer undersøgt ved hjælp af en dertil udviklet TEG emulator. Den elektriske karakterisering af CMO-modulet blev anvendt til at danne en 30-moduls TEG for at matche I-V karakteristikken for konverterens effektive arbejdspunkt. 30-moduls TEG'en blev modelleret ved hjælp af en programmerbar DC strømforsyning tilsluttet via en kommerciel non-inverting buck-boost konverter til en resistiv belastning. MPPT statiske og dynamiske virkningsgrader blev analyseret for forskellige cases relateret til eksisterende praktiske forhold i TEG-applikationer.

Hidtil er det teoretiske MPP i TEG-systemer bestemt ud fra teorien om maksimal effektoverførsel, der finder sted, når last-resistansen matcher resistansen af TEG-systemet. Denne betingelse er dog dannet ud fra et rent elektrisk synspunkt, og der tages ikke højde for termiske interaktioner i TEG-systemet. Denne afhandling viser gennem eksperimentel analyse, at Peltier-effekten kan maksimere effekten

genereret af et TEG-system, hvilket betyder i, at der findes en reel MPP, der er højere end den bestemt af teorien. Ved at ændre arbejdspunktet af TE-enheden (dvs. sætte spændingen højere end halvdelen af tomgangsspændingen), løber der mindre strøm gennem modulet. På grund af den aktuelle ændring, er Peltier-effekten mindre udpræget og den termiske ledningsevne af enheden er reduceret. Varmefluxen gennem modulet er derfor reduceret, hvilket medfører en stigning i temperaturforskelen over enheden og en højere effekt. Dette koncept blev først undersøgt på en enkelt-modul prøveopsætning og bagefter på et udviklet TEG varm gas system ved hjælp Bi_2Te_3 moduler. Resultater viser, at effekten genereret af TEG- systemet kan stige op til 8% ved aktivt at reducere Peltier-effekten.

Selvom forskning for det meste fokuserer på at udvikle mere effektive TE materialer/moduler, viser dette arbejde en ny tilgang til at maksimere effekten genereret af et TEG-system kun ved at ændre arbejdspunktet af TEG'en. Betingelserne for at få TEG'en til at operere på det rigtige MPP varierer hovedsageligt med varmestrømmen gennem TEG'en. Ikke desto mindre er den termiske respons af Peltier-effekten og derved resultatet på TEG-systemet langsom (dvs. minutter), og hurtige MPPT metoder (typisk reaktion i ms) tillader ikke systemet termisk at reagere på eventuelle elektriske ændringer. Det betyder, at de rette MPPT-algoritmer skal være kompatible med den reelle MPP operation af TEG-systemer og tage højde for den gavnlige, men langsomme Peltier-effekt.

ACKNOWLEDGEMENTS

Having to write this part only means the milestone of finishing my PhD thesis has been reached. I deeply appreciate every person that helped me in any way during this interesting three-year "journey".

First, I am deeply thankful to my supervisors Erik Schalz and Lasse Rosendahl for giving me the opportunity to experience the life of a PhD student, for their support and helpful guidance throughout this period.

Many thanks to my colleagues from the Department of Energy Technology. In particular to Alireza Rezaniakolaei and Waruna Dissanayaka Wijesooriyage_for all the productive talks and debates we shared in the office and also to Dezso Sera and Laszlo Mathe for our challenging but well acknowledged collaboration.

I am deeply grateful to the Thermoelectrics team at The University of Glasgow for their patience, support and valuable advice. In particular to Andrew Know, Andrea Montecucco, Jonathan Siviter and Paul Mullen. May the future bring us together for many curries!

I thank my family for their unconditional love and endless support. I also dedicate this thesis to Emanuel-Petre Eni whose kind and motivational words kept me going through tough times. You were right, I could do it.

I could not have done it without you! Cheers A.

TABLE OF CONTENTS

List of Figures ..... **xii**
List of Tables ..... **xvi**
List of Acronyms ..... **xvii**
Chapter 1. Introduction **1**
1.1. Background and motivation 1
1.2. Project objectives 8
1.3. Thesis outline 9
1.4. Original contributions 10
1.5. List of publications 11
1.5.1. Journal papers 11
1.5.2. Conference papers 11
1.5.3. Award 11
Chapter 2. Theory of Thermoelectric Devices **13**
2.1. Introduction to thermoelectric phenomena 13
2.1.1. The Seebeck effect 13
2.1.2. The Peltier effect 14
2.1.3. The Thomson effect 16
2.1.4. The Kelvin relationships 16
2.1.5. The Joule effect 17
2.2. Figure of merit of thermoelectric devices 17
2.3. TEG systems generalities 20
2.3.1. Components of the TEG system 21
2.3.2. TEG electrical equivalent 23
2.3.3. Maximum power versus maximum efficiency 25
2.3.4. Thermal analysis of the TEG system 27
2.4. Conclusions 29
Chapter 3. Current State of the Art **31**
3.1. Thermoelectric materials and applications 31
3.2. Temperature profiles analysis for TEG systems 34

3.3. TEG performance curves 37
3.4. Temperature mismatch impact on power generation 38
3.5. Maximizing power generation from TEGs 40
3.5.1. DC-DC Converters in TEG systems 40
3.5.2. Control algorithms in TEG systems 43
3.5.3. Energy storage device 47
3.6. Conclusions 48
Chapter 4. TEG Emulator for MPPT Testing 51
4.1. Electrical characterization of oxide-based TEG 51
4.2. TEG emulator 53
4.2.1. Configuration for steady-state conditions 55
4.2.2. Configuration for dynamic conditions 57
4.3. Maximum power point tracking algorithms 60
4.3.1. Perturb & Observe 61
4.3.2. Incremental Conductance 62
4.3.3. Fractional open-circuit voltage 62
4.4. Experimental analysis of MPPT using the TEG emulator 63
4.4.1. Setup description and test conditions 63
4.4.2. Steady-state MPPT testing 66
4.4.3. Dynamic MPPT testing 67
4.5. Conclusions 77
Chapter 5. Constant Heat Characterization of TE Modules 79
5.1. Theoretical analysis of the MPP in TEG systems 79
5.2. Maximizing power generation through Peltier effect 79
5.3. Description of the test setup 80
5.3.1. Mechanical structure 80
5.3.2. Heat isolation 84
5.3.3. Electrical and control structures 84
5.4. Heat losses characterization 84
5.5. TEG characterization in constant heat operation 90
5.6. MPP in constant heat operation 101

5.7. Conclusions 110
Chapter 6. MPP in Constant Heat Systems 114
6.1. Hot gas TEG system 114
6.2. Mechanical side 114
6.3. Electrical and control side 118
6.4. Test conditions 123
6.5. Experimental validation of the real MPP in TEG systems 126
6.6. Optimal resistance ratio for constant heat operation 131
6.7. Conclusions 136
Chapter 7. General Conclusions 139
7.1. Conclusions 139
7.2. Future work 140
Literature list 143
Appendices 154

LIST OF FIGURES

Figure 1-1 World energy flow, 2011, by Lawrence Livermore National Laboratory (available online at https://flowcharts.llnl.gov/) 1
Figure 1-2 Simplified TEG system – main four units. 3
Figure 1-3 Efficiency levels of common energy conversion technologies compared to TE potential for different figure-of-merit values. The data are presented for the heat source temperature range 0°C to 1400°C and considering a constant cold side temperature of 25°C (11). 4
Figure 1-4 Diagram for the cascade calcium-manganese oxide and Bi_2Te_3 TE module. 6
Figure 2-1 Two element TE device functioning as a) power generator b) thermoelectric heat pump for cooling and c) thermoelectric heat pump for heating (8). 15
Figure 2-2 Interdependence of the Seebeck coefficient, the electrical and the thermal conductivities related to the doping concentration. Trends are modeled for Bi_2Te_3 (34). 18
Figure 2-3 General schematic of TE system. 22
Figure 2-4 Thermoelectric material versus system efficiencies for water heater, automotive exhaust and industrial furnace TEG applications (47). 23
Figure 2-5 Basic configuration of a TE module. 24
Figure 2-6 Equivalent electric circuit of TEG. 24
Figure 2-7 Generalized structure of TEG. 25
Figure 2-8 General P-V curves of a TEG for different temperature gradients (22). 26
Figure 2-9 Rate of output power and voltage change due to temperature gradient change (51). 28
Figure 2-10 Equivalent thermal circuit of a TE module placed between heat source and heat sink. 28
Figure 3-1 State of the art zT n- and p-type materials (34). 32
Figure 4-1 TEGeta block diagram. 52
Figure 4-2 Placement of the thermocouples (T_2-T_9) in the reference blocks. 52
Figure 4-3 a) P-V and b) I-V characteristics for CMO-25-42S tested for the following temperature gradients ΔT = 134°C, 184°C, 236°C, 289°C, 343°C and 401°C, at 1.3MPa clamping pressure. 53
Figure 4-4 Oxide module I-V and P-V curves configured using Keysight simulator in a) SAS mode and b) table mode at ΔT = 401°C. 56
Figure 4-5 Voltage (Voff = +0.5V) and b) current (Ioff = +0.5A) offsets set to a pre-defined table for oxide TEG at ΔT = 401°C. 58
Figure 4-6 Flow chart with implementation of the oxide TEG emulator. 59
Figure 4-7 Real and new offset SAS I-V characteristics of a TEG module composed of 15 series-connected modules in 2 parallel arrays operating at same MPP for ΔT = {134, 184, 236, 289, 343, 401}°C. 60
Figure 4-8 The flowchart of the P&O algorithm. 61

Figure 4-9 Block diagram of the experimental setup. 64
Figure 4-10 Trapezoidal temperature sequences for dynamic MPPT testing..... 65
Figure 4-11 Ideal MPP power (blue) and TEG emulator output power (red) analyzed for f_{MPPT} a) 2.5Hz, b) 5Hz, c) 7.5Hz d) 10Hz, and e) 12.5Hz for ramp rate of 5°C/s. 72
Figure 4-12 Ideal MPP voltage (blue) and TEG emulator output voltage (red) analyzed for f_{MPPT} a) 2.5Hz, b) 5Hz, c) 7.5Hz d) 10Hz and e)12.5 Hz. 75
Figure 4-13 Instantaneous P&O efficiencies for f_{MPPT} a) 2.5Hz, b) 5Hz, c) 7.5Hz d) 10Hz and e) 12.5Hz. 76
Figure 5-1 TEG measuring system..... 81
Figure 5-2 Diagram of the test setup used for TE module characterization. 82
Figure 5-3 Top view of the aluminium heater block and the position of the two hot side thermocouples..... 83
Figure 5-4 Diagram of the laboratory setup for characterization of heat losses in constant heat operation..... 86
Figure 5-5 Relative error of the heat losses between the two test cases $T_{chiller}$ = 12°C and $T_{chiller}$ = 25°C for heater power range from 2W to 10W. 89
Figure 5-6 Heat losses plotted against temperature difference for the two test cases $T_{chiller}$ = 12°C and $T_{chiller}$ = 25°C..... 89
Figure 5-7 Comparison of the heat losses plotted against T_h for the two test cases $T_{chiller}$ = 12°C and $T_{chiller}$ = 25°C..... 90
Figure 5-8 Heat losses characterization plotted against T_h with chiller temperature set to 25°C..... 90
Figure 5-9 Temperature difference change from open-circuit to short-circuit test for 110W constant power to the TEG. 92
Figure 5-10 Flow diagram of the Agilent VEE Pro program to obtain the I-V and P-V characteristics in constant heat operation 93
Figure 5-11 a) Output power versus output voltage and b) output current versus output voltage for GM250-241-10-12. The module was tested two times in constant heat starting at 30W to 130W with 20W increments. 95
Figure 5-12 a) Output power versus output voltage and b) output current versus output voltage for GM250-241-10-16. The module was tested in constant heat starting at 30W to 110W with 20W increments. 96
Figure 5-13 Open-circuit voltage for modules GM250-241-10-12 (solid line) and GM250-241-10-16 (dased line) in constant heat operation 97
Figure 5-14 The relative error between measured V_{OC} and calculated V_{OC} based on mathematical fitting (equation (5-6)) at constant heat flow through the GM250-241-10-12 module from 30W to 130W. 98
Figure 5-15 The relative error between measured V_{OC} and calculated V_{OC} based on mathematical fitting (equation (5-7)) at constant heat flow through the GM250-241-10-12 module from 30W to 130W. 98
Figure 5-16 The Seebeck coefficient of the TE modules GM250-241-10-12 and GM250-241-10-16. 99

Figure 5-17 The internal resistance of the TE modules GM250-241-10-12 and GM250-241-10-16 in constant heat operation. 99
Figure 5-18 Thermal conductivity of the GM250-241-10-12 and GM250-241-10-16 modules for open- and short-circuit conditions and constant heat operation. 100
Figure 5-19 P-V and I-V curves for the GM250-241-10-12 module in constant temperature condition at $\Delta T = 154°C$. 102
Figure 5-20 Heater power variation with output current value change for the GM250-241-10-12 module in constant temperature condition at $\Delta T = 154°C$. 102
Figure 5-21a) Output power versus temperature gradient (constant heat) and b)output current versus output voltage (constant temperature). The green "theoretical" MPP1 point corresponds to the green I-V curve plotted for the condition when the output voltage is half of V_{OC}. The magenta MPP2 point corresponding to the magenta I-V curve is the real MPP point at 130W. 104
Figure 5-22 The fraction between the voltage and V_{OC} (β) that sets the conditions to achieve MPP in constant heat operation for the GM250-241-10-12 module. The β values are calculated for the heat flow range of 30W to 130W. Each bar displays the corresponding temperature gradient across the module at thermal equilibrium..... 105
Figure 5-23 The fraction between the voltage and V_{OC} (β) that sets the conditions to achieve MPP in constant heat operation for the GM250-241-10-16 module. The β values are calculated for the heat flow range of 30W to 110W. Each bar displays the corresponding temperature gradient across the module at thermal equilibrium..... 106
Figure 5-24 a) I-V, b) P-V and c) ΔT-V constant heat characteristics of the module that show the MPP (Point 2 - magenta) set by $\beta = 0.5$ and the MPP (Point 4 - green) set by $\beta = 0.56$. 108
Figure 5-25 Conversion efficiency of the GM250-241-10-12 and GM250-241-1016 modules. 109
Figure 6-1 The hot air system used for measurements in constant heat operation. 115
Figure 6-2 Schematic of the heater side of the hot gas system where the ambient air is heated. 116
Figure 6-3 a)Front view and b) side view of the heater plate with blowing-air type igniters attached. 117
Figure 6-4 Initial testing of the heaters and the additional holes made to the heater plate from Figure 6-3 to prevent from over-heating..... 117
Figure 6-5 TEG cold side heat exchanger with labyrinth view for water path..... 118
Figure 6-6 The data acquisition and control unit of the hot gas system. 119
Figure 6-7 Inlet fan output frequency versus voltage reference of the PWM control (measurements and mathematical fitting). 120
Figure 6-8 Dispersal fan output frequency versus voltage reference of the PWM control (measurements and mathematical fitting). 120
Figure 6-9 Total heater power against control voltage for the inlet fan output frequency range of 20Hz to 160Hz in steps of 20Hz. 123
Figure 6-10 The TEG structure integrated into the hot air system's top side heat exchanger 124

Figure 6-11 Flow diagram of the Agilent VEE Pro program that controls the hot air system 125
Figure 6-12 TEG output power variation caused by the hysteresis control of the chiller and the averaging process of the TEG output power. 128
Figure 6-13 Average TEG output power against β with P_{heater} = 6.7kW, $f_{fan,inlet}$ = 80Hz and $f_{fan,dispersal}$ = 60Hz. 128
Figure 6-14 Average TEG output power against β with P_{heater} = 1kW, $f_{fan,inlet}$ = 40Hz and $f_{fan,dispersal}$ = 60Hz. 130
Figure 6-15 Calculated ZT values for the GM250-241-10-12 module based on the constant heat parameter characterization 135
Figure 6-16 Theoretical $R_{load}/R_{teg} = \sqrt{1+ZT}$ plotted against the experimentally obtained R_{load}/R_{teg} values calculated for GM250-241-10-12 module. 136

LIST OF TABLES

Table 3-1 Temperature profile for TEG applications - literature survey..... 36
Table 4-1 Pre-programmed parameter list for simulator to generate I-V curve for oxide TEG at 401°C and P_{MPP} = 1.009428W..... 55
Table 4-2 Table with 7 pairs of voltage – current values to emulate an oxide TEG at 401°C and P_{MPP} = 1.009428W. 57
Table 4-3 Comparison between experimentally measured MPP (P_{MPP}) with the MPP generated by the simulator in SAS ($P_{MPP,Table}$) and Table ($P_{MPP,SAS}$) mode. 57
Table 4-4 Measured static efficiencies normalized to the maximum DC power ($P_{DC,r}$ = 30.14W). 66
Table 4-5 Steady-state MPPT efficiencies for low/high resolution of the I-V curve at 400°C and f_{MPPT} = 2.5Hz..... 67
Table 4-6 Dynamic MPPT efficiencies for various P&O perturbation frequency and three temperature sequences. 68
Table 5-1 Characterization of the heat losses for two cases of the chiller temperature (Test 1 with $T_{chiller}$ = 25°C and Test 2 with $T_{chiller}$ = 12°C). 88
Table 5-2 The variance in the thermal conductivity at open- and short-circuit for the GM250-241-10-12. 100
Table 5-3 The variance in the thermal conductivity at open- and short-circuit for the GM250-241-10-16. 101
Table 5-4 Comparison between the power generated with the conditions from the maximum power transfer theorem ($\beta = 0.5$) and the power generated using the Peltier effect to decrease the thermal conductivity of the module ($\beta \neq 0.5$) for 30W to 130W constant heat flow..... 110
Table 6-1 Polynomial coefficient values of the second order fitting of the heater power against voltage control for inlet fan output frequency range 20Hz–100Hz. 122
Table 6-2 Polynomial coefficient values of the third order fitting of the heater power against voltage control for inlet fan output frequency range 100Hz–160Hz..... 122
Table 6-3 Calculation of R_{load} /R_{teg} for GM250-241-10-12, GM250-241-10-16 and GM250-127-28-10 modules..... 133

LIST OF ACRONYMS

ADC	Analog to digital converter
Bi_2Se_3	Bismuth antimony
Bi_2Te_3	Bismuth telluride
CMO	Calcium-manganese oxide
DAQ	Data acquisition and control unit
DSP	Digital signal processor
GPIB	General-purpose interface bus
INC	Incremental conductance
MPP	Maximum power point
MPPT	Maximum power point tracking
NEDC	New European driving cycle
ORC	Organic Rankine cycle
PbSnTe	Lead tin telluride
PbTe	Lead telluride
PC	Personal computer
PCM	Phase-change material
PV	Photovoltaic
PWM	Pulse width modulation
P&O	Perturb&Observe
RTG	Radioisotope thermoelectric generators

SAS	Solar Array Simulator
Sb_2Te_3	Antimony telluride
SiGe	Silicon germanium
TAGS	Tellurides of antimony, germanium and silver
TE	Thermoelectric
TEG	Thermoelectric generator
USB	Universal serial bus

CHAPTER 1. INTRODUCTION

This chapter first analyses the current state of the world energy and the potential for thermoelectric waste heat recovery in the form of background and motivation of the PhD thesis. Afterwards, the objectives are presented along with the main contributions and a summary of the thesis outline.

1.1. BACKGROUND AND MOTIVATION

Nowadays, more energy is wasted than used. Figure 1-1 shows the global energy flow diagram made available online by Lawrence Livermore National Laboratory. In 2011, the world used ~534EJ of energy of which 54% was accounted as losses and it means that not all the consumed energy is put to use. The unused energy is mainly discharged as thermal losses into the atmosphere. Between 2007 and 2011, the energy consumption increased by 9% and the energy losses by 16%. Recent predictions forecast continuous growth in the amount of waste heat *i.e.* 6.8% between 2016 and 2022.

The enormous percentage of rejected energy is due to the inefficient conversion of other necessary processes. Even worse, the losses from non-renewable energy sources *i.e.* fossil fuels are the major cause of greenhouse gas emissions. To diminish the negative impact on the environment, increasing renewable energy production has been a worldwide target for the last decade.

Thermoelectric (TE) technology is a relatively new and promising technology considered to recover the waste heat and convert it to useful electrical energy. This technology could cover a broad range of applications from ultra-low power to high-power large scale industrial applications (1). The electrical energy is produced when a TE device is exposed to a temperature difference. The amount of power production is dependent on the magnitude of the temperature gradient ΔT across the device, but also on the corresponding hot and cold temperatures (T_h and T_c). Although it is an emerging technology, potential TE applications are intensively studied (2-5). Thermoelectric generators (TEGs) have significant opportunities in large scale industrial applications due to the high quantities of available thermal energy discharged as waste heat.

The quality of the waste heat (*e.g.* temperature, density, accessibility) varies with the source emanating it. In many industrial processes, dilution air is added to reduce the exhaust temperature. The gaseous industrial waste heat at 150°C represents a low-quality heat which makes it an inefficient source for TE conversion. The majority of TEGs present better efficiency when operating at higher hot side temperatures (>300°C). Medium to high temperature large scale industrial applications such as

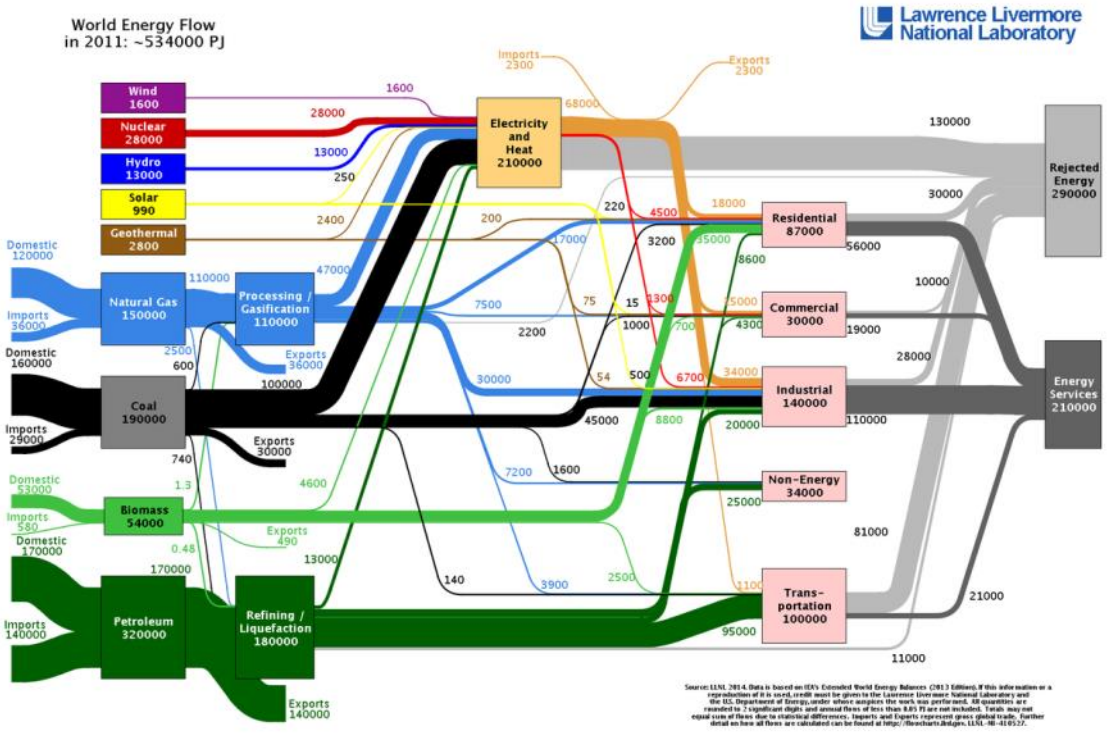

Figure 1-1 World energy flow, 2011, by Lawrence Livermore National Laboratory (available online at https://flowcharts.llnl.gov/).

furnaces, cement works, steel plants and engines (485°C to 1400°C) can offer significant commercial potential to TEG developers due to their suitable heat quality and high operational efficiency of the energy recovery process.

The first TEG was built in 1942 in the former Soviet Union and had a conversion efficiency of 1.5% – 2% (1). Between 1950s and the 1990s, the efficiency of the TE modules was still below 5% and the progress of improving the materials' figure-of-merit was slow. The modules were based on Bi_2Te_3, PbTe and SiGe with usage in small niche applications, mainly space and military missions. After 1990, the interest in TE energy generation was renewed and significant progress was achieved in device efficiency improvements, diversification of materials and applications (6).

TE power generation is achieved by combining the four unit TEG system: TE module(s), hot side heat exchanger, cold side heat sink and power control, as seen in Figure 1-2.

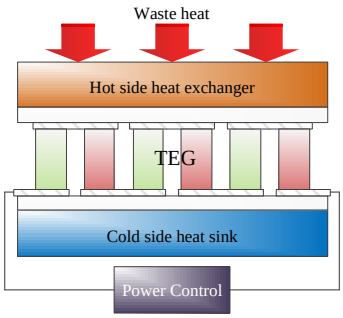

Figure 1-2 Simplified TEG system – main four units.

The main advantage of thermoelectricity over other renewable technologies (*e.g.* wind turbines) is the fact that the energy conversion is accomplished by a non-moving device that allows a silent operation. The device presents high reliability when used on more constant heat sources and exhibit long lifetime comparable to other technologies (*e.g.* PV panels, wind turbines). For example, the TE modules used on the *Voyager* spacecraft lunched in 1977 are still operational and expected to be so until 2025 when they will no longer supply enough power to operate any of the instruments (7). The use of TEGs is still limited to mainly small-scale applications where the primary concerns are not costs and efficiency, but reliability, low noise, vibration free or remote operation of the devices. At the same time, TEG systems are being integrated into industrial applications for the opportunity to gather valuable practical knowledge until advances in TE materials are achieved.

The conversion efficiency of the laboratory TE modules may reach 20%, but commercial parts have a figure of merit *ZT* of unity and only reach 10% efficiency. Figure 1-3 presents the efficiency of a few energy conversion processes and the TE efficiency for different *ZT* values up to the maximum theoretical ZT = ∞ given by the Carnot limit ($\eta_{Carnot} = (T_h - T_c)/T_h$). Even though large efforts have been made to improve the *ZT* of materials, progress is slow. The TEG efficiency is currently not high enough to compete against the more mature and established technologies *i.e.* based on the Rankine cycle, but can be comparable to solar thermal plants and some of the PVs. However, the small physical size of a TEG makes it an attractive power source in some applications. A 56mm x 56 mm x 4.5mm TEG (*e.g.* TE-MOD-22W7V-56 from TEGpro or 2411G-7L31-15CX1 from Custom Thermoelectric) can produce over 20W and when coupled to an appropriate power converter, it provides sufficient energy for a wide range of processes or computational tasks.

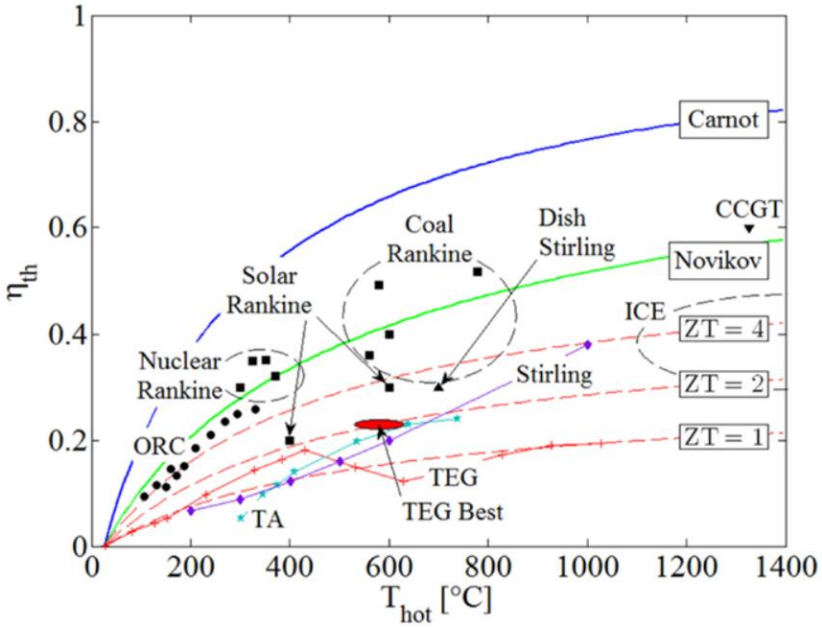

Figure 1-3 Efficiency levels of common energy conversion technologies compared to TE potential for different figure-of-merit values. The data are presented for the heat source temperature range 0°C to 1400°C and considering a constant cold side temperature of 25°C (8).

Even though in the future TE technology may not hold a large share of the installed renewable energy, it certainly has good potential to produce energy from the already available waste heat especially when the TEG system costs become more competitive. Continuous research and optimization is invested in any potential viable renewable technology and thermoelectricity is no exception. The

optimizations brought at material, module and system levels have always the same two main end targets: minimized system costs and maximized power output. Maximization of power output from a TEG system is a theme that runs throughout this thesis.

For most TEG systems, the dominant costs are for ceramic plates and heat exchangers. Breakeven system costs are constantly analyzed and predictions are made when the TEG systems will reach these targets (9,10). However, cheaper manufacturing techniques are necessary as well as mass production to reduce system costs. More recently, a new technology that uses thermal spray for oxide module construction is under research. It is said that the spray technology has the potential to significantly reduce system costs and become competitive with the organic Rankine cycle (ORC). The cost for ORC systems is approx. €5–7/W (11).

In terms of TE materials, the current market is dominated by modules manufactured from Bi_2Te_3 alloys. The modules exhibit acceptable performance at reasonable costs. Most improvements brought to the material remain at research level because of the additional costs involved that make them unfit for production. The best commercial TEGs barely reach 10% conversion efficiency. Other relatively new materials such as oxides are regarded as potential candidates, but the device efficiency is <1%.

The use of Bi_2Te_3 devices in practical applications is currently limited at a maximum hot side temperature of around 250°C – 330°C. Above this temperature, the efficiency of the Bi_2Te_3 module decreases. For this reason, low temperature and low cost solders are used in manufacturing the devices. This temperature limitation of Bi_2Te_3 devices impedes the coverage of the broad range of possible TEG integrated applications. Therefore, the challenge for the future is to use new materials that could cover a wider temperature range to take advantage of the full spectrum of available waste heat. Even though currently oxide modules have low efficiency, they are considered potential TE devices that are able to cover the temperature requirements. In this project, commercially available Bi_2Te_3 and calcium-manganese oxide (CMO) modules will be investigated at their full operating temperature range.

To still make use of the relatively good efficiency of the Bi_2Te_3 modules and the high temperature capabilities of oxide modules, a cascade combination of the two is possible. The oxide hot side is placed on the hot side heat exchanger, the cold side of the oxide is coupled with the hot side of the Bi_2Te_3 and the cold side of the Bi_2Te_3 is positioned on the cold side heat sink, as shown in Figure 1-4. One constraint for the cascade module is to keep the temperature at the interface between the two materials lower than the maximum limit for Bi_2Te_3. Even with this limitation, the power generated by the cascade module is higher compared to each of the two devices, albeit at higher cost.

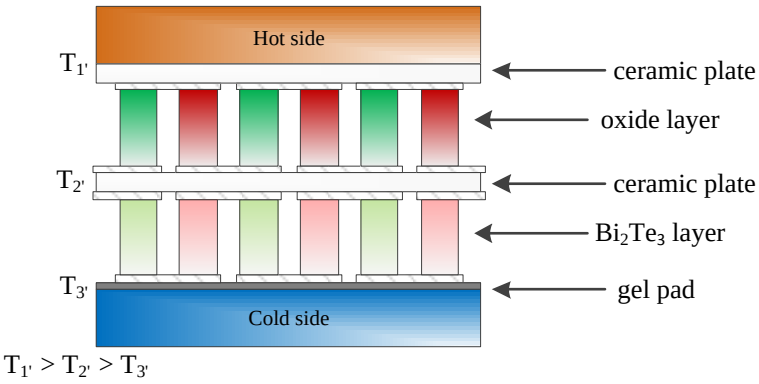

Figure 1-4 Diagram for the cascade calcium-manganese oxide and Bi_2Te_3 TE module.

The waste heat availabilities for TEG generation are fluctuating, but not according to consumer power demands. The electrical energy surplus can be stored into batteries. However, the TEG systems implemented in remote areas (*e.g.* desert) can be affected by harsh environmental conditions that can compromise the battery capacity. In these situations, there is a need for energy harvesters that can power the electronics in the system and that do not rely on batteries.

Such applications are low-power (tens of μW to mW) and usually involve powering wireless sensor systems for measurement or control, *e.g.* seismic monitoring, weather or military surveillance. TE devices are used for energy harvesting and are able to completely power the system from a few °C temperature gradients and as low as 0.6°C (12). Instead of batteries, capacitors are used to provide the necessary intermittent power. DC-DC converters are used to boost the voltage generated by the module to the level required by the sensor. Control algorithms are often avoided in low power application due to their additional power consumption. This also means that the internal module impedance cannot be matched to the impedance of the load and the system does not perform at its maximum power point (MPP). However, the main constrain in TE harvesting under low temperature gradients is maximizing the output voltage of the module for the system to be active. TE modules for harvesters are usually constructed from a large number of pellets to have high open-circuit voltages. At the same time, harvester TEGs have very large internal resistance and therefore generate low output power. Today's converters for harvesters are able to start from as little as 20mV (*e.g.* LTC3108 from Linear Technology).

For any other TEG application, the best choice for energy storage remains the battery. Even though, the temperature gradients can reach up to a few hundreds °C, the low conversion efficiency of the TEGs limit the power generation capabilities.

During periods when this temperature is below the operating threshold, batteries are used to provide power to the loads.

When charging the batteries, the power control unit is composed of a DC-DC converter that operates the TEG at its MPP to extract the maximum available power. This operation is called maximum power point tracking (MPPT) and can be performed with various existing control algorithms.

The conversion efficiency from TEGs to the loads depends on the equivalent converter and MPPT efficiencies, and it is not ideal. Part of the power is lost because of the parasitic components of the DC-DC converters and another small percentage is lost because of the inability of the control methods to continuously and perfectly track the MPP. This means that only a percentage of the power extracted from the TEGs is delivered to the loads or stored into the battery. The long-standing target of the MPPT efficiency is to reach the ideal 100% or come as close as possible. This can be achieved by adapting the design of the converter and control algorithm to match the existing operating input conditions to the load requirements. In this project, the focus will be on the optimization of the TEG power generation from the control perspective.

For many years, electrical engineers attempted to design and model power electronics for TEG systems. The general focus was on experimentally testing the power converters and control methods using a TEG emulation consisting of a voltage source in series with a resistor instead of an actual TEG (4,13-19). This method mimics the important electrical characteristics of a TEG, but clearly disregards the thermal dynamics present in the actual TEG systems (order of minutes) which are significantly higher than the electrical response speed from the electronic part (order of nanoseconds). The thermal transients play a significant role especially in testing the dynamic efficiency of MPPT algorithms which need to be optimized according to the actual conditions of the desired TEG application.

The second most used TEG test system is composed of a controlled electrical heater that gives the hot side temperature to the TEG (20-24). This method gives a degree of freedom to the user to control the thermal transients on the hot part of the TEG which do not necessarily reflect the thermal behaviour of a real TEG system.

A TEG system is composed of various parts and materials with different thermal conductivities. The waste heat source and the thermal characteristics of the heat exchanger dictate the rate of temperature change on the hot side of the TEG during transients. At the same time, the rate of change in the cold side temperature is influenced by the thermal characteristics of the cooling system. The thermal interactions of these components are important to be considered when designing the TEG power conditioning system to ensure its compatibility when placed in the actual application.

A further complication arises due to the way the thermal conductivity of the TEG itself varies with the current flowing through the device. This phenomenon is caused by the Peltier effect. Any current change in the module can lead to either a positive or negative Peltier effect over the system. This behaviour, in conjunction with the non-linear voltage/ power characterization of the TEG leads to significant difficulty in finding the real MPP of a TEG system. This is discussed further in Chapter 5.

Acquiring the electrical and thermal parameters of TE devices is usually performed with controllable apparatus built for research purposes. One example is the test fixture presented in Chapter 5 where the pressure applied to the TEG system is automatically adjusted using feedback control for any changes of the input settings. Additionally, the apparatus can maintain a set temperature difference across the module or a specific heat flux through the TEG depending on the user preferences. Such options are not found in practical TEG applications. The modules in TEG integrated systems are fixed at a specific pressure which varies with the temperature gradient across the devices. The hot-side temperature or the heat flux is given by the heat source and it is uncontrollable. Moreover, the TEG systems are also influenced by other uncontrollable parameters such as the environment (*e.g.* atmospheric pressure, humidity). These environmental effect influence the operation of TEGs integrated into applications which will be shown and discussed in Chapter 6.

For this reason, the concept of maximizing the power generated by a TEG system needs to be validated not only by a test apparatus, but also by a system that resembles as much as possible the real TEG application. A hot gas system was constructed and described in Chapter 6 with the purpose of analyzing the real MPP in TEG systems.

1.2. PROJECT OBJECTIVES

Current TEG systems are temperature limited by the commercial low temperature Bi_2Te_3 modules and power limited by MPPT control methods initially designed for PV systems. The MPPT algorithms are derived from consideration of the constant temperature operation of the TEG systems which all have the common issue of masking the parasitic Peltier effect which can vary the output power generation of TEGs. The Peltier effect can be manipulated by the fast electrical changes in TE modules however it has a slow thermal effect on the TEG systems. This thermal effect has been so far disregarded by the MPPT algorithms for TEG systems because they were initially designed for PV systems which are not affected by thermal component interactions. Moreover, experimental investigation of the dynamic MPPT efficiency is also limited because of the lack of TEG simulators that can record the necessary data.

In order to improve the overall power generation of the TEG systems, the following challenges need to be overcome:

- How can the *I-V* characteristic of the TEG be matched to the converter's efficient operating point?
- How can the dynamic MPPT efficiency of TEG systems be experimentally investigated?
- Can a TEG system generate more power than the limit set by the *maximum power transfer theorem*?
- How much influence does the Peltier effect have on the TEG power generation?

Based on the above mentioned challenges, the main objectives of the PhD project are:

i. Parametric characterization of commercially available oxide TE modules for high temperature applications.

ii. Design of a TEG emulator to investigate control algorithms for constant temperature operation.

iii. Static and dynamic efficiency analysis of control algorithms using the designed TEG emulator and temperature profiles of realistic TEG applications.

iv. Constant heat parametric characterization of TE modules compatible with realistic conditions from TEG applications.

v. Experimental investigation of the Peltier effect potential in maximizing the power generated by TEG systems operating in constant heat condition.

vi. Validation of the MPP that incorporates the positive Peltier effect on a viable TEG application (hot gas system).

1.3. THESIS OUTLINE

The thesis is presented as a monograph structured into 7 chapters as follows:

Chapter 2 Theory of thermoelectric devices describes the basic thermoelectric effects, the TE device operation and an overview of the components that summarize a TEG system. This information is vital in understanding the contents of this thesis.

Chapter 3 Current state of the art covers general information and explanations about trends in TE materials with focus on Bi_2Te_3 and oxides, temperature profiles of actual TEG systems, followed by module and overall system design characteristics and considerations.

Chapter 4 TEG emulator for MPPT testing presents the design and implementation of an oxide-based TEG emulator. The emulator was designed to eliminate the limitation to steady-state testing of TEG equivalents consisting of voltage sources with series resistors. A step-by-step description of modeling the emulator is given. Afterwards, steady-state and dynamic MPPT efficiencies are analyzed.

Chapter 5 Constant heat characterization of TEGs presents the *constant heat* parameter characterization of a TE module using a test fixture compatible with the conditions of the actual TEG integrated applications. Moreover, experimental results demonstrate that the Peltier effect can be manipulated to have a positive outcome on the power generation of TEG systems.

Chapter 6 MPP in Constant heat TEG systems describes the design of a hot gas system build for testing TE modules with operating conditions consistent with those of real TEG applications. Furthermore, a TE device was tested in *constant heat* and the experimental results validate the necessary additional conditions to the *maximum power transfer theorem* for the TEG system to operate at its real MPP.

Chapter 7 Conclusions and future work summarize the general conclusion of the thesis and suggest possible future work.

1.4. ORIGINAL CONTRIBUTIONS

The original contributions of the PhD project are as follows:

- A high temperature parametric constant temperature characterization of an oxide-based TEG using a commercial test system.
- Design and implementation of a TEG emulator using a programmable DC power supply for power electronics testing.
- Static and dynamic MPPT efficiency analysis using the TEG emulator for various test case scenarios, including rapidly changing temperature profile acquired from real application data.
- Heat loss characterization for the TEG measuring system.
- A constant heat characterization method for TEGs compatible with realistic conditions of TEG applications.
- Additional conditions for controlling the TEG systems that includes the Peltier effect to operate at the real MPP compared to the MPP at matched impedances (*i.e.* "theoretical" MPP).

- Experimental validation of the TEG system power increase using a controllable test apparatus for TEG parametric characterization.
- Experimental verification of the existence of the real MPP using a hot gas system for TEG integration that can be correlated to a viable TEG application.

1.5. LIST OF PUBLICATIONS

Part of the work carried out in this thesis has been published as follows:

1.5.1. JOURNAL PAPERS

[J1] Man, E. A., Sera, D., Mathe, L., Schaltz, E., Rosendahl, L., *Dynamic performance of maximum power point trackers in TEG systems under rapidly changing temperature conditions*, published in Journal of Electronic Materials, 2016.

[J2] Man, E. A., Schaltz, E., Rosendahl, L., Rezaniakolaei, A., Platzek, D., *A high temperature experimental characterization procedure for thermoelectric generator modules under transient conditions*, published in Energies, 2015.

1.5.2. CONFERENCE PAPERS

[C1] Man, E. A., Schaltz, E., Rosendahl, L., *Thermoelectric generator power converter system configurations: A review*, published in the proceedings of the 11th European Conference on Thermoelectrics, ECT 2013.

[C2] Man, E. A., Sera, D., Mathe, L., Schaltz, E., Rosendahl, L., *Thermoelectric generator emulator for MPPT testing*, published in the proceedings of the ACEMP-OPTIM-Electromotion International Conference, IEEE Press, 2015.

1.5.3. AWARD

The Outstanding Application Paper Award was received at the International/ European Conference on Thermoelectrics (ICT & ECT 2015) held in Dresden Germany for the article “Dynamic performance of maximum power point trackers in TEG systems under rapidly changing temperature conditions”.

CHAPTER 2. THEORY OF THERMOELECTRIC DEVICES

This chapter covers basic thermoelectric theory starting at the material level with the thermoelectric effects, continues with the performance analysis of modules and finishes with overall information regarding TEG systems.

2.1. INTRODUCTION TO THERMOELECTRIC PHENOMENA

Charge carriers are particles that move freely in a material and have the ability to transport heat and electric charge. In semiconductors, electrons and holes are the charge carriers. The electric current is driven by electrons in *n*-type materials and by holes in *p*-type materials. The movement of holes and electrons requires energy and when they recombine, the energy is released. The energy removal is equivalent to a cooling effect, whereas the released energy is in the form of heat (25).

A thermocouple is the basic TE unit and it consists of a pair of dissimilar metals or *n*-type and *p*-type semiconductor elements, electrically connected in series usually by conducting copper strips. A TE module is composed of more thermocouples in series electrical connection and coupled thermally in parallel between ceramic substrates. The device can operate either as a heat pump (for cooling or heating) or as an electrical generator. Only the power generation mode of the TEGs will be further investigated in this thesis.

The conversion of temperature difference into an electric voltage and *viceversa* in solids is called the TE phenomena and it is based on three different thermoelectric effects: Seebeck, Peltier and Thomson. These effects allow the TE devices to work in heat pumping or power generation mode (26).

2.1.1. THE SEEBECK EFFECT

The Seebeck effect is defined as the creation of an electric potential between two joined semiconductors when subjected to a temperature difference.

When a temperature difference is applied across a thermocouple, the charge carriers in the materials are thermally excited and diffuse towards the cold region. The diffusion of the carriers across the thermocouple forms a heat flux though each material (Q_n and Q_p). In the case of open-circuit condition, the accumulation of the

carriers at the cold junction creates an electric potential between the two terminals called the Seebeck voltage V_{OC} and can be expressed using the following formula:

$$V_{OC} = \alpha \Delta T \qquad (2\text{-}1)$$

Where α *(V/K)* is the Seebeck coefficient and ΔT *(K)* is the temperature difference between the hot and cold sides of the thermocouple. In general, the Seebeck voltage for the *n*- and *p*- type materials will be different and the resultant is the scalar sum of the individual potentials.

The Seebeck coefficient is quantified as the built up voltage in response to an applied temperature difference across the two junctions:

$$\alpha = \frac{V_{OC}}{\Delta T} \qquad (2\text{-}2)$$

The value of α can be either positive or negative depending on the material type and its dominant charge carriers (27)**.** Metals and metal alloys were first considered for thermoelectric materials, but their Seebeck coefficients are only in the range of few to tens of $\mu V/K$. Their usage is also limited by the fact that some metals are toxic. Another disadvantage to note is their behaviour when operating at high temperatures (around 700°C); they can easily oxidize, vaporize or melt. It was only after the 1920's that semiconductors were discovered as better TE material candidates with Seebeck coefficients in the range of hundreds of $\mu V/K$ (28)**.**

A thermocouple or a TE device acts as a *generator* when placed in a closed circuit, between a heat source and a heat sink that creates the temperature difference. The heat source drives the electrons in the *n*-type material toward the cooler region creating a current through the circuit flowing in the opposite direction. The charges then cross into the *p*-type material though the metallic interconnect. The holes in the *p*-type material then flow in the direction of the current. Thus, thermal energy is converted into electrical energy.

2.1.2. THE PELTIER EFFECT

The Peltier effect is the reverse of the Seebeck effect and it is defined as the conversion of current flow into a temperature difference between two dissimilar materials. Depending on the direction of the current flow, heat is absorbed at one side and released at the other. The Peltier coefficient π_P is expressed with the formula:

$$\pi_p = \frac{P_P}{I} \qquad (2\text{-}3)$$

where P_P is the amount of heat produced or absorbed and I is the current flowing though the circuit.

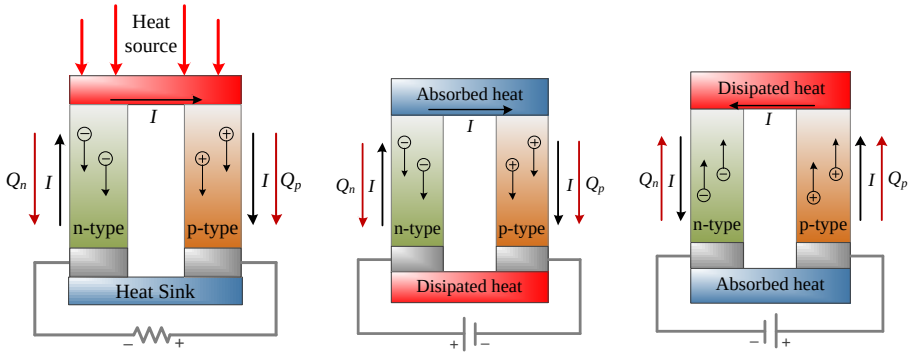

Figure 2-1 Two element TE device functioning as a) power generator b) thermoelectric heat pump for cooling and c) thermoelectric heat pump for heating (8).

A thermocouple or a TE device works as a *thermoelectric heat pump (THP)* when an external power source supplies the electrical excitation in the circuit. Figure 2-1b) presents how a thermocouple works as a cooler. When a voltage is applied across a *p-n* junction, pairs of electrons and holes will be created near the junction. These charge carriers will flow away from the junction. The energy required by the charge carriers to move will have a cooling effect on the junction, transporting thermal energy Q_n or Q_p. On the opposite side of the material, the heat is released and heats the junctions as the electrons and holes recombine. Though the process of heat absorption and release, the conductors aim to return to the equilibrium that existed before the current was applied. Reversal of the applied electric polarity reverses the direction of the heat transport and the device starts working as a heater as shown in Figure 2-1c).

In thermoelectric power generation, the Peltier effect is considered parasitic because it increases the thermal conductivity of the device by pumping heat from the hot to the cold side. This heat pumping leads to a decrease in the temperature gradient across the device and corresponding reduction in the electric potential established. The Peltier impact on the effective thermal resistance of a TE device is dependent on the magnitude of the current and varies in a non-linear way. Its effect on system design and performance is discussed in more detail in Chapter 5.

2.1.3. THE THOMSON EFFECT

The Thomson effect is defined as the reversible heat that is generated or absorbed in a current-carrying homogeneous material when subjected to a temperature difference. In contrast with the Seebeck and Peltier effects that are defined for junctions between two materials, the Thomson effect is characteristic for single conductor. The heat P_T absorbed or rejected is proportional to the product of the electric current I that flows though the conductor and the temperature gradient ΔT:

$$P_T = \tau I \Delta T \tag{2-4}$$

Where τ *(V/K)* is the Thomson coefficient.

In TE device modeling, the Thomson effect is often stated to have a minor influence compared to the Joule effect and therefore it is usually neglected. However, a few researched how this effect impacts the performance of TE modules (29,30). Their conclusion was that the Thomson heat can reduce the power generated by a module by means of voltage, but does not alter its internal resistance**.** It can have a more significant effect in the case of large temperature gradients and therefore some recommend that it should not be neglected (31).

2.1.4. THE KELVIN RELATIONSHIPS

The interaction between the Seebeck and Peltier effects is expressed by the Kelvin relationship in the following formula:

$$\pi_P = \alpha T_j \tag{2-5}$$

where T_j is the junction temperature. It indicates that the same materials can be employed in both power generation and heat pumping (32).

The relationship between the Seebeck and the Thomson coefficients is defined as follows:

$$\tau = T_{AVG} \frac{d\alpha}{dT} \tag{2-6}$$

Where T_{AVG} is the average temperature of the material.

The Kelvin relationships indicate that the three effects exist together in any TE device when they are thermally or electrically excited, no matter the operation mode (26).

2.1.5. THE JOULE EFFECT

Although this effect is not a characteristic specific to TE phenomena, the Joule effect should be included because of its correlation between heat and electrical energy. The Joule effect is defined as the heat P_J released along the length of a conductor when an electric current I is flowing through and can be expressed as:

$$P_J = R_{cond} I^2 \qquad (2\text{-}7)$$

where R_{cond} is the electrical resistance of the conductor.

Unlike the heating caused by the Peltier effect, the Joule heating is independent of the direction of the current flow. In contrast with the Seebeck, Peltier and Thompson effects, the Joule effect is thermodynamically irreversible and is accounted for as a heat loss (33).

2.2. FIGURE OF MERIT OF THERMOELECTRIC DEVICES

The widely accepted parameter that describes the potential performance of TE materials and their utility in applications is called the dimensionless figure of merit:

$$zT = \frac{\alpha^2 \sigma T}{\kappa} = \frac{\alpha^2 T}{\rho \kappa} \qquad (2\text{-}8)$$

and depends on the Seebeck coefficient α, thermal conductivity κ, electrical conductivity σ or electrical resistivity ρ and the absolute temperature T.

To be useful in TE applications, materials need to have a large power factor $(\alpha^2\sigma)$ which means a large Seebeck coefficient and electrical conductivity, and a low thermal conductivity. These parameters need to be optimized concurrently to maximize the zT of the material. This manipulation can become quite challenging because of the parameters' interdependence, *i.e.* electrical conductivity proportionally dependent on thermal conductivity, but inversely proportional with the Seebeck coefficient, as seen also in Figure 2-2.

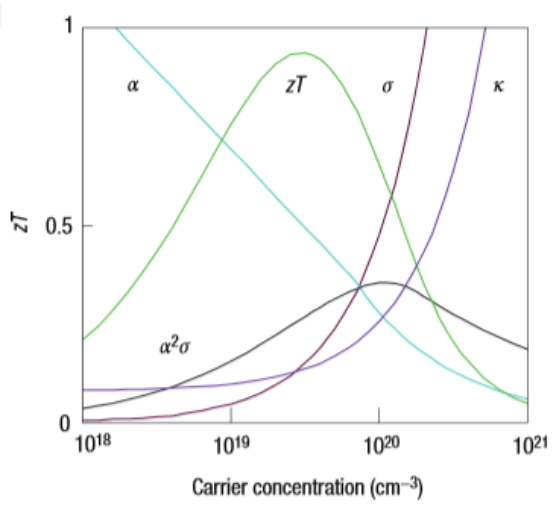

Figure 2-2 Interdependence of the Seebeck coefficient, the electrical and the thermal conductivities related to the doping concentration. Trends are modeled for Bi_2Te_3 (34).

Low carrier concentration insulators and semiconductors have a large Seebeck coefficient but a low electrical conductivity. Because the electrical conductivity is inverse proportional to the Seebeck coefficient and both values are desired to be as large as possible, a compromise between the two values must be made. A large α can be established if a single type of carrier is used (either *n* or *p*), otherwise both charge carriers will migrate to the cold side, cancelling out the induced voltages (34). A high electrical conductivity is also beneficial to minimize the losses caused by Joule heating (35).

A low thermal conductivity signifies a lower rate of heat transfer across the materials which ensures a higher temperature difference between the junctions. On the contrary, materials that are used for heat sinks have high thermal conductivities which allows for a fast heat transfer rate (heat flux) between the hot surface and the ambient environment.

The two components that when added form the thermal conductivity are κ_e which comes from the electrons and holes transporting heat and κ_l from phonons travelling through the lattice. The electrical conductivity and the estimated electronic contribution of the thermal conductivity are defined as proportional by the Wiedemann–Franz law (36). Because of this law, it is difficult to increase one without increasing the other.

In other words, a large power factor means that the charge carriers provide an efficient heat to electricity conversion and a small thermal conductivity maintains a higher temperature difference across the device.

The power factor maximizes somewhere between common metals and semiconductors (Figure 2-2). The peak occurs at carrier concentrations between 10^{19} and 10^{21} carriers per cm^3 and corresponds to heavily doped semiconductors which are proven to be good TE materials (37).

An actual TE device is usually constructed from two materials (*n*-type and *p*-type) and, therefore, their electric and thermal properties differ. For more accurate calculations, the figure of merit of a *p*-*n* couple that accounts for the TE capacity of both materials can be used and is given as:

$$ZT = \frac{\left(\alpha_p - \alpha_n\right)^2 T}{\left[\left(\rho_n \kappa_n\right)^{1/2} + \left(\rho_p \kappa_p\right)^{1/2}\right]^2} \qquad (2\text{-}9)$$

where the *n* and *p* suffixes of the parameters correspond to the *n*- and *p*-type materials. Although the equation considers both material properties for the efficiency calculation, other parasitic contributions that affect the performance of the device are ignored (*e.g.* contact resistance) (38). A simpler option often used is to assume that the figure of merit of the material *zT* equals the one of the device *ZT*. However, ZT ≈ zT is most of the times an unrealistic approximation. For this to happen, the temperature must be independent and the *n*- and *p*-type TE properties need to be matched (34,39).

Presently, there is no information on the largest value *ZT* can reach. The theoretical maximum of $ZT = \infty$ is equivalent to the Carnot efficiency which is the theoretical limit for any thermal process. Current *ZT* values are around 1→2 which is not enough to compete with the primary technologies such as steam turbines or internal combustion engines (Figure 1-3). Harman *et al.* (40) announced in 2005 one of the highest *ZT* values in research of around 3. Other good figures of merit reported in the last decade are in the range of 1.2 - 2.2 at 300°C – 650°C (41). The goal of the TE material research community is to obtain *ZT* values in the range of 3-4 in order for the TE materials to have a competitive efficiency and to be suitable for large-scale applications (42,43).

Equation *(2-8)* is limited by the assumption that *Z* is defined for small temperature differences. Min *et al.* (31) show that the value of *ZT* calculated at $\Delta T = 10°C$ is significantly higher than the one obtained for a larger temperature difference ($\Delta T = 90°C$). Their investigation continued by integrating the Thomson effect and proposing the following modified equation for calculating the figure of merit:

$$Z_m T = \frac{\alpha_e^{\,2}}{\rho\kappa} T = \frac{\left(\alpha_h - \beta\Delta T\right)^2}{\rho\kappa} T \qquad (2\text{-}10)$$

The Thomson effect is most of the time neglected on the assumption that is relatively small; however, Min *et al*. (31) showed that more accurate *ZT* values under large temperature differences can be achieved if this effect is considered.

2.3. TEG SYSTEMS GENERALITIES

There are three operating scenarios for TEG systems: (1) constant temperature, (2) constant heat and (3) "dynamic" constant heat.

Constant temperature operation is the most common for TEG system analysis. The hot and cold source temperatures are maintained at constant values by varying the thermal input power depending on the electrical load changes. The recurrent application example of constant temperature operation of TEGs is the electric heater used in parameter characterization apparatus. Even TEG manufacturers use such test setups to obtain product datasheets.

One possible hot source for TEG applications that would maintain a constant temperature are phase-change materials (PCMs) (44). PCMs integrated into TEG systems can release the stored heat at variable rate corresponding to the electrical and thermal operating conditions of TE devices. For example, if the load current in a TEG system was increased, the thermal conductivity of the module would increase and more heat would be pumped from the hot to the cold side. Typically, this would lead to a temperature gradient drop across the TEG. However, because the thermal conductivity of the TEG was increased, PCMs would release heat at a higher rate, maintaining the hot temperature at the same value as before the load current change.

Constant heat operation is less researched, but mostly found in waste heat applications. The thermal input power is constant, but the temperatures at both the cold and hot side of the TEG are varying depending on the parasitic effects given by the load current. A fairly constant heat source example is the Plutonium-238 (Pu-238) used by the National Aeronautics and Space Administration (NASA) for radioisotope TEGs in space applications. This radioactive isotope has a half-life of 87.7 years. NASA reported 0.8% decay per year which makes Pu-238 a fairly constant heat source (7).

Both NASA and European Space Agency (ESA) are now considering Americium 241 (Am-241) as alternative heat source for Pu-238 in low power satellite applications. Am-241 has a half-life approximately five times that of Pu-238 and it

is less expensive. Hence, Am-241 is an attractive option for long duration flights such as the nanosatellites considered for interplanetary missions.

A deviation of the constant heat operation is the "dynamic" constant heat and it means that heat is available from the equivalent application, but the amount varies in time shorter than the thermal time constant of the TEG system response. The vast majority of the TEG applications operate under these "dynamic" constant heat conditions. Application examples include the heat generated by the fire in a stove, by the mass flow in the exhaust pipes of vehicles etc.

2.3.1. COMPONENTS OF THE TEG SYSTEM

Figure 2-3 represents the general schematic of a practical TEG system which consists of the following elements (45):

- *The support structure*, also referred to as *heat exchanger*, is used as housing for the modules. The structure holds the modules and the interface materials sandwiched together at a specific pressure. The structure material is usually modified to absorb as much waste heat as possible to provide a high temperature on the hot side of the TEG.
- *TE module or TEG;* the size, material and number of modules are chosen according to temperature application range and power output required.
- *Heat dissipation system*, also called *heat sink*, enables the heat transmission though the modules and maintains a temperature gradient across the module.
- *Power conditioning system*, which is the electrical interface that delivers processed power from the TEG to the loads. It generally consists of a DC-DC converter (with step-up and/or step-down capabilities) and a control algorithm to either maximize or stabilize the power delivered to loads.
- *Energy storage device*, usually *battery*, to provide the additional necessary power when there is a mismatch between generation and *load* demand.

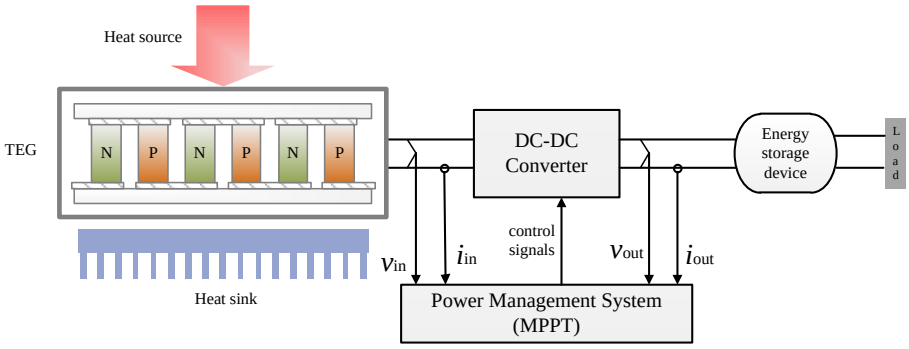

Figure 2-3 General schematic of TE system.

In a TEG system not all the available waste heat is transferred to the TE device. Moreover, the effectiveness of the heat exchangers impacts the amount of heat transferred between the heat source and the TE material. Therefore, the performance of a system cannot be predicted based on the efficiency values of the modules or the corresponding materials. The efficiency of the commercial modules is currently 5% – 10%, but the system efficiency is always less than this. For example, in the case of TEG integration on the exhaust pipe of vehicles, the alterations to the pipe shape and the additional cooling load and weight lead to issues that limit the efficiency of exhaust heat recovery. More precisely, the integration of TEGs was initially suspected to increase the vehicle cooling load up to 50% and to cause a back pressure increase in the exhaust gas system which could increase the fuel consumption (46). Conversely, Kühn *et al.* investigated the impact of the TEG position on the back pressure. They report that the inclusion of the TEG system in the exhaust can reduce back pressure if properly implemented. The energy extracted from the gas increases its density (through cooling) and, although the mass flow rate is preserved, volumetric flow rate (and hence muffler back pressure) is reduced.

Oetringer *et al.* (46) estimate a 3% potential fuel savings corresponding to a CO_2-emission reduction of 0.8g/100 km for an Opel Ampera with 5% efficiency half-Heusler modules. The data collected by LeBlanc (47) show 33% efficiency decrease from material to system level in automotive exhaust, 32% decrease in water heater application and 59% decrease in industrial furnace TEG integration as detailed in Figure 2-4.

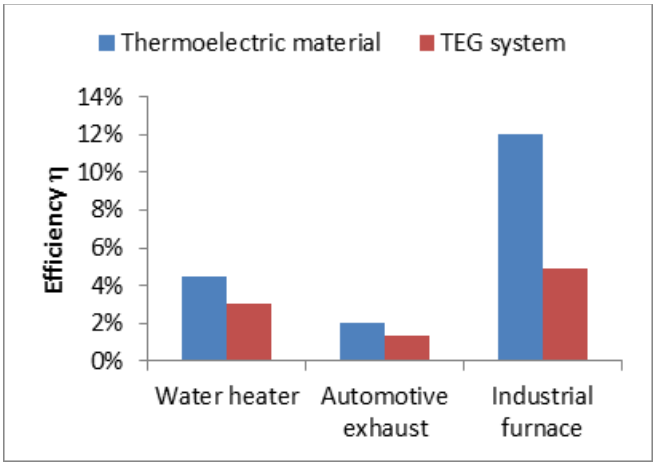

Figure 2-4 Thermoelectric material versus system efficiencies for water heater, automotive exhaust and industrial furnace TEG applications (47).

2.3.2. TEG ELECTRICAL EQUIVALENT

A standard TE module (Figure 2-5) is formed by connecting a number of *n*- and *p*-type thermoelements electrically in series and thermally in parallel. Each thermocouple contains two pellets, one of which is doped to create the *p*-type pellet and the other, the *n*-type pellet. The elements are linked together usually by small copper strips and positioned between two ceramic plates that also serve as electrical insulators and thermal conductors.

A TEG is a solid-state device used to produce electric energy as a result of a temperature gradient between its cold and hot sides. Commercial modules are available in a wide range of sizes to be compatible with application requirements. The pellet size influences greatly the internal electrical and thermal resistances of the module as well as the voltage-current rating. A fixed sized module can accommodate either a small number of pellets with large cross-sectional area or a higher number of pellets with small cross sectional area.

A module with large cross-sectional area pellets has smaller internal resistance but also generates lower voltage and higher current. Multiple modules can be connected in series to obtain a higher voltage output, in parallel for higher current or a combination of series/parallel to meet both voltage and current demands. From a system's perspective, it is important that the output from the TEG array is matched to a) the available heat flux, and b) produces a level of voltage and current that enables the power converter to be operated efficiently. Overall, the TEG output ratings depend on the number of thermocouples in the module, number of

constituent modules, their configuration/connection, the material properties of the thermoelements and the temperature gradient.

The advantages of being noiseless, non-polluting, physically small and having a long lifetime make the TEGs attractive for a wide range of applications, both domestic and industrial. However, the low efficiency of the generator continues to be a widely discussed issue and remains to be improved.

At constant temperature difference maintained across a TEG, the steady-state electrical parameters form almost linear relationships, so to a first approximation, the electrical equivalent can be modeled as a DC source in series with an internal resistance. Figure 2-6 shows the equivalent electric circuit corresponding to a module which consists of a voltage source connected in series to a resistance that represents the internal resistance of the generator. For a TEG the voltage and internal resistance values are temperature dependent *i.e.* temperature gradient and average temperature respectively, and this is examined in greater detail in Chapter 4.

When there is no load connection, V_{OC} of a module is the sum of the Seebeck voltages generated by the thermocouples. At load connection, the voltage becomes:

$$V_{load} = V_{OC} - R_{teg} I \quad where \quad V_{load} = R_{load} I \tag{2-11}$$

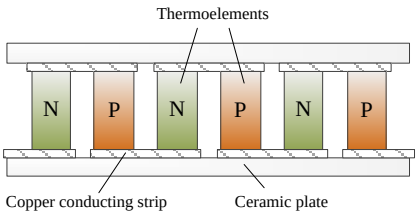

Figure 2-5 Basic configuration of a TE module.

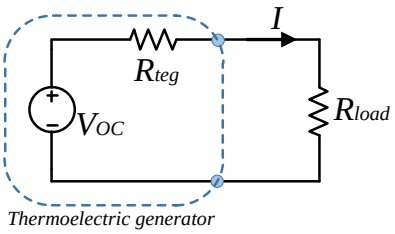

Figure 2-6 Equivalent electric circuit of TEG.

And the current though the circuit can be written as:

$$I = \frac{V_{OC}}{R_{teg} + R_{load}} = \frac{\alpha \cdot \Delta T}{R_{teg} + R_{load}} \tag{2-12}$$

The output power can be then formulated as:

$$P_{load} = V_{load} I_{load} = R_{load} I_{load}^2 = \frac{R_{load} \cdot \alpha^2 \cdot \Delta T^2}{\left(R_{teg} + R_{load}\right)^2} \qquad (2\text{-}13)$$

Often only one module will not provide the necessary power output for the application. As a result, more modules are interconnected depending on the load requirements and temperature gradient availabilities. A generalised structure of a TEG array is illustrated in Figure 2-7 and consists of *nt* modules with *ns* connected in series and *np* connected in parallel. The total number of modules in the generator array is $n_t = n_s \cdot n_p$.

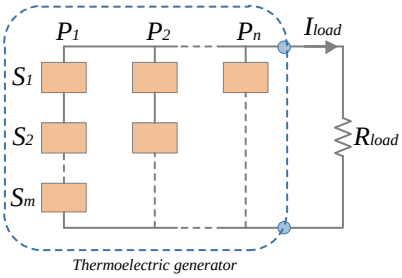

Figure 2-7 Generalized structure of TEG.

For this typical configuration, each module is assumed to have the same electrical characteristics and subject to the same thermal gradient, therefore the load current formula *(2-12)* becomes:

$$I_{load} = \frac{n_s \alpha \Delta T}{R_{gen} + R_{load}}, \qquad where \quad R_{gen} = \frac{n_s \cdot R_{teg}}{n_p} \qquad (2\text{-}14)$$

In general for a practical TEG array system, the temperature gradient is not uniform for all modules. This results in circulating currents within the array that decrease system efficiency and has been extensively examined by Montecucco *et al.* (48).

2.3.3. MAXIMUM POWER VERSUS MAXIMUM EFFICIENCY

The *maximum power transfer theorem* states that the power produced by a TEG is maximized when the ratio *m* between the load resistance and that of the internal module resistance equals unity. In other words, the resistances are matched:

$$P_{\max 1} = RI_{load}^2 = \frac{(\alpha\Delta T)^2}{4R}, \quad where \quad R_{teg} = R_{load} = R \tag{2-15}$$

$$\text{Or } P_{\max 2} = RI_{load}^2 = \frac{n_t(\alpha\Delta T)^2}{4R}, \quad where \quad R_{gen} = R_{load} = \frac{n_s \cdot R_{teg}}{n_p} = R \tag{2-16}$$

The point at which the TEG generates the highest possible power to the load at a given temperature gradient is defined as half of the open-circuit voltage ($V_{OC}/2$) or short-circuit current ($I_{SC}/2$), and is referred to as the maximum power point (MPP).

In Figure 2-8 the temperature gradients ΔT_1, ΔT_2, ΔT_3, ΔT_4 and ΔT_5 represent general samples to illustrate the dependency of TEG voltage V_{TEG} on the temperature difference. It can be seen that an increase in the temperature difference results in an increase in the open-circuit output voltage as well as in the maximum output power of the module. The output power reaches its maximum value when the output voltage is half of the open-circuit voltage. A MPPT control is necessary to repeatedly perform resistance matching between the TEG and the load to extract the maximum power.

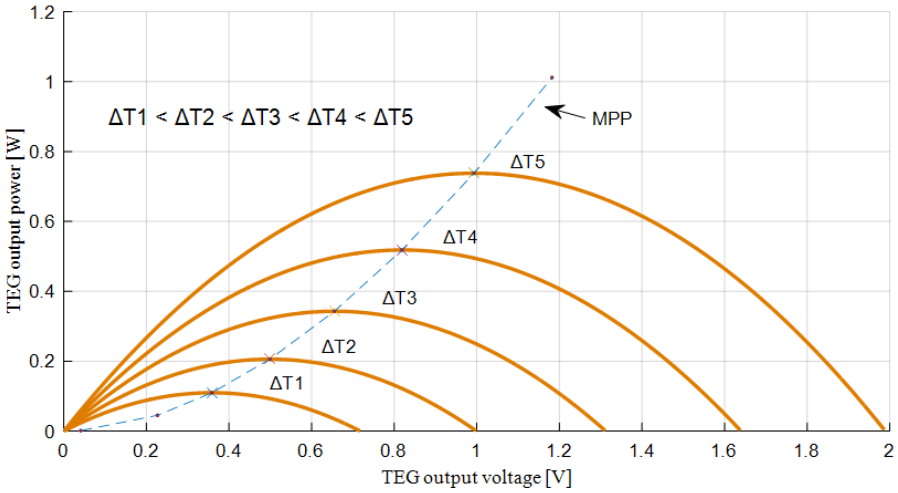

Figure 2-8 General P-V curves of a TEG for different temperature gradients (22).

Initial TE theory utilized the matched condition between the load and TEG resistance for maximum power and maximum efficiency (49,50). In 1909, a separate condition for maximum efficiency ($m = R_{load}/R_{teg} = \sqrt{1+ZT}$) was derived different from the one for maximum power ($m = R_{load}/R_{teg} = 1$). Since then the majority of textbooks and research describe these two separate conditions. These

assumptions are valid for the constructed modules. However, Baranovski *et al.* (50) demonstrate that in design stage, the TEG geometry can be optimized to reach maximum efficiency and maximum power at the same operating condition: $m = R_{load} / R_{teg} = \sqrt{1+ZT}$.

2.3.4. THERMAL ANALYSIS OF THE TEG SYSTEM

The electrical conductivity σ and the thermal conductivity κ of a TE module govern the current and heat flow through the device. A low thermal conductivity ensures the temperatures of the heat exchangers are preserved at hot and cold junctions which maintain larger temperature gradients across the module. A high value of the electrical conductivity is desired to minimize the Joule heating.

At open-circuit condition, there is no current flowing though the device and therefore no Peltier effect altering the heat flow. Nor is heat lost due to Joule effect. When a load is connected, the heat loss due to Joule effect and the effective thermal resistance are influenced by the magnitude of the current. The load current gives rise to the unwanted Peltier effect which acts to pump heat from the cold to the hot side. The temperature at the hot side decreases, the temperature at the cold side increases and, as consequence, the temperature gradient is reduced. A lower temperature difference across a module decreases the voltage available at the device terminals. Power is proportional to V^2 and therefore a small change in temperature gradient can result in a large power change. Figure 2-9 shows the *P-I* and *V-I* curves of a Bi_2Te_3 commercial module. A 50°C change from 100°C to 150°C causes an increase of 2.36V of the V_{OC} and 3.32W of the *MPP*. On the other hand, a change from 150°C to 200°C results in a smaller voltage increase (2.2V), but a larger power increase (3.46W).

The total thermal resistance of the TEG system (Θ_{system}) is composed of the thermal resistances of the hot and cold thermal masses $(\Theta_{hot}, \Theta_{cold})$, the interface materials on both the hot and cold sides $(\Theta_{h,interface}, \Theta_{c,interface})$ and the module (Θ_{module}) as follows:

$$\Theta_{system} = \Theta_{hot} + \Theta_{h,interface} + \Theta_{module} + \Theta_{c,interface} + \Theta_{cold} \qquad (2\text{-}17)$$

Figure 2-10 shows a typical thermal equivalent circuit of module placed between heat source and heat sink. At open-circuit condition, the heat flow though the device is governed only by the Fourier law $Q = K(T_h - T_c)$. In close circuit condition, the ideal heat flow is composed of the Fourier, the Peltier $(\alpha I T_j)$ and the Joule $(1/2 I^2 R)$ terms. A small amount of the thermal input power is lost from the system through convection and radiation (Q_{loss} in Figure 2-10). Typically, the power losses are minimized and therefore they will be excluded from the analysis.

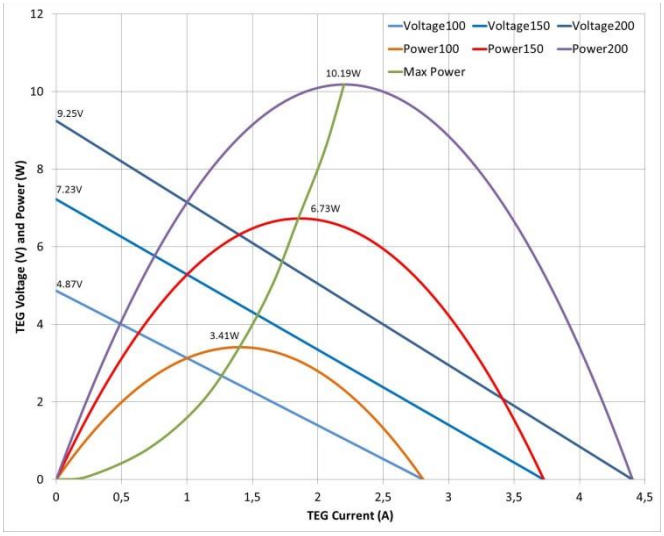

Figure 2-9 Rate of output power and voltage change due to temperature gradient change (51).

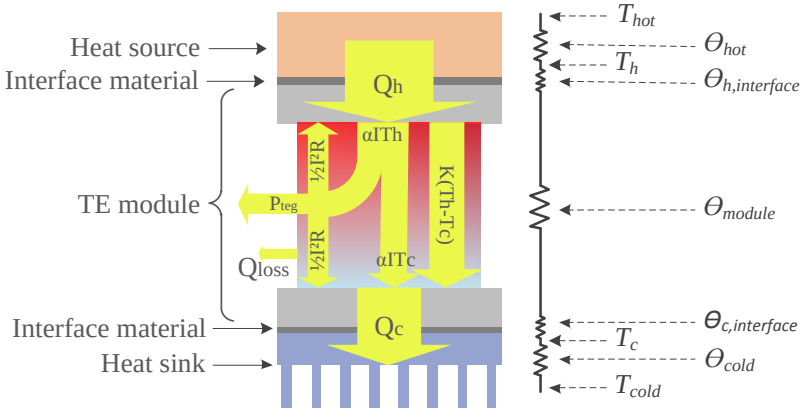

Figure 2-10 Equivalent thermal circuit of a TE module placed between heat source and heat sink.

Considering the Thomson effect small and therefore negligible, the equivalent heat flow balance equations of the hot and cold junctions are:

$$Q_h = \alpha I T_h + K\left(T_h - T_c\right) - 1/2\, I^2 R_{teg} \qquad (2\text{-}18)$$

$$Q_c = \alpha I T_c + K\left(T_h - T_c\right) + 1/2\, I^2 R_{teg} \qquad (2\text{-}19)$$

Where K = (κA)/l is the thermal conductance, κ is the thermal conductivity, A is the area and l the thickness of the module.

The thermodynamic efficiency is the ratio of the electrical power generated by the TEG P_{teg} divided by the thermal power Q_h at the hot junction:

$$\eta = \frac{electrical\ power\ to\ the\ load}{heat\ power\ absorbed\ at\ the\ hot\ junction} = \frac{Q_h - Q_c}{Q_h} = \frac{P_{teg}}{Q_h} = \frac{P_{teg}}{P_{teg} + Q_c} \qquad (2\text{-}20)$$

Where Q_c is the heat removed from the cold side.

The maximum conversion efficiency of a TEG is thermodynamically limited by the Carnot efficiency and it is defined as:

$$\eta_{\max} = \frac{T_H - T_C}{T_H} \frac{\sqrt{1+ZT} - 1}{\sqrt{1+ZT} + T_C/T_H}, \quad T = \frac{T_H + T_C}{2} \qquad (2\text{-}21)$$

To determine the efficiency, the heat removed Q_c and the power generated by the module P_{teg} need to be accurately measured. However, measuring the heat flow can be a difficult task. The alternative method requires the calculation of ZT by measuring the Seebeck coefficient, electrical and thermal conductivities. The latter needs more coefficient measurements and may be more inaccurate. Both methods introduce measurement error and therefore the efficiency calculation is generally a difficult parameter to accurately determine.

2.4. CONCLUSIONS

The theory presented in this chapter is the basis for the TE topics that will be further investigated in this thesis. First, the TE effects were briefly introduced to aid in understanding how a TE device operates as a generator or a heat pump. Because this thesis focuses only on waste heat recovery, the discussions mostly revolved around the TE device operating as generator.

The current performance limits that TEGs face start at material level due to the parameter interdependency of the materials. For this reason, since their discovery, the progress in improving the figure of merit of TE modules has been slow, especially for the commercial ones. Significant progress in the figure of merit of materials and TE devices is necessary to compete with the current more efficient and established technologies.

The concepts of constant heat and constant temperature were clearly divided. This clarification is mostly important as the current module characterization methods revolve around constant temperature condition with unlimited thermal input, but the actual availability in practical application is the limited heat. In other words, the method currently used to determine the TEG characteristics and predict the performance of that device integrated in an actual TEG system is faulty.

A general electrical and thermal description of the components that form a TEG system was given. Similar to module level, also at system level, the interdependency of all the components seriously affect the efficiency of the TEG system leading to a reduced efficiency compared to the one of the TEG. As generally recommended, the TE module should not only be regarded as a “black box” that generates electrical energy from a temperature gradient input. Designing an efficient TEG system proves to be challenging as it requires the engineers to deeply understand the interconnected behaviour between the electrical and thermal parameters of the system. A complete thermal and electrical analysis of the module and the entire system is critical to accurately predict the behaviour of TEG systems integrated into applications.

CHAPTER 3. CURRENT STATE OF THE ART

This chapter presents the literature review of the thermoelectric subjects that will be further investigated in this thesis. First, an update on thermoelectric materials and applications is given. Afterwards, the temperature profiles for real systems are analyzed, followed by considerations of the performance curves of the modules and temperature mismatch impact on efficiency. Finally, discussions conclude with various means to optimize the power generation in TEG systems.

3.1. THERMOELECTRIC MATERIALS AND APPLICATIONS

Initially, metals and metal alloys were favored as TE materials due to their advantage of being good electrical conductors. By the late 1960's, semiconductors with zT values higher than in metals or alloys were discovered, classifying them as good TE materials. Semiconductors can offer higher conversion efficiency due to their flexibility of changing their material properties and geometry. Among the investigated materials, there were bismuth telluride, lead telluride and silicon germanium with optimum operating temperatures around 200°C, 600°C and 1100°C respectively.

Waste heat depends on the ambient temperature and can reach high temperatures (> 1000°C) in absolute terms. There is no single TE material with a high average zT for a full application temperature range. Each material type has highest zT values at a particular temperature range as shown in Figure 3-1.

To produce high efficiency TE modules, large zT values for the materials are necessary, but not sufficient. Other aspects need to be considered for materials to become good TEG candidates, such as cost, availability, environmental impact, reliability or large-scale manufacturing capabilities (52). Cost is the second key issue after performance in large-scale applications. Materials such as some of the skutterudites compounds have in their structure rare earth elements and therefore their availability is limited. Most commercial TEGs are made from Bi_2Te_3, but the future price and availability of tellurium is becoming an issue. Lead (Pb) based materials ideally will be avoided in future TE device construction because of toxicity concerns. However, at present there is nothing commercially available that can match their performance.

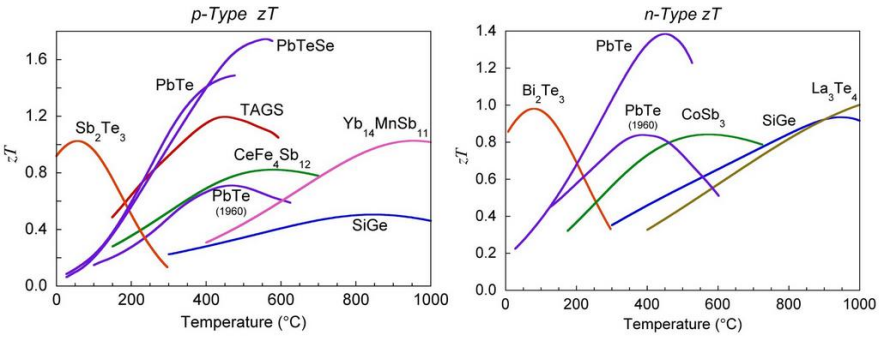

Figure 3-1 State of the art zT n- and p-type materials (34).

TE modules have to endure periodically changing conditions that can seriously affect their reliability. Because of the continuous exposure to thermal cycling, the chemical structure of the materials changes. A TE material needs also to have good mechanical properties to avoid fracture and breakage when exposed to long-term fatigue loading. These mechanical issues lead to the performance decrease of the module and ultimately to its destruction (53).

The modules used in low temperature TEG applications are primarily made from bismuth telluride alloys (Bi_2Te_3, Sb_2Te_3 and Bi_2Se_3) (54-57). For a long time, TEG integration on stoves for remote areas subject to prolonged disruptions in electrical supply or with no grid connection is a popular low-medium temperature application that uses Bi_2Te_3 modules.

In 1966, Killander and Bass (58) designed a TEG system integrated in a wood fired stove top. They estimated the need of a device able to produce 20W to 40W and chose to mount in series two HZ-20 modules from Hi-Z Technology Inc. The rated power of a module was 20W at matched load conditions, hot side temperature of 230°C and 30°C on the cold side. During the day, the temperature of the stove top varied between 150°C and 250°C and the heat sink between 60°C and 90°C. The power generated by the TEG was only 4W – 7W with a morning peak of 10W. Killander and Bass analyzed the lower than expected power generation of their TEG system prototype. They observed and discussed the potential problems that caused the lower power output, *i.e.* irregular surface of the of the stove top, lack of MPPT, too high cold side temperature and lack of clamping pressure for the system. The issues reported by Killander and Bass helped others to search and propose solutions to increase the overall system performance, but also broaden the research interest in TEG integration on stoves in the following years (59-64).

Because of their relatively high *zT* and wide commercial availability, attempts have been made to integrate Bi_2Te_3 modules in medium temperature TEG applications

and more specifically in automotive applications. Since the module is temperature limited, an additional thermal bypass system was necessary for protection against damage at the hot side. However, there is a lot of waste heat recovery potential in applications such as car exhausts with temperatures higher than the Bi_2Te_3 limit (*i.e.* 300°C – 600°C for diesel and 500°C – 1000°C for petrol).

Other materials such as skutterudites and half-Heuslers are being extensively investigated as potential TE candidates for exhaust heat recovery, but opinions differ on which material is the most suitable. As yet no clear commercially viable demonstration has been produced.

Between 2009 and 2012, the International Energy Agency group under the Implementing Agreement for Advanced Materials for Transportation (IEA-AMT) performed round-robins (65,66) to assess the potential TE materials for automotive applications. The data were collected from eleven laboratories representing six countries. The three main material classes were found to be: skutterudites, PbTe (*n*-type) and half-Heusler (*n*-type). Even though skutterudites have high average zT values and good mechanical properties, they undergo sublimation and oxidation (especially *p*-type) at high temperatures. For this reason, they were eliminated from the study. On the other hand, PbTe has been used in radioisotope thermoelectric generators (RTGs) for space missions and exhibits minimal sublimation and oxidation. TEGs based on PbTe can exhibit good reliability and long life-time if operated under constant temperature gradient. PbTe was dismissed because when operated under repeated thermal cycles that are present during service for automotive applications, it presents weak mechanical properties and poor thermal shock resistance. The remaining candidate was the half-Heusler compound because of its strong mechanical properties and thermal stability.

In contrast, Schock *et al.* (5) chose skutterudite-based TEGs for integration into a heavy-duty truck engine at a working temperature range of 300°C – 600°C. The selection criteria for the material were: (a) accommodation of the operating temperature range; (b) good mechanical properties, especially high durability; and (c) availability. For these materials, the main issue is protection against sublimation. The selection of insulators showed no significant change in the sublimation process using gas seal, whereas on aerogel was found to be more promising.

The first TEG used in space applications was constructed with telluride-based materials and was developed by NASA. The modules were composed of PbTe for the *n*-type thermoelements and TAGS[1]/PbSnTe for the *p*-type (7). The segmentation

[1] Tellurides of antimony, germanium and silver

of the *p*- leg was done to improve the device reliability[2]. The current target is to reduce costs of a mission, which mainly means reducing the Pu-238 use by having more efficient TEGs. NASA tasked Jet Propulsion Lab (JPL) and Teledyne Energy Systems, Inc. (TESI) to bring *n*- and *p*-type skutterudite materials to production status for future space missions (67). Am-241 is also a strong contender and has a number of advantages over Pu-238, including a longer half-life and being more easily screened to protect the power electronics.

In many applications, the area that can be covered by modules is large and the temperature distribution is non-uniform. To take advantage of the available temperatures, modules from different materials can be used together. Luo *et al.* (68) simulated the thermoelectric potential recovery from cement rotary kilns using data from a kiln operated in China. To avoid interference with the rotation of the kiln, TEGs were simulated on a coaxial secondary shell. The heat exchangers were proposed to be built from stainless steel with high absorbing coefficient coating to recover as much radiant heat as possible. Because of the temperature distribution along the longitudinal direction of the kiln, modules from different materials (i.e. Bi_2Te_3 and PbTe) were proposed. Although not explicitly stated by the authors, matching the TEG thermal conductivity to the available heat flux per unit area is critical if the desired temperature difference is to be achieved. In addition to material choice, the system designer also has the pellet height as a tunable parameter for system optimization (69).

3.2. TEMPERATURE PROFILES ANALYSIS FOR TEG SYSTEMS

The output power dynamics of a module are proportional to the thermal transients of the temperature gradient input. Such thermal time constants are necessary to be considered when modeling a TEG system. For PV systems, the irradiance varies at a fast rate during passing clouds. Control algorithms have difficulties in accurately tracking the MPP during such fast transient periods. Because the same control methods are used in TEG systems, the issues concerning fast dynamics need to be addressed. On the other hand, thermal rates of change are not as fast as irradiation changes in PV systems.

However, TEG systems present an additional challenge not seen in PV systems: the interaction between the MPP set-point of the converter and the parasitic Peltier effect which leads to a slow response temperature change on the hot and cold side heat exchangers. This in turn affects the temperature gradient available across the module and hence the available power for extraction by the converter. TEGs respond

[2] The desired sublimation rate of TAGS for the corresponding application is crossed above 400 °C. To avoid temperature limiting the TEG due to sublimation, TAGS was segmented to PbSnTe which was able to operate between 400 °C and 700 °C.

in a few nanoseconds to changes in current but it may take several minutes for the thermal effects to manifest themselves. Response times in ~12 orders of magnitude have to be accommodated by the MPPT algorithms for TEG systems to allow the system to thermally react to any electrical changes.

In Table 3-1, a summary of the maximum hot and cold side temperature slopes as described in the literature are presented. The slope values are based on an extensive literature review on TEGs integrated into real applications. Because the information regarding temperature dynamics in TEG system is rather limited, the focus was placed on two most common applications – stove and exhaust pipe. The fastest temperature slope was found to be 4.8°C/s in a biomass stove (62).

However, the surface of exhaust pipes is also expected to reach fast temperature changes. Unfortunately, TEG on exhaust pipes involve testing using the new European driving cycle (NEDC) which does not necessarily reflect one's way of driving. Indeed, the NEDC is widely recognized as being inadequate for the system designer to use when planning a TEG system, not least because it tends to underestimate the maximum heat flux a system will be subject to, and hence the worst-case operating temperature is likely to lead to permanent damage if not properly considered.

By way of example, a gasoline engine on a dynamometer may be operated continuously at maximum power output for extended periods of time. When the engine switches from idling to full throttle, the exhaust manifold may be seen to become a bright red colour in as little as 20 seconds. Assuming the metal to have a surface temperature of ~950°C at full load and 150°C at idle, a ΔT of 800°C in 20 seconds corresponds to a slew rate of 40°C/s.

The observed rate of change is an order of magnitude faster than that published to date, suggesting there are some significant challenges yet to address in peer-reviewed academic work but that are almost certainly already under investigation by the large automotive manufacturers as they develop commercial TEG exhaust gas systems.

Table 3-1 Temperature profile for TEG applications - literature survey.

Application type	Temp. range (°C)	Max. hot side slope (°C/s)		Max. cold side slope (°C/s)		Max. ΔT slope (°C/s)	
		Ramp up	Ramp down	Ramp up	Ramp down	Ramp up	Ramp down
Biomass boiler (70)	AT – 200	0.16	–	Tc – constant (25-27 °C)		0.16	–
Portable device (71)	AT – 200	0.7	–	0.4	–	0.3	-
Microburner (72)	AT – 200	–		–		0.6	–
Stove (58)	AT – 250	0.15	0.05	0.05	0.02	0.1	0.03
Wood stove (73)	AT – 300	0.1	–	0.03	–	0.07	–
Biomass stove (63)	AT – 300	0.25	0.1	0.03	0.02	0.22	0.08
Wood stove (60)	AT – 300	2.25	–	0.05	–	2	–
Biomass stove (62)	AT – 400	5.5	0.8	0.07	0.06	4.8	0.74
Solar cooker (74)	AT – 550	0.3	–	Tc – constant (50 °C)		0.3	–
Exhaust pipe (75)	AT – 300	–	–	–	–	0.5	–
Cooling pipe (75)	AT – 150	–	–	–	–	0.3	–
Exhaust pipe (76)	AT – 300	0.2	–	Tc – constant (80 °C)		0.2	–
Exhaust pipe (77)	AT – 400	3.25	0.75	–		3.25	0.75

**AT = Ambient temperature*

3.3. TEG PERFORMANCE CURVES

Acknowledge of the electrical parameters of a module are vital for designing the overall TEG system (*i.e.* power conditioning system). Typically, the TEG manufacturers provide the necessary data for the TEG in the form of a single power figure at a specific ΔT. Because there is no standard method to perform electrical characterization of a TE device, the electrical and thermal parameters can differ depending on the measurement apparatus and test conditions. The setup and the test conditions in which the manufacturers obtain the datasheet values for their modules are individual and can vary from those used by users or even in TEG practical applications. This means that the expected power generation from a specific module at a certain temperature gradient in practice will most probably not follow the expected datasheet specifications. For example, testing under vacuum is sometimes used to show "improved" TEG parameters. The vacuum significantly decreases the convection losses and the power generated by the module will be higher than the same module tested under open air. However, placing the TEGs under vacuum is seldom used in practical terrestrial TEG applications.

The data mismatch issue becomes more significant in large-scale applications. In this case, a high amount of modules *(few hundreds)* are used and it can become difficult to predict how the system will behave. At least one module should be tested using the conditions experienced in the individual application to test for any discrepancies to the datasheet.

Furthermore, the TEG parameters from the datasheets are exclusively obtained in constant temperature operation *i.e.* unlimited heat flux. In reality, the heat source available for the TEGs is constant. Therefore, this parameter mismatch will always exist until the manufacturers perform the appropriate tests for their modules' datasheets.

There exist some commercially available measurements systems and many have been constructed for research purposes to study the TEG electrical characteristics (78-83).

The first step when characterizing a TE module is to experimentally obtain voltage and current values for various electrical loads, as well as for open- and short-circuit. Based on these results, the *I-V* and *P-I* curves can be plotted. From these characteristics, other TEG parameters such as Seebeck coefficient, electrical resistance, thermal conductance and *ZT* can be computed. A typical curve was shown in Figure 2-9.

Pierce and Stevens (84) experimentally compared the TEG parameters using four characterization methods available in literature: steady-state, rapid steady-state,

Harman and Gao Min's method. The tests were performed under constant heat operation, using a self-made test setup and one module for all four methods. Results clearly show undefined discrepancies between the four methods for each calculated parameter. The authors assume the mismatches are due to thermal resistance of the substrates, electrical contact resistance or Thomson effect, but they do not give a precise explanation. The conclusion of this work only strengthens the need for a standardized method to perform TEG parameter characterization.

3.4. TEMPERATURE MISMATCH IMPACT ON POWER GENERATION

Very often in TEG applications, instead of a single module, TEG arrays are employed to reach certain power ratings. The modules can be connected electrically in series, parallel or a combination of both. For the purpose of the discussion here, an array of TEGs is defined as two or more modules connected to a single power converter. The total surface area covered by the TEG becomes larger and the position of the modules relative to the thermal input power becomes asymmetric. For this reason, the modules are prone to experience variable temperature distributions. Temperature mismatch situations are mainly caused by thermal variability of the heat source but also by other factors such as the uneven distribution of the mechanical clamping force among the modules or different module thermal conductivity.

Su *et al.* (85) explored the surface temperature variation of different heat exchangers for automotive waste heat recovery. Temperature readings taken with an infrared thermal imaging system show a temperature variation from 286.1°C to 322.2°C and from 262.2°C to 322.8°C on two types of exhaust pipe heat exchangers. These findings are supported by other research on this topic (61,72,73,75,86). The investigations confirm that the non-uniform temperature distributions are very common in present TEG systems and that researchers are working to mitigate the problem mostly by optimization of the heat exchangers.

The main consequence of an array of modules working at different temperature gradients is the fact that some operate at a different *I-V* point which is not necessarily the MPP. This leads to a total output power reduction of the TEG compared to the ideal case in which all modules are operating at the same MPP.

Vadstrup *et al.* (87) and Montecucco *et al.* (48) analysed and quantified the power loss in series- and parallel- connected modules operating at different temperature gradients. In both connection types, there is a significant power drop. Vadstrup *et al.* quantified a power drop of 8.4% for series connection and 16.7% for parallel connection relative to the case when modules were individually controlled.

Montecucco *et al.* followed up with 9.22% and 12.90% for the series and parallel connection respectively. Furthermore, the results from both studies reflect the same conclusion that paralleling modules results in a higher total power reduction. Montecucco *et al.* attribute the cause of higher losses in the parallel-connection to the higher current generated by the TEG which leads to higher I^2R losses in the wiring and converter due to the Joule effect. Moreover, the work by Montecucco *et al.* adds information on the position of the operation points on the *I-V* curve of the modules at different temperature inputs and the corresponding thermal efficiencies of the system.

The recurring solution given to avoid power reduction in temperature mismatch conditions is the distributed MPPT (DMPPT) configuration which means controlling each module independently (88). However, this would involve each module to have its own MPPT power converter which would increase the overall system costs, weight and size. The addition of converters to each module for individual control could present an economical problem in large scale applications where cost is the main concern. The extra electronics costs may not be economically viable because of the current low TEG system efficiency. At the same time, there are no available investigations focusing on the economics of the individual module control issue, but a compromise between the numbers of modules and converters must be found if this option is chosen to be implemented.

Min Chen (89) proposes a control concept which involves disconnecting for a period of time the modules that reduce the system power generation due to the uneven temperature distribution. The control algorithm compares the performance of a pre-defined simulation model with the real TEGs and acts upon the modules that are underperforming. When the disconnected modules become viable again, they are reconnected into the system. The results show that the power losses due to temperature mismatch can be reduced using the proposed removal & revival method. However, the authors acknowledge that for any parameter change in the system, the pre-defined database needs to be updated. For example, degradation of TE modules can cause issues of power mismatch between the pre-defined combinations of maximum power output and the actual power readings. Moreover, the algorithm limits the TEG configuration to series connecting two parallel modules as presented in the paper. If both modules in the parallel connection need to be disconnected, this would mean an open connection of the entire TEG array and the loss of any power generation. Moreover, the algorithm needs significant computational resources to monitor and control all modules in real-time.

Similar to individual module control in series-connected strings, another solution to DMPPT presented in PV systems could be applied to TEG systems. It is called differential power processing (DPP) and consists of converters connected to neighbouring modules (90,91). Compared to each module connected to one converter, the DPP configuration has one converter less. Moreover, the converters

are rated to only process the small power difference between series-connected modules (92). This means slightly better system efficiency and reduced costs compared to the case where each module is connected to its individual converter.

3.5. MAXIMIZING POWER GENERATION FROM TEGS

A TE device directly connected to a load operates at a specific point on the *I-V* curve which is often not the MPP. At the same time, the power produced by a TEG is fluctuating dependent on the temperature gradient across it produced by the waste heat source and therefore it cannot deliver a constant power to loads. A DC-DC converter interfaced between the TEG and the load can solve these issues. The iterative matching of the TEG internal resistance to the virtual load seen by the device is performed by a MPPT algorithm that regulates the duty cycle of the converter accordingly. This MPPT converter configuration is used to maximize the power generated by the TEGs for any operating conditions. MPPTs rely on iterative methods, often based on current or voltage measurements, to track the maximum operating point of the system. The performance of the algorithms is referred to as MPPT efficiency. A basic consideration of this type of system is that the converter runs with a short delay between the sampling of the TEG operating point and the subsequent adjustment (if any) of the converter operating condition – typically less than 1 ms. Present control algorithms do not consider the long-term impact on the thermal circuit caused by modification of the electrical operating point.

3.5.1. DC-DC CONVERTERS IN TEG SYSTEMS

TEGs have specific features that need to be considered when choosing the converter topologies. Most of the time, the voltage level generated by the TEG does not meet the load requirements so the converter needs step-up and/or step-down capabilities to solve the issue.

Depending on the design (pellet number, size and thickness), a TE module can either produce low voltage and high current or high voltage and low current output. The first option is not favourable for DC-DC converter because there is a minimum voltage threshold necessary to power the converter's electronics and operate the control algorithm. At the same time, high input current levels can cause significant power losses due to Joule heating. In this case, the voltage can be increased by connecting more modules in series or using a step-up converter. However, to keep relatively high converter efficiency, the conversion ratio is limited. The second module design case is more desired for TEG applications. A high voltage generation can mean high efficiency step up and/or down converters or less module connections to meet the load requirements.

The number and connections of the modules used to form a TEG for a practical application depends on the waste heat availability and the equivalent hot temperature range. The corresponding DC-DC converter is designed to match the voltage and current values generated by the TEG and at the same time the load demands.

So-called *energy harvesters* operating in the mV region have a specific set of design issues that will be included here for completeness of this review.

There are a variety of DC-DC power converter integrated circuits (ICs) designed specifically for low power operation (*e.g.* LTC3108 from Linear Technology, BQ25504 from Texas Instruments, SPV1050 from STMicroelectrics). All expect to receive a low input voltage (20mV→750mV) which is transformer-coupled to achieve a high step-up ratio to between 2.4V and 5V, depending on the IC. MPPT is not considered in these converters.

A typical TEG, such as the commercial Bi_2Te_3 modules have a low internal resistance (few ohms) with many couples (few hundreds) electrically in series to develop the highest possible V_{OC} from the lowest ΔT. Once the converter has self-started, energy extraction from the TEG is possible from either a lower ΔT or close to MPP. Ideally a TEG would be specifically designed for the converter IC such that its internal resistance equalled the converter's input impedance at nominal load. With the use of commercially available TEGs this is not the case and, for low ΔT, the system behaviour is dominated by the V_{OC}.

For TEGs with high internal resistance (e.g. thin film O-Flexx devices) the opposite problem occurs. When the starting threshold voltage is reached, as the converter tries to start, the additional current required causes the voltage to collapse and self-start fails. The failed start-up causes additional heat transfer from the hot to cold side heat exchangers due to the parasitic Peltier effect, further delaying the next start-up attempt.

These problems are expected to drive the development of a new range of TEGs with internal resistance in the 20Ω to 50Ω region with upwards of 1000 couples devices specifically targeting environmental energy harvesting applications.

In most TEG applications, the temperature varies over a wide range. To process as much power as possible from the power source, DC-DC converters need to be able to operate over a wide input voltage range. A high conversion ratio of the converter means a maximized delivery of the power generated by the source to loads. The conversion ratio is altered by several circuit imperfections such as parasitic and switching components. Low current ripple is desired at the converter input to avoid interference with the control algorithms. Obviously, the converter needs to maintain

a high operating efficiency over the entire input voltage range, providing an additional challenge to the system designer.

So far, the most popular DC-DC converters in TEG applications are buck (93), boost (61,94), non-inverting buck-boost (51,87,95-98) and boost-cascaded-with-buck (99-103). These converters are simple, cost-effective, low-weight, easy to control and present high-efficiency.

For TEGs that generate low voltages and high currents (*i.e.* skutterudites-based), the equivalent interleaved topology of the converters can be used (104,105). In this way, the magnitude of the input current is reduced by splitting the input current among each level of the interleaved configuration. If the current value for each level is smaller, the inductances can also be greatly reduced. The only disadvantage of this topology is that it requires more power devices which increase the hardware costs and the control complexity.

In energy harvesting applications, the flyback converter is the most popular and used to step up the small voltage generated by the harvester (106,107). It offers high conversion ratio at a compromise with a lower converter efficiency (<70%) compared to the transformerless boost converter used in TEG applications (typically >90%). The flyback converter is also used in DMPPT TEG systems to process the small amount of power mismatch between series connected TE modules (88).

The buck-boost topology is one of the most attractive choices in TEG integrated applications. Maganga *et al.* (97) used a non-inverting synchronous buck-boost to analyse MPPT algorithms for TEG applications. The converter had a nominal power of 35W (17.5V and 2A) and reached 88.2% efficiency at 34W input. The buck-boost used by Champier *et al.* (61) to charge a lead-acid battery was integrated into a TEG stove application. The efficiency of the converter was in the range of 85% - 92% when the TEG produced more than 5W. During a 2h cooking experiment, the TEG power varied between 8W and 14.5W and therefore the converter had an average efficiency of 90%. Montecucco *et al.* (51) designed a synchronous buck-boost for a wide range of input voltages (3V – 13.5V). The efficiency of the converter was tested with a power supply in series with a fixed resistor and varied from 78.1% at 1.5W input power to 92.6% at 30.38W.

In Chapter 4, the buck-boost converter was also used to test the designed TEG emulator and the performance of the P&O control algorithm for various operating conditions. Because the main focus was on the MPPT efficiency analysis, the efficiency of the converter itself was not further investigated.

3.5.2. CONTROL ALGORITHMS IN TEG SYSTEMS

Power management in a system can be split between two main categories: power output control of the energy source and converter power output control. The first class focuses on optimizing the energy that can be drawn from the renewable power sources (*i.e.* TEGs, PVs) and the latter focuses on maintaining a constant power to the loads.

In case of TEG systems to operate at MPP, the control algorithms need to periodically match the input impedance of the converter to the TEG internal resistance for any temperature difference variation. The power delivered to the loads can be monitored and controlled through a closed loop. Any deviations in the load voltage compared to a set-reference create an error. A controller acts upon minimizing or eliminating the error by changing the control variable: duty-cycle (voltage mode), peak current (current mode) or the switching frequency.

This thesis focuses on extracting as much power as possible from the TEGs and therefore on the first mentioned control category. This class contains either a MPPT algorithm that controls directly the duty cycle of the DC-DC converters or a combination of MPPT with voltage or current control.

MPPT methods are based on an iterative approach that varies a system parameter to make the TEG deliver the maximum available power to the load. The tasks of the MPPT are to detect the power variations of the source and to continuously match the converter impedance to the one of the power supply as stated by the *maximum power transfer theorem*. A presumption of the work presented here is that the converter is connected to an infinite sink and does not accumulate charge. Thus, the converter is always able to operate at the MPP and absorb all available power[3].

A microcontroller or a digital signal processor (DSP) are the usual choices that are used to run the control methods and of course, they consume part of the TEG generated power to perform the necessary computations. The amount of the power used is dependent on the complexity of the control method. A more complex algorithm (*e.g.* P&O) has more mathematical equations compared to *e.g.* fractional open-circuit voltage or short-circuit current *(fractional I_{SC})* methods. The former is preferred because use of the short-circuit current, even briefly, increases the Peltier heat pump effect, affecting system efficiency and increased I^2R losses in the electrical system. For the fractional methods the microcontroller or the DSP requires less computational power. For this reason, in case of applications that have

[3] Practically speaking, a large battery is used as the infinite sink and is periodically discharged to prevent overvoltage.

constant or slowly changing temperature gradients, a lower sampling frequency[4] for the voltage and current readings can be used (*i.e.* f_{samp} = 1Hz) and still maintaining a high efficiency MPPT. Furthermore, a control method that has less computational burden may be more efficient in terms of microcontroller power consumption.

The MPP power is calculated based on voltage and current readings at a specific sampling frequency using an analog to digital converter (ADC). A compromise between a high performance and low-power consumption ADC can be achieved by reducing the bandwidth requirements and measuring average current/voltage values (108). This means that the usage of the MPPT method becomes optimal for systems that have slower changing power sources that the algorithm can track successfully. Any sudden variations may not be seen nor followed by the controller because of its low bandwidth and as determined by the Nyquist limit.

In any practical TEG system, the thermal inertia of the hot and cold side heat exchangers limits the rate of temperature change and hence undersampling is rarely if ever a problem. Large changes in successive sample values can, however, lead to a significant transient in the time response of the algorithm which, if not critically damped, may lead to considerable loss of system efficiency during the setting time.

The state of the art MPPT algorithm used in not only in PV but also TEG systems is P&O. Because it is a "hill-climbing" algorithm, this method can never reach the absolute goal of 100% efficiency. Instead, it will continuously oscillate around the MPP even in steady-state conditions. The main issue of P&O is its inability to track fast changing transients, no matter the compromise between its sampling frequency and the perturbation amplitude. A secondary issue with P&O concerns the algorithm's ability to find the "real" MPP: the required sampling frequency masks the beneficial effect in limited heat flux systems of operating slightly to the left of the MPP on a typical *I-V* curve. This is returned to in Chapter 5.

P&O relies on accurate current and voltage measurements, which are affected by electrical noise and may lead to false power calculations. A large enough magnitude of the oscillations is necessary for better accuracy of the measurements. Still, a tradeoff needs to be ensured, because a too large oscillation can reduce the efficiency of the control method and may cause perturbation in the heat flux through the system.

The performance of the incremental conductance (INC) control method has been repeatedly compared to the P&O throughout the years. Recently, Dezso *et al.* (109)

[4] Note that during the sampling period no energy is extracted from the TEG and this further reduces the overall system efficiency. A 50μs sampling event at 1Hz equates to 0.005% efficiency reduction.

demonstrated mathematically and experimentally, that both methods share the same principle, behaviour and performance and therefore, INC is not a completely different MPPT, but a variation of the P&O. The experimental investigation of the steady-state and dynamic MPPT for both algorithms reveal efficiency deviations below 0.02% and 0.15% respectively. INC is slightly more complex to implement digitally than P&O and it cannot be implemented in pure analogue form (110).

Fractional open-circuit voltage (*fractional Voc*) is a popular control method in TEG systems because of the approximately linear electrical characteristics of the TEGs; it is least computationally intensive and does not need current sensing. The algorithm measures *Voc* iteratively and determines the duty cycle based on half of the *Voc* value.

Compared to the "hill-climbing" algorithms, *fractional Voc* requires only one parameter measurement and lower computational requirements which means less power is used by the controller unit on which the MPPT is implemented, and no oscillations around the MPP.

Conversely, to measure the *Voc*, the energy source needs to be periodically disconnected from the load by means of an additional input switch. This repeated disconnection can lead to unwanted transients and, as already noted, reduced efficiency during dynamic temperature operation. For steady-state operation of the input temperature, the frequency of disconnection can be lowered. This reduction is not recommended in dynamic operation because it will affect the ability of the converter to track changes in the power supply.

Laird *et al.* (111) investigated and compared the steady-state performance of P&O and *fractional Voc* at different temperature gradient inputs and various loads. Results clearly show that *fractional Voc* delivers a more stable output voltage than P&O.

The input switch of converters (*i.e.* buck, buck-boost) can be used to perform *Voc* readings by disconnecting the switch and wait until capacitor charges to *Voc*. The waiting time depends on the size of the capacitor (*i.e.* tens of μs for a capacitor in the order of tens of μF).

Montecucco *et al.* (51) proposed a new method to measure the *Voc* of a TEG, by adding an extra switch in series with the input capacitor of the converter. Instead of disconnecting with the input switch, this method disconnects the input capacitor for a faster *Voc* acquisition (in the range of *ns*). This *Voc* measuring technique is however limited to converter topologies that have a switch at the input to avoid disrupting the continuous current flow in converters that have an inductor at the input (*i.e.* boost).

Due to its popularity, P&O is often the reference for any research that works on improving its performance especially in transient operation or simply compared with other algorithms. Many experimental results show that the efficiency of this algorithm reaches easily ~90% or more.

Phillip *et al.* (96) emulated a TEG system model suitable for exhaust pipe applications. The simulated steady-state efficiencies at different temperature input values for the P&O are reported between 97.10% - 98.19%. Laird *et al.* (14) experimentally tested the P&O algorithm, however, the TEG was implemented by using a voltage source in series with a fixed resistor[5]. This emulation is viable only for steady-state testing. The performance characterization of the MPPT algorithm showed a maximum of 94.78% efficiency. *Kim et al*. (94) focused on tuning the P&O parameters for a TEG system using an experimental setup with an electrical heater for the hot side of the module. They presented simulation and experimental results with various sampling periods and perturbation steps. Although they show the transient response for the TEG power output for a pulse input, they report only the steady state efficiencies for two heater power inputs (87.83% and 90.23%). Champier *et al.* (61) present well-structured results starting with simulation, experimental testing of the MPPT with voltage source as TEG emulator and subsequently, the TEG system integration into a stove application. Both simulation and experimental characterization show a >99% efficiency of the P&O, but no efficiency results are reported for the stove application.

The experimental investigation of any MPPT algorithm is indispensable before it can be implemented in real systems; however the efficiency values are difficult to acquire, especially in dynamic operation. Specifically for this situation, programmable power supplies that can emulate the behaviours of renewable power sources (*i.e.* PVs) have been developed. Reference (98) describes the analysis of the instantaneous and average efficiency of a standard P&O using an innovative oxide-based TEG emulator developed using a Solar Array Simulator.

So far, there are no MPPT algorithms reported in literature specifically developed for TEG systems operating under constant thermal power that take into account the slow thermal response of the system. Based on the constant heat TEG experimental analysis from Chapter 5 and Chapter 6, it is proposed that such an algorithm requires performing three additional functions:

[5] This approach also fails to replicate the reactive components (especially capacitance) in the actual TEG system that, due to oscillatory behaviour after a voltage transient, may affect the accuracy of the *Voc* sample obtained.

I. The algorithm must be able to track high heat exchanger slew rates accurately (so must be able to accommodate transients without oscillatory behaviour).
II. The algorithm must be able to account for the very slow thermal response of the hot and cold side heat exchangers as a consequence of operating at a fraction of *Voc* which does not correspond to that predicted by conventional application of the *maximum power transfer theorem*.
III. The algorithm must incorporate a computationally efficient method of combining both electrical and thermal system time constants to enable tracking of the real MPP.

3.5.3. ENERGY STORAGE DEVICE

The purpose of the energy storage device is to provide the additional necessary energy when there is a mismatch between generation and load demand. Usually, such a device is a battery or a supercapacitor.

The charging current of a battery is less than or equal to a maximum permissible value, defined by the *C rating*. This current is provided by the converter and varies with the temperature gradient on the TEG. The battery voltage depends on the charging current and its state of charge.

In a battery charging application, a MPPT algorithm is used to deliver the maximum available charging current but below the rated value. The voltage battery is also monitored so as not to exceed a specific value which corresponds to the overcharging condition. In this case, the charging current needs to be reduced. After the battery is fully charged, the current is kept to a low value known as the "holding charge". This is typically 0.001 of the *C rating*.

Montecucco *et al.* (93) used a similar battery charging approach as Koutroulis and Kalaitzakis (112). The concept was used for a 12V lead-acid battery in a TEG system. The MPPT algorithm becomes active when the battery voltage reaches 10.2V. Each time the battery voltage reaches the overcharge limit, the charge current is decreased as a fraction of the charge capacity and the voltage is thus kept between 10.2V – 14.4V. The process is repeated until the battery is fully charged. Afterwards, the current is reduced to a few milliamperes and the battery is maintained at a floating voltage.

In general, the maximum battery charging voltage has a temperature dependence and for temperatures other than 20°C a convection factor of -0.003V per all °C should be used for lead-acid battery types.

3.6. CONCLUSIONS

The current state of the art was presented for TE devices that operate as electrical generators with waste heat as source. The chapter has examined a range of materials suited to different temperature ranges and their corresponding figure of merit *ZT*. Their long-term stability and factors affecting their inclusion in a range of practical and economically viable applications has also been reviewed.

Considerations of how the method used to characterize TEG modules differs from actual usage, where the available heat flux is limited, shows that the design engineer faces several different challenges in translating a paper design into a well-performing system.

The historical application of MPPT algorithms, originally derived for PV systems to TEG systems, has been examined in some detail. Moreover, a number of TEG-specific issues have been identified that limit the performance of these current control methods.

Finally, the importance of matching the TE materials to both the heat flux and the electronic power converter such that the whole system is properly balanced has been explored for both steady-state and transient conditions.

The chapter concludes with a discussion of the different factors that affect the overall system efficiency. Related topics such as embedded energy storage and its proper charging by the power converter are also briefly mentioned.

The academic and industrial interest in TEG systems from small to large scale applications is growing. Following this trend, this thesis contributes to the existing knowledge by presenting original research addressing the following topics:

1. Determination of TE properties: a method was developed to extrapolate the electric and thermal properties of TE modules based on a few steady-state readings at different temperature gradient for constant temperature and constant heat operation.
2. Emulation of thermoelectric generator: A TEG emulator was designed and implemented to improve the classical voltage source in series with resistor connection. The emulator mainly contributes to the dynamic testing of MPPTs in TEG systems.
3. Power generation maximization in TEG systems. A method was developed to maximize the power generated by TEG systems compared to the theoretical power obtained using the *maximum power transfer theorem* conditions.

The thesis concludes with a critical examination of system performance enhancement when the work presented here is applied to a constrained heat flux application.

CHAPTER 4. TEG EMULATOR FOR MPPT TESTING

This chapter first introduces a constant temperature experimental characterization of the electrical parameters of an oxide-based module using a commercial system. Afterwards, a TEG emulator is designed based on the oxide module data and using a programmable DC power supply. Finally, the P&O algorithm was tested on the TEG emulator and the static and dynamic MPPT efficiencies analyzed.

4.1. ELECTRICAL CHARACTERIZATION OF OXIDE-BASED TEG

The first step in designing a TEG emulator is to obtain the steady-state parametric characterization of a real module at different temperature gradients. The thermal input power needs to be carefully controlled to maintain a constant temperature on the hot side of the device when testing from open-circuit to short-circuit conditions.

At present, there is no standardised system or method to perform electrical characterization of TEGs, therefore the parameters were tested using the steady-state method on a commercial system called TEGeta from PANCO GmbH. Figure 4-1 shows the equivalent block diagram of the system.

The test setup can perform parameter characterization of one module at a time. It consists of a 1kW electrical heater that can reach up to 1000°C, water based cooling system, reference blocks for heat flow calculation, two stainless steel plates to sandwich the components together and a bottom spring to calibrate the clamping pressure. Ten thermocouples (denoted *T1* to *T10*) are placed in the system for temperature measurements: one in the heater, one in the cooling block and four in each reference block at the distances presented in Figure 4-2. *T1* was chosen to be at "position 0". The temperature in the heater can be manually set to a desired value and it is controlled using the feedback readings from *T1*.

The material used for the reference blocks is homogeneous and therefore the temperatures at the hot and cold side of the module under test can be extrapolated from the readings of *T2* to *T5* and *T6* to *T9* respectively. A more detailed description of the TEG setup is published in (113).

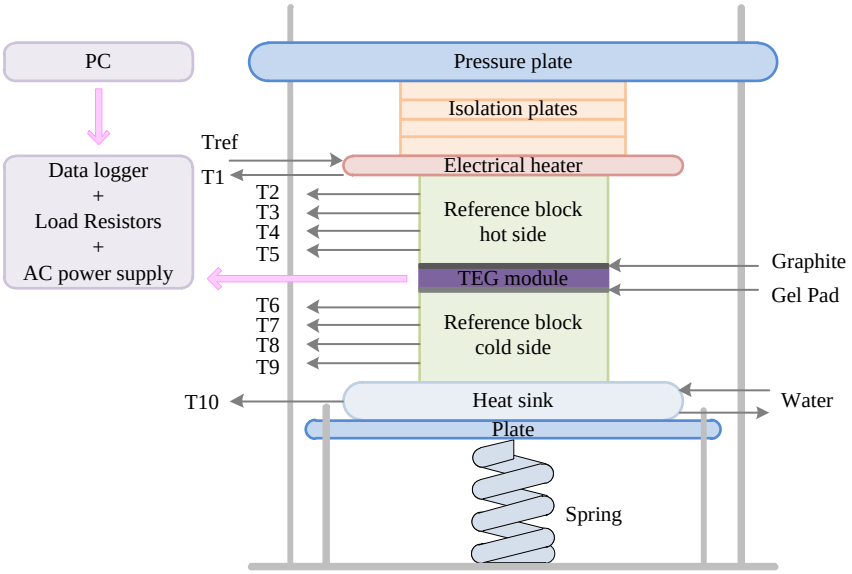

Figure 4-1 TEGeta block diagram.

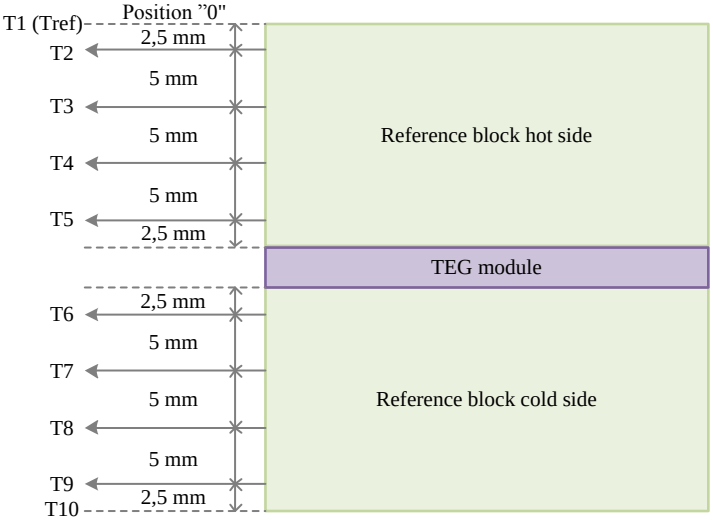

Figure 4-2 Placement of the thermocouples (T_2-T_9) in the reference blocks.

A commercial 42mm×42mm CMO-25-42S module was tested at various steady-state temperatures to acquire the *I-V* and *P-V* characteristics using the TEGeta system. Tests were carried at 1.3MPa clamping pressure as generally recommended by Custom Thermoelectric and the characteristics can be seen in Figure 4-3. The green points are the experimental values obtained with the measuring system and the

orange line is the curve fitting. The current cooling system for the measuring setup is not yet optimized and therefore the cold side temperature was not kept as low as possible. Having cold side temperature above 30°C – 50°C on a module that has less than 1% conversion efficiency significantly reduces the power output.

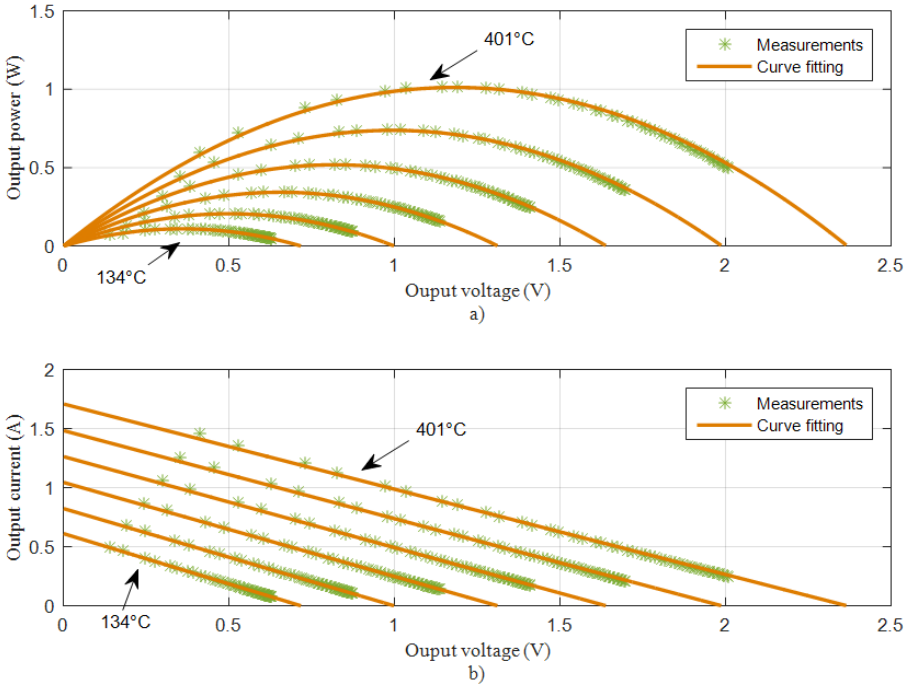

Figure 4-3 a) P-V and b) I-V characteristics for CMO-25-42S tested for the following temperature gradients ΔT = 134°C, 184°C, 236°C, 289°C, 343°C and 401°C, at 1.3MPa clamping pressure.

The oxide module performed poorly and generated only 0.1W at 134°C across the device. The highest temperature gradient that could be obtained with the system was 401°C where the power output reached ~1W and the V_{OC} was ~2.4V. In case this module was placed in a TEG system and if operated at its MPP, it would only output ~1.2V at 400°C which is usually not enough to activate the switching devices in most electronic power converters.

4.2. TEG EMULATOR

In contrast with PV systems where the voltage-current relationship is logarithmic, TEG exhibit linear electrical characteristics in steady-state for each constant temperature gradient maintained across the device. For this reason, the simple way

to experimentally emulate a TEG is using a DC power supply as voltage source in series with a resistor equivalent to the Seebeck voltage and the internal resistance respectively. However, the TEG resistance varies dependent on the average temperature between the hot and cold sides of the module. This simple TEG emulation is limited to only one steady-state temperature difference input because of the fixed resistor value.

As a standalone unit, a TE device is small in size and has a light weight. As soon as it is integrated in a TEG system, the module needs a support structure, heat exchanger, heat sink or water/air cooling and some means of applying clamping pressure. This last part can pose certain difficulties since the hot and cold side heat exchangers have to be pushed together without introducing a thermal short-circuit in the system. These significantly increase the overall system volume, weight and complexity. For this reason, alternative ways to emulate TEGs such as a power supply and a series resistor can offer simplicity and flexibility for power electronics testing.

Currently, there are no TEG simulators available on the market, but there exist programmable power supplies that operate as PV simulators. The Keysight E4360A is a Solar Array Simulator (SAS) designed to emulate the output characteristics of PV strings with the purpose of testing converters and MPPT algorithms without the need of the actual PV panels. The SAS is programmed using data from the actual *I-V* and *P-V* characteristics. Testing the power electronics in both PV and TEG systems can be more flexible with a smaller and more compact programmable supply compared to the real system. The SAS can accommodate various test conditions and most importantly, it offers testing repeatability, which in some cases is a requirement.

The Keysight can be programmed to operate in three different modes:

1. *SAS mode*. The SAS uses an internal-based algorithm to approximate the *I-V* curve based on a list of four parameters given by the user: open-circuit voltage V_{OC}, short-circuit current I_{SC}, voltage at maximum power point on curve V_{MPP} and current at the peak point on the curve I_{MPP}.
2. *Table mode*. In this mode, the user defines a table containing voltage – current points based on which the simulator extrapolates the *I-V* curve.
3. *Fixed mode*. The supply behaves as a standard DC power supply and because this operation has been already extensively discussed and implemented in literature, it will not be further analysed in this thesis.

The user can choose in both SAS and Table mode either high resolution option for a smother *I-V* curve generated within 350ms or low resolution for fast *I-V* curve generation within 30ms.

The characteristic of the oxide module obtained in 4.1 and presented in Figure 4-3 will be further used to show the implementation steps of the simulator to operate as a TEG.

4.2.1. CONFIGURATION FOR STEADY-STATE CONDITIONS

As mentioned before, the easiest way to emulate a TEG in steady-state operation is using a power supply and a series resistor. However, to test different temperature gradient input conditions, the resistor needs to be manually changed with one that matches the resistance of the TEG. No attempt was made to replicate the inductive and capacitive reactances inherent in a real TEG system. Although a TEG is nominally a DC device, the power converter usually changes the voltage and current drawn from the device during MPPT operation and hence these reactive components can affect the accuracy of the adjustment process. Sometimes a perfect match cannot be made due to limited availabilities in resistor values. The simulator can be programmed in both SAS and Table modes to operate in steady-state at different temperature levels without the need for manual labour.

In SAS mode, a set of up to 512 "lists" (*i.e.* table rows) containing the four necessary parameters (V_{OC}, I_{SC}, $V_{MPP,}$ I_{MPP}) can be pre-programmed. Table 4-1 contains one list with the parameters that the simulator needs to emulate the oxide module at 401°C. A dwell time can be set by user and as soon as this time has passed, the simulator switches to the next *I-V* curve (if programmed) from the list which is equivalent to a temperature gradient change for the TEG[6].

Table 4-1 Pre-programmed parameter list for simulator to generate I-V curve for oxide TEG at 401°C and P_{MPP} = 1.009428W.

V_{OC}	I_{SC}	V_{MPP}	I_{MPP}
2.364	1.708	0.854	1.182

The equations used by the SAS to construct the *I-V* characteristic can be found in Appendix A (114). To emulate a TEG, the V_{MPP} was set as half of the V_{OC}. Figure 4-4a) shows the *I-V* and *P*-V curves of the oxide TEG displayed by the web interface of the simulator.

In Table mode, a point corresponds to a specific voltage *V* and current *I* value. A minimum of 3 and a maximum of 4000 points can be defined within a table. The volatile and non-volatile memories of the simulator can store up to 30 tables. The SAS can switch among the tables to emulate a temperature change for the TEG.

[6] In this respect, the emulator can offer superior performance to that from a physical TEG system: the thermal time constants of the system are for all practical purposes zero.

Table 4-2 contains a set of 7 voltage - current points for the oxide module at 401°C. The TEG characteristics produced by the SAS are shown in Figure 4-4b).

Even though in Table mode three sets of voltage – current points might be enough for the SAS to construct the *P-V* characteristics, for a TEG more points are necessary. This situation can be expected keeping in mind the SAS is custom made for PVs and also that the characteristics of PV and TEG differ. If not enough points are defined in the table, the resulting *I-V* curve will be a combination of the PV and TEG characteristics. This happens because the SAS needs to extrapolate the extra points to generate the new *I-V* curve and it is done based on PV equations.

An accuracy analysis was performed for six different temperature inputs by comparing the MPP of the TEG with the power generated by the simulator in both SAS and Table modes. The results are shown in Table 4-3 with the calculated relative errors. In conclusion, it can be stated that the simulator can accurately emulate a TEG in steady-state conditions with relative error lower than 0.25%.

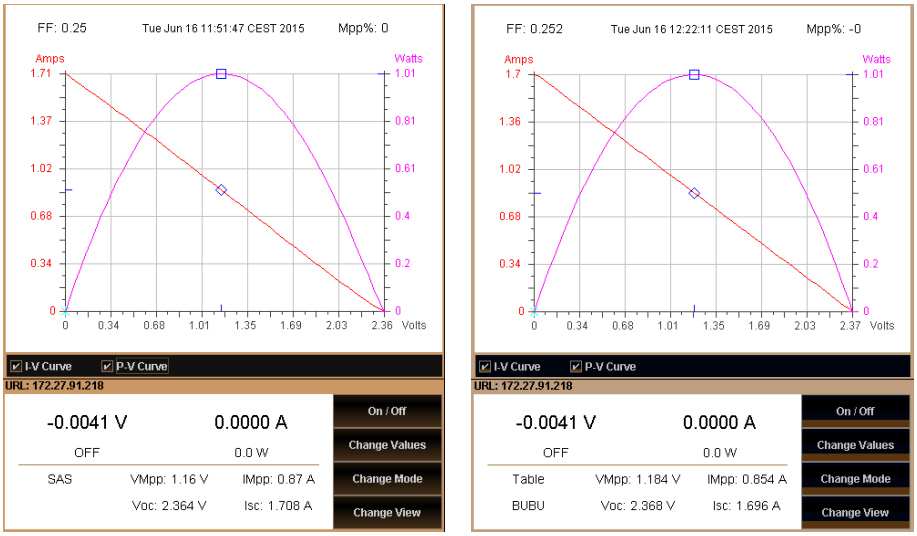

a) **b)**

Figure 4-4 Oxide module I-V and P-V curves configured using Keysight simulator in a) SAS mode and b) table mode at ΔT = 401°C (low resolution).

Table 4-2 Table with 7 pairs of voltage – current values to emulate an oxide TEG at 401°C and P_{MPP} = 1.009428W.

Current (A)	1.70	1.40	1.10	0.80	0.50	0.20	0.01
Voltage (V)	0.02	0.43	0.85	1.26	1.68	2.10	2.36

Table 4-3 Comparison between experimentally measured MPP (P_{MPP}) with the MPP generated by the simulator in SAS ($P_{MPP,Table}$) and Table ($P_{MPP,SAS}$) mode (low resolution).

ΔT (°C)	**P_{MPP} (W)**	**$P_{MPP,Table}$ (W)**	**$P_{MPP,SAS}$ (W)**	**$err_{PMPP,Table}$ (%)**	**$err_{PMPP,SAS}$ (%)**
134	0.109627	0.109662	0.109736	0.0322	0.0997
184	0.2055	0.2058	0.2058	0.1459	0.1459
236	0.3425	0.343339	0.342818	0.2453	0.0932
289	0.5172	0.517914	0.5176	0.1383	0.0776
343	0.73668	0.738036	0.736542	0.1840	0.0187
401	1.009428	1.011664	1.009188	0.2215	0.0237

4.2.2. CONFIGURATION FOR DYNAMIC CONDITIONS

For dynamic operating conditions, SAS and Table modes can be used by pre-configuring tables and lists for the corresponding temperature profile that is going to be used. Because of the limited number of lists or tables that can be programed into the simulator, the TEG can only be tested for a limited temperature range. More important, in both cases the change between lists or tables is performed without considering any thermal system dynamics.

A more suitable option for dynamic TEG operation without the above mentioned limitations is the use of the simulator in Table mode with offsets. This implies pre-setting a table with voltage and current points as a reference table. For every temperature gradient change it means that the simulator needs to switch to another *I-V* characteristic. A program can be designed to calculate the I_{SC} or V_{OC} of the new *I-V* curve corresponding to the temperature change. The offset current or voltage between the I_{SC} or V_{OC} and those of the reference table is then sent to the simulator which updates the new TEG characteristics. Since only the reference table is pre-set into the simulator, there are no limitations on the number of offsets that it can

change. Therefore, the simulator can frequently switch the TEG characteristics even with small increments. Thus, the user can control the timing of the changes and include the thermal dynamics of the temperature gradient across the device.

In table mode, the SAS can accept both positive and negative offset values. However, the simulator cannot be used with voltage offsets to perform as a TEG because the resulting *I-V* curve is a combination of the linear TEG characteristic and the non-linear PV one. Figure 4-5a) shows the resulting characteristic for a voltage offset of V_{off} = +0.5V given to the reference table at ΔT = 401°C. However, the SAS does not preset this limitation when used with current offsets (I_{off} = +0.5A) as seen from Figure 4-5b).

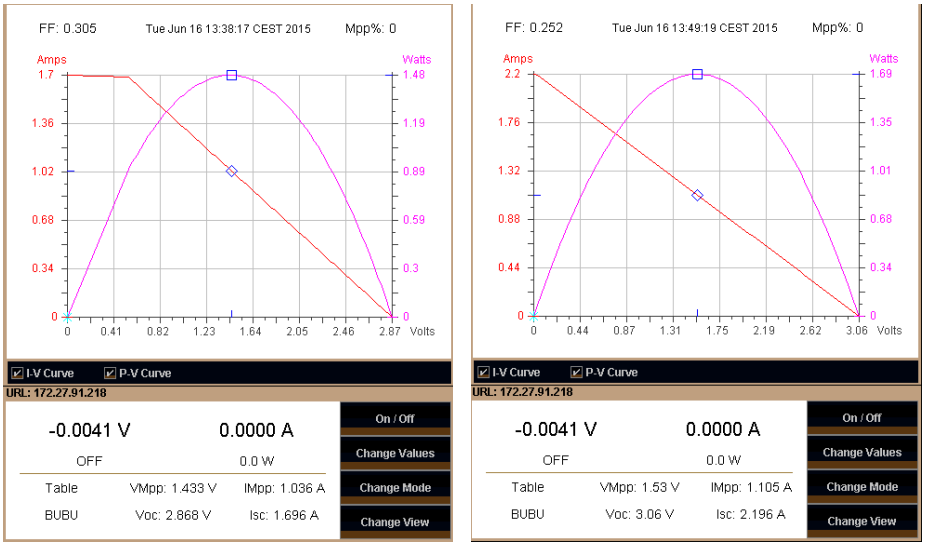

a) **b)**

Figure 4-5 Voltage (Voff = +0.5V) and b) current (Ioff = +0.5A) offsets set to a pre-defined table for oxide TEG at ΔT = 401°C.

The information flow chart of the TEG emulator is presented in Figure 4-6. A MATLAB/Simulink program was designed to contain the oxide TEG *I-V* curves from Figure 4-3 and the desired profile of the temperature gradient across the module. The table with the current and voltage points for the oxide module characterization at ΔT = 401°C from Table 4-2 is chosen as the reference.

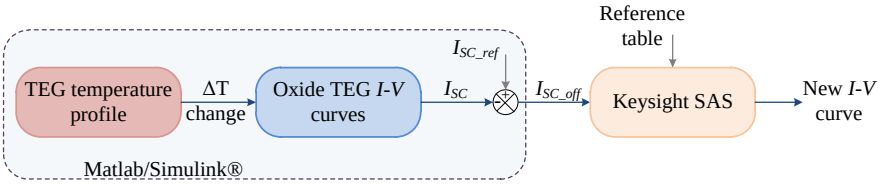

Figure 4-6 Flow chart with implementation of the oxide TEG emulator.

The option of the rate of temperature change that mimics the thermal dynamics is also included in the script. However, there is a minimum frequency at which the SAS can perform the *I-V* change corresponding to the temperature variation *i.e.* $f_{min,\Delta Tchange}$ = 33.33Hz. Generally, thermal dynamics in real TEG systems are slow and therefore a 30ms wait time to update the *I-V* curves does not present a limitation.

The desired gradient temperature profile can be modelled by the user. Each temperature change is fed to the lookup table that contains the *I-V* curves for the module. The new I_{SC} value is subtracted from the reference I_{SC_ref} and the offset I_{SC_off} is sent to the SAS which updates the new *I-V* curve accordingly.

However, performing a current offset change to the reference *I-V* curve means the variation in the value of the internal module resistance is linear which is not the case for TEGs. The internal resistance of TEGs varies dependent on the average temperature between the hot and the cold side and often can be approximated by a second order polynomial. In other words, the new *I-V* curves do not overlap with the actual TEG characteristics. To overcome this limitation, a new set of current offset values can be calculated taking into consideration the TEG resistance values also. This solution makes the new I-V curves overlap the real TEG characteristics in a limited range around the MPP where the control algorithm usually performs as shown in Figure 4-7. The small deviation is considered acceptable since it is operation at the MPP that is of interest.

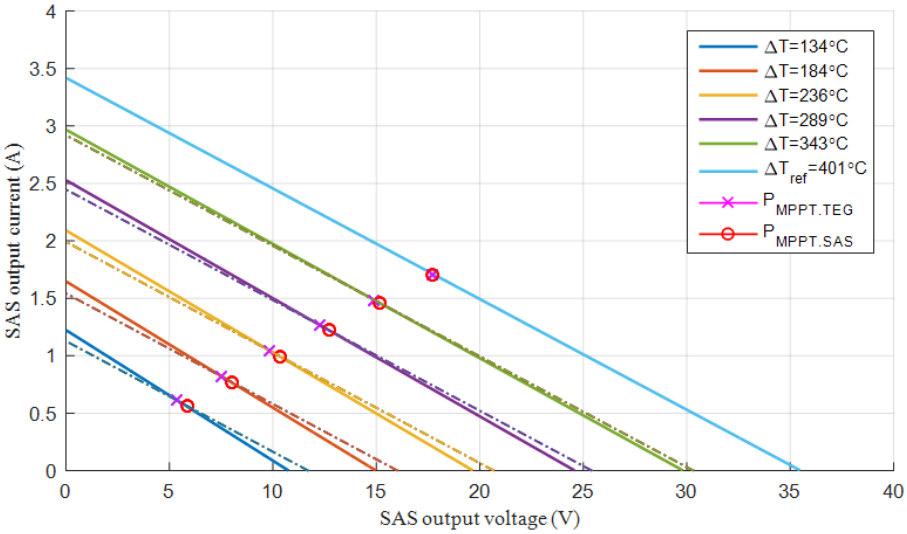

Figure 4-7 Real and new offset SAS I-V characteristics of a TEG module composed of 15 series-connected modules in 2 parallel arrays operating at same MPP for ΔT = {134, 184, 236, 289, 343, 401}°C.

4.3. MAXIMUM POWER POINT TRACKING ALGORITHMS

The goal of MPPT algorithms is to set the TEG system to operate at its optimum power output according to the temperature conditions. There exist many control algorithms in literature originally developed for PVs, but there are a few that are frequently used for TEG systems. The P&O is perhaps the most used hill-climbing method due to its simplicity and high efficiency. The INC is another hill-climbing algorithm often used instead of P&O with very similar efficiencies, but slightly more complex to implement. Both methods require voltage and current measurements and significant computational power to perform the MPP search. The *fractional* open-circuit voltage V_{OC} method is less frequently used for PVs because their MPPs differ among the various panel technologies. In case of TEGs it is known from the *maximum power transfer theorem* that no matter the material the module is constructed from, it will operate at the MPP when the load voltage is at half of the open-circuit voltage. For this reason, the *fractional* V_{OC} method is a very good choice for TEG systems and it requires only one voltage measurement (and no current measurement) that significantly reduces the computational demand. However, as will be shown in Chapter 5, operating the module at the MPP does not necessarily mean the *system* is operating at the MPP.

4.3.1. PERTURB & OBSERVE

The P&O method continuously searches for the MPP on the *P-V* characteristic at a designed step and frequency. The P&O oscillates around the MPP and so it will never achieve 100% efficiency, even if the temperature of the TEG system is in completely steady-state. Another issue of the P&O is the poor tracking under rapidly changing conditions.

The flowchart of the P&O is shown in Figure 4-8 where V_{ref} is the desired voltage at the source. The algorithm acquires the voltage and current measurements of the TEG, calculates the corresponding power and compares it to the power from the previous perturbation step. It further compares the current voltage with the previous value and finally takes a decision in which direction to perturb next. If the variation of the power against voltage $dP/dV > 0$ then the P&O perturbs on the left of the MPP and if $dP/dV < 0$ it perturbs on the right side.

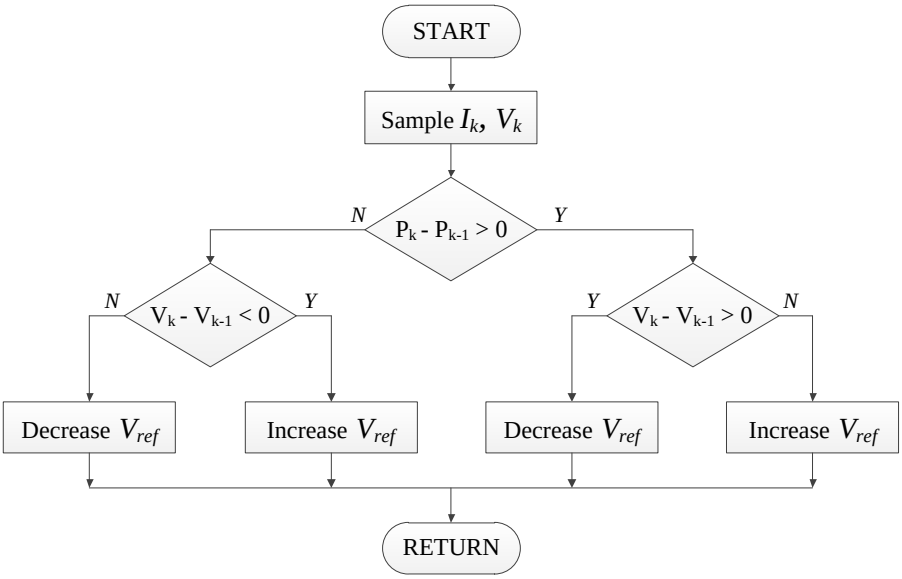

Figure 4-8 The flowchart of the P&O algorithm.

Optimization of the P&O involves adjusting the perturbation magnitude and/or the frequency according to specific applications. For example, in applications where the temperature is constant, a small perturbation step and low frequency are preferred. In the case of dynamic applications, the perturbation magnitude or the frequency need to be higher than for steady state, to accommodate the total power change caused by the temperature variation and the previous perturbation step. In this case,

a compromise between perturbation magnitude and frequency needs to be reached for the algorithm to achieve high MPPT efficiency.

4.3.2. INCREMENTAL CONDUCTANCE

The INC method performs similarly to P&O, even though the INC was designed with the purpose of avoiding the P&O drawbacks (115). However, the INC algorithm uses the observation that the slope of the *P-I* curve is zero at the MPP, $dP/dI > 0$ to the left of MPP and $dP/dI < 0$ to its right. The algorithm tracks the MPP by comparing the instantaneous *(I/V)* and the incremental *(dI/dV)* conductances, according to equation *(4-1)*:

$$\frac{dP}{dI} = \frac{d(VI)}{dI} = V + I\frac{dV}{dI} \qquad (4\text{-}1)$$

The performance of the INC method has been repeatedly compared to P&O. Often it was reported that the INC performance is superior because of its ability to stop perturbing when the MPP is reached *i.e.* $dP/dI = 0$. However, this equality is seldom obtained as mentioned by (115). For rapidly changing conditions, the INC method encounters the same problem as P&O and can track in the wrong direction.

4.3.3. FRACTIONAL OPEN-CIRCUIT VOLTAGE

Unlike P&O and INC, the *fractional* V_{OC} is not a hill-climbing method and it does not require TEG current measurements. This method needs only to measure the TEG's open-circuit voltage and set the load voltage to be half of V_{OC}. Typically, the converter's inductor needs to be disconnected from the TEG for a period of time to let the input capacitor charge up to V_{OC} before performing the voltage measurement. This also can mean that for a few hundreds μs, no energy is transferred from the TEG to the converter. Sometimes, an additional switch can be added at the input of the converter, before the input capacitor to avoid intermittent converter operation. However, there is always an interruption to the energy flow from the TEG to the power converter and hence a small impact on the overall system efficiency.

Overall, the *fractional* V_{OC} is the most easily implemented control method, cheap because it does not need a complicated control system and has low computational demand. For most TEG systems the rate of temperature change is slow, therefore this method can be most suitable even if used with a low frequency V_{OC} reading.

4.4. EXPERIMENTAL ANALYSIS OF MPPT USING THE TEG EMULATOR

The TEG emulator that has been designed and is presented in this chapter has the main purpose of aiding in static and dynamic MPPT testing without the requirement of the actual complex TEG system.

The P&O algorithm was selected to be implemented and tested with the TEG emulator. Among the three described control methods, only the P&O and INC need both voltage and current measurements to perform MPP tracking. *Fractional* V_{OC} is the easiest to implement because it needs only a load voltage setting based on a V_{OC} reading. However, a repetitive disconnection of the converter from the emulator to measure the V_{OC} is necessary. The converter used for the MPPT analysis does not have an extra input switch to perform the disconnection, therefore this method was discarded. Furthermore, the P&O and INC algorithms do not interrupt the energy flow between the TEG and the converter to perform measurements. Between P&O and INC, the choice was P&O because it is easier to implement and it has similar behaviour with the INC method. The purpose of the experiment is to show the successful operation and MPPT efficiency results of the P&O algorithm on the TEG emulator. For this reason no optimization was performed on the control algorithm.

The SAS unit is limited to 5A and the converter needs a minimum of 5V to operate up to a maximum of 42V. A TEG array consisting of two parallel-connected arrays each with 15 series-connected modules was used. The temperature gradient that satisfies the converter's minimum voltage requirement of 5V is 134°C where the TEG array gives a V_{OC} = 10.76V and I_{SC} = 1.223A. At 401°C temperature gradient, the TEG array has V_{OC} = 35.46V and I_{SC} = 3.417A.

The TEG was modelled into the MATLAB/Simulink program of the emulator based on the *I-V* characteristics of the oxide module. Three assumptions were made: 1) the temperature gradient is distributed uniformly across all modules, 2) all modules have the same *I-V* characteristic and, 3) all modules operate at constant temperature.

4.4.1. SETUP DESCRIPTION AND TEST CONDITIONS

Figure 4-9 shows the block diagram of the experimental setup consisting of the following components: a 600W simulator (E4360A from Keisight), a 400W DC-DC buck-boost converter connected to a variable load resistor, a LEM module for voltage/current measurements and a PC that runs the MATLAB codes that control the SAS and the converter.

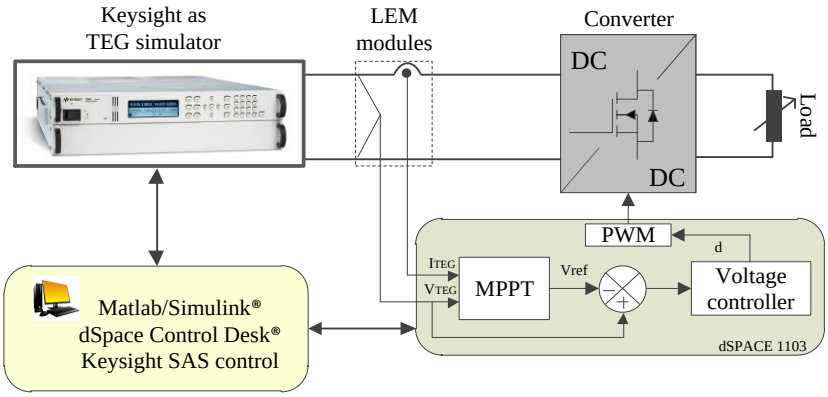

Figure 4-9 Block diagram of the experimental setup.

PV technology is more mature and established compared to thermoelectrics and there already exists a standard way of testing MPPTs. The EN 50530 (116) standard proposes a trapezoidal irradiance profile with different slope values to test the MPPTs for different (slow/fast) irradiance change conditions. The fast irradiance change test is important as algorithms tend to have difficulties tracking accurately the MPP in these conditions.

For dynamic MPPT investigation, a trapezoidal sequence for the gradient temperature input is proposed (Figure 4-10) because it resembles many temperature profiles for TEG applications (*e.g.* stove (58,61,117), biomass boiler (118), car exhaust (119,120)).

As mentioned, the input voltage of the converter is limited at 42V. At 400°C, the TEG has an open-voltage of ~35V and the MPP voltage is ~17.5V. The 5V voltage threshold is set by the control unit of the converter's switching components because they are powered from the TEG voltage. The TEG operating at a temperature gradient of 134°C would provide the necessary 5V to the converter if the MPPT control was ideal. However, the P&O is repeatedly perturbing the operation point of the converter and could go below the threshold voltage. To satisfy all voltage and current limitations of the system during all experiments, the lower and upper limits for the temperature gradients were set to 150°C and 400°C respectively. This range mostly corresponds to medium temperature TEG applications.

Based on the literature review of the practical temperature profile for TEG applications from section 3.2, three trapezoidal sequences were chosen for investigation and are shown in Figure 4-10. The slopes were set to 0.5°C/s, 2°C/s and 5°C/s. The last can be used to test MPPTs under rapidly changing temperature conditions.

The SAS was used in Table mode with current offsets and had a pre-programmed table for the TEG at 401°C. It was controlled by using MATLAB via a LAN interface. The current offset corresponding to each temperature change was sent by the MATLAB program to the SAS at a rate selected by the user. The converter was controlled in real time by the DS1103 dSPACE system based on the P&O algorithm. The voltage and current readings of the TEG emulator necessary for the MPPT were measured with the LEM module. The MPPT unit outputs the voltage reference for the voltage controller which then calculates the duty cycle for the converter.

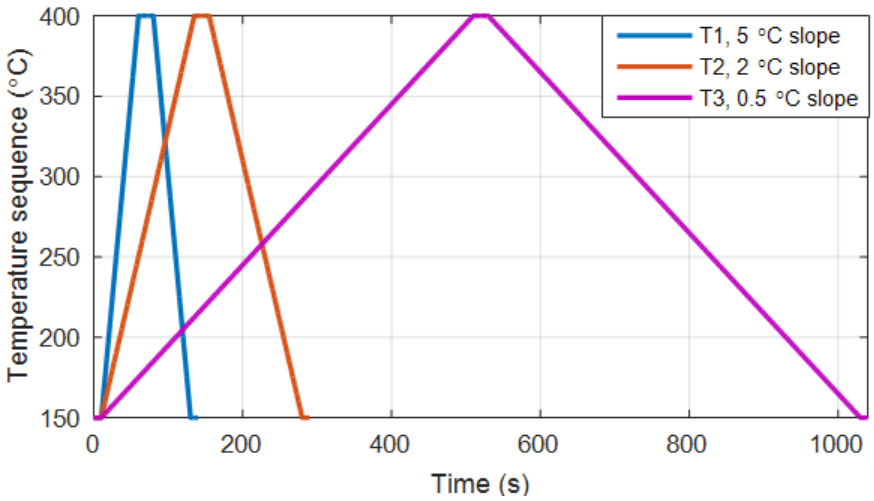

Figure 4-10 Trapezoidal temperature sequences for dynamic MPPT testing.

The switching frequency of the converter and the sampling frequency of the control system were set to 48kHz. A simple proportional *(P)* control was added to the system to regulate the voltage from the MPPT unit at the same rate as the sampling frequency[7]. The proportional gain of the voltage controller was set to a low value of 0.01 to avoid enlarging the amplitude of the noise introduced in the system by the voltage reading. The voltage perturbation increment was set to 2V. The datasheet of the SAS states that it can generate an *I-V* curve as fast as 30ms (33.33Hz). However, during tests, it was observed that occasionally the simulator had issues generating the new curves at this rate and some of the curves were omitted. Therefore 50ms (20Hz) between each *I-V* curve was set to avoid SAS operating at its critical lower limit for curve generation. This setting was experimentally tested and it was found that the SAS experienced no issues in changing the *I-V* curves.

[7] Typically a proportional-integral (PI) control is preferred to also eliminate the steady-state error. However, no control optimization was further investigated as the focus was the validation of the TEG emulator.

4.4.2. STEADY-STATE MPPT TESTING

The steady-state performance of the P&O algorithm was tested for various power levels (15%, 50% and 100% of the maximum TEG array power). Because of the current limitation of the SAS and the input voltage limitation of the power converter, the maximum TEG array power was set to $P_{DC,r}$ = 30.14W and achieved at ΔT = 400°C. The formula used to calculate the static efficiencies was taken from the EN 50530 standard and it is as follows:

$$\eta_{MPPTstat} = \frac{1}{P_{MPP,TEG} \cdot t_M} \sum_i U_{DC,i} \cdot I_{DC,i} \cdot \Delta t_{sam} \qquad (4\text{-}2)$$

Where i is the total number of measured samples, $U_{DC,i}$ is the sampled value of converter input voltage, $I_{DC,i}$ is the sampled value of converter input current, t_M is the overall measuring period and Δt_{sam} is the period between two subsequent sample voltages.

A 10 second dwell time was set before each power level measurements to ensure steady-state operation of the MPPT. The overall measuring period for each test was t_M = 50 seconds. Both $U_{DC,i}$ and $I_{DC,i}$ were sampled with Δt_{sam} = 20.83μs. To also investigate the SAS resolution effect on the accuracy of the MPPT efficiency, the *I-V* curves were set to low resolution first. Tests were carried out for two MPPT frequency values (f_{MPPT1} = 2.5Hz, f_{MPPT2} = 10Hz) and results are shown in Table 4-4.

Table 4-4 Measured static efficiencies normalized to the maximum DC power ($P_{DC,r}$ = 30.14W).

$P_{DC}/P_{DC,r}$	P&O efficiency $\eta_{MPPTstat}$ (%)	
	f_{MPPT} = 2.5 Hz	f_{MPPT} = 10 Hz
$p_{DC,0.15}$ = 0.15	92.91	94.18
$p_{DC,0.50}$ = 0.5	97.68	98.50
$p_{DC,1}$ = 1	98.10	98.58

The measurements in Table 4-4 were performed with the low resolution option. An additional test was performed with the *I-V* curves were set to high resolution. The test was carried out at 400°C corresponding to p_{DC_1} = 1, f_{MPPT} was set to 2.5Hz and the results are shown in Table 4-5.

Table 4-5 Steady-state MPPT efficiencies for low/high resolution of the I-V curve at 400°C and f_{MPPT} = 2.5Hz.

Test conditions	**P&O efficiency $\eta_{MPPTstat}$ (%)**	
	Low resolution	***High resolution***
$\Delta T = 400°C$/ $P_{MPP,Table} = 30.14W$ ($p_{DC,1} = 1$)	98.13	98.74

Two important conclusions can be drawn when comparing the results from these experimental tests. Firstly, looking at Table 4-5 it can be seen that the deviation between the MPPT efficiency values for the two resolution settings is significant (*i.e.* 0.61%). This clearly means that the resolution of the *I-V* curves has an important effect on the efficiency value, therefore, if possible, the high resolution should be chosen for the TEG emulator for steady-state MPPT testing.

Secondly, Table 4-4 and Table 4-5 contain the results of two separate tests with the same conditions *i.e.* $p_{DC,1} = 1$, $f_{MPPT} = 2.5$Hz, and low resolution *I-V* curve setting. The efficiency values are 98.10% and 98.13% with a deviation of 0.03%. This signifies that the emulator offers repeatability testing with deviations in the acceptable range between successive tests of the same control algorithm.

4.4.3. DYNAMIC MPPT TESTING

The dynamic MPPT testing was carried out on the trapezoidal sequences with the three different slopes: 0.5°C/s, 2°C/s and 5°C/s presented in Figure 4-10. For all profiles, the temperature starts from 150°C. After 10s, the temperature rises with a slope value up to 400°C, stops for 20s and decreases back to 150°C with the same slope. To mimic the temperature dynamics, the rate at which the SAS updates the *I-V* characteristic corresponding to a temperature change needs to be faster than the MPPT frequency. As mentioned in 4.4.1, the frequency of the temperature change was set to 20Hz. The frequency of the P&O was varied from 2.5Hz to 12.5Hz with 2.5Hz increments.

The average efficiencies of the P&O in dynamic operation for the three temperature sequences were calculated using equation (4-3) and are summarized in Table 4-6.

$$\eta_{MPPTdyn} = \frac{1}{\sum_j P_{MPP,TEG,j} \cdot \Delta t_j} \sum_i U_{DC,i} \cdot I_{DC,i} \cdot \Delta t_i \qquad (4\text{-}3)$$

Where *i* is the total number of measured samples, *j* is the total number of calculated samples, Δt_j is the period in which the power $P_{MPP,TEG,j}$ is provided and Δt_i is the period in which $U_{DC,i}$ and $I_{DC,i}$ are sampled.

Table 4-6 Dynamic MPPT efficiencies for various P&O perturbation frequency and three temperature sequences.

f_{MPPT}	P&O efficiency $\eta_{MPPTdyn}$ (%)		
	Temp. seq. 1 ***(5°C/s slope)***	***Temp. seq. 2*** ***(2°C/s slope)***	***Temp. seq. 3*** ***(0.5°C/s slope)***
2.5Hz	94.98	95.94	96.24
5Hz	95.68	96.21	96.46
7.5Hz	95.85	96.28	96.62
10Hz	95.92	96.30	96.80
12.5Hz	95.87	96.07	96.52

Figure 4-11 and Figure 4-12 present the theoretical MPP and voltage compared to the TEG emulator power and voltage respectively and Figure 4-13 shows the instantaneous efficiencies. The results are given for f_{MPPT} equal to a) 2.5Hz, b) 5Hz, c) 7.5Hz d) 10Hz and e) 12.5Hz. It is generally known that the P&O has more difficulties in accurately tracking under rapidly changing conditions, therefore the MPPT performance will be further analyzed for the fastest temperature sequence *i.e.* 5°C/s slope.

From Figure 4-7, the voltage change relative to the temperature difference variation can be approximated to 100mV/°C. The temperature is varied at a fixed rate (every 50ms) which is equivalent to 0.25°C and 25mV change. When t_{MPPT} = 400ms (f_{MPPT} = 2.5Hz – case a)), the total temperature difference change is 2°C and 200mV for every MPPT period. The TEG emulator's operation voltage range 1 is ~(6V,18V). The magnitude of the perturbation is composed of multiplying the fixed perturbation step with the proportional constant and the measured voltage (*i.e.* in the range (120mV,360mV)). It can be noticed that there two scenarios:1) at lower TEG voltage values, the set perturbation magnitude is smaller than the magnitude of the voltage caused by the temperature difference change and 2) larger at higher TEG voltage values. In contrast, when f_{MPPT} = 12.5Hz (case e)), the total temperature difference change is 0.4°C and 40mV[8] for every MPPT period which means the

[8] All calculations were made for one MPPT period. The MPPT frequency and the frequency at which the temperature difference is changed are not synchronized. However, this does not affect the assumptions described.

perturbation magnitude is always higher than that caused by the temperature change for the full sequence.

For any power change caused by the temperature gradient larger than that caused by the voltage perturbation, the P&O interprets the change as an effect of its action. Depending on the direction of the previous perturbation, the algorithm has two options to either perturb in the right or the wrong direction. In case of a ramped change in the temperature such as the trapezoidal sequence (Figure 4-12), the algorithm cannot recover the correct direction until the temperature change stops. This can happen when the MPPT frequency is too low and the total power change caused by the temperature change is more significant than the change caused by the perturbation. The effect can be also noticed in Figure 4-12, more significant on the rising slope of the trapezoidal temperature sequence. For all perturbation frequency values, the P&O simply cannot track the rapidly changing temperature and only oscillates around the theoretical TEG voltage. The amplitude and frequency of these oscillations are dependent on the MPPT frequency[9]. At lower P&O frequency, the amplitude of the oscillations is higher, which significantly affects the average efficiency on the rising temperature part, as shown in Figure 4-13a).

During the falling slope the tracking difficulties of the P&O become less significant. Fewer oscillations can be noticed whatever the direction of the perturbation, the output power drops continuously due to the decrease in the input temperature difference. More tracking difficulties can be observed at low MPPT frequencies where the power change due to the input temperature drop is more significant. Slightly more oscillation around the theoretical voltage can be noticed in case of higher MPPT frequencies. In this case, the power drop caused by the temperature input is smaller and depending on the previous power sample and its location on the *P-V* curve, the algorithm can detect a slight power increase. However, this erroneous tracking is most probably rectified in the next few iterations.

[9] Generally, the oscillations around the theoretical voltage value are dependent on both the magnitude and the frequency of the perturbation. However, in these experiments, the perturbation magnitude was fixed at 2V and only the effects of variable perturbation frequencies were investigated.

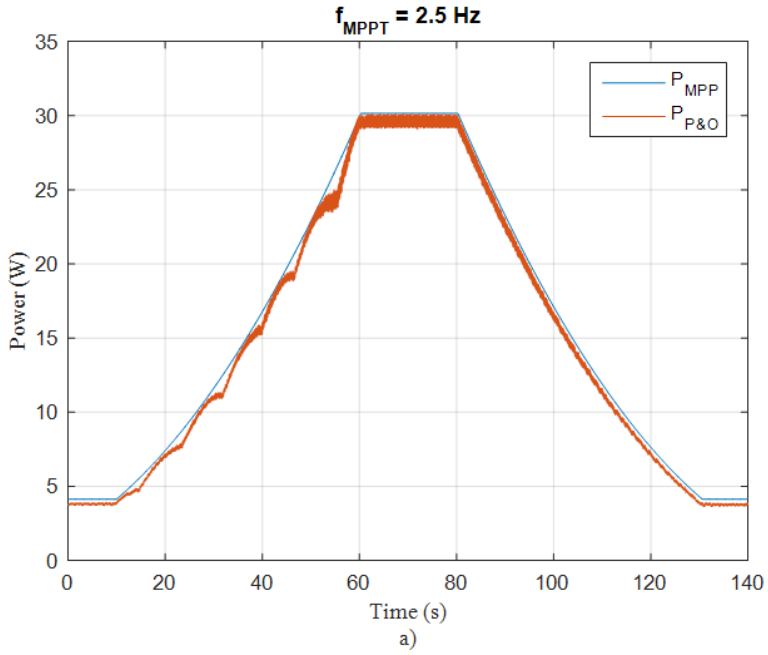
f_{MPPT} = 2.5 Hz
P_{MPP}
$P_{P\&O}$
Power (W)
Time (s)
0
5
10
15
20
25
30
35
0
20
40
60
80
100
120
140

a)

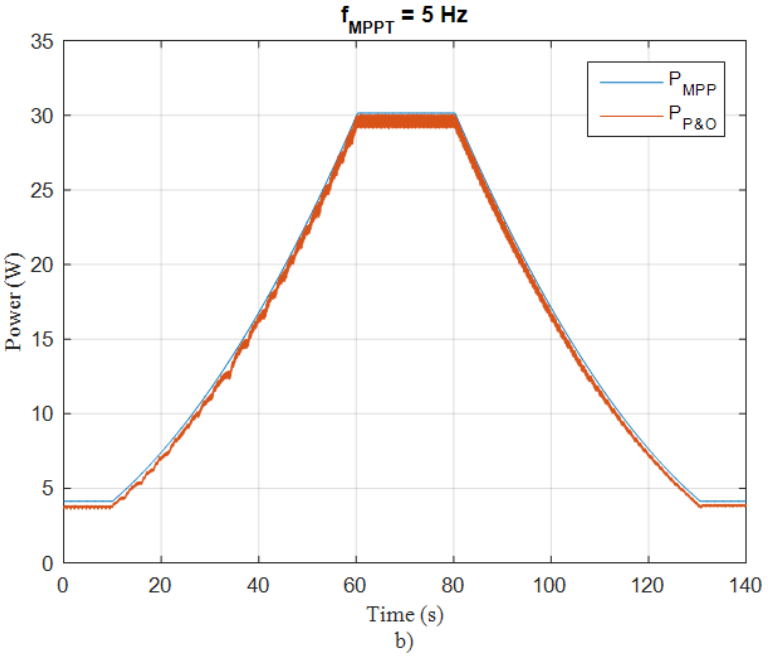
f_{MPPT} = 5 Hz
P_{MPP}
$P_{P\&O}$
Power (W)
Time (s)
0
5
10
15
20
25
30
35
0
20
40
60
80
100
120
140

b)

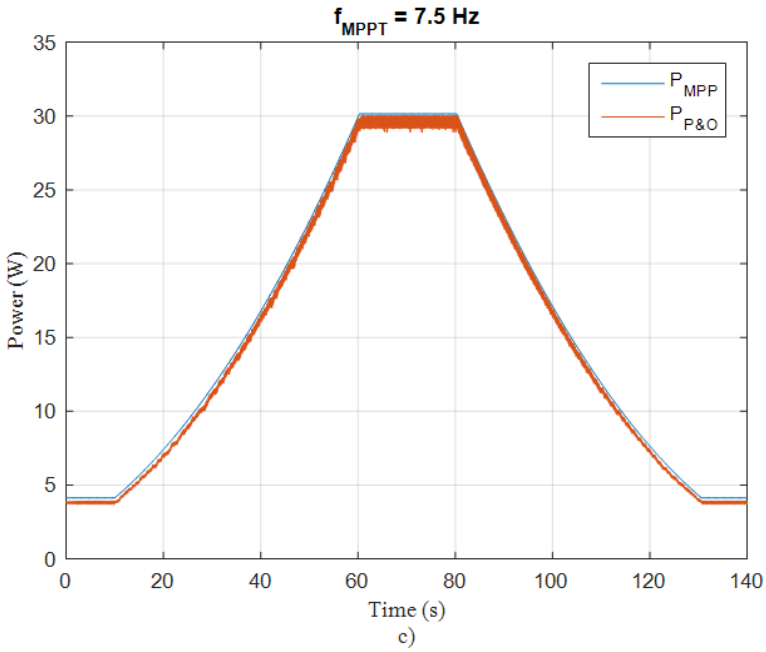
f_{MPPT} = 7.5 Hz
P_{MPP}
$P_{P\&O}$
Power (W)
Time (s)
0
5
10
15
20
25
30
35
0
20
40
60
80
100
120
140

c)

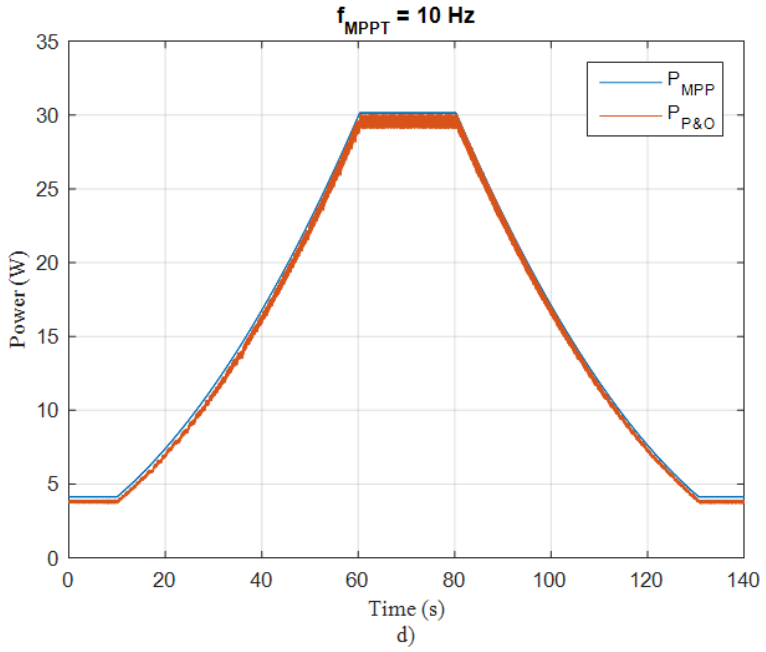
f_{MPPT} = 10 Hz
P_{MPP}
$P_{P\&O}$
Power (W)
Time (s)
0
5
10
15
20
25
30
35
0
20
40
60
80
100
120
140

d)

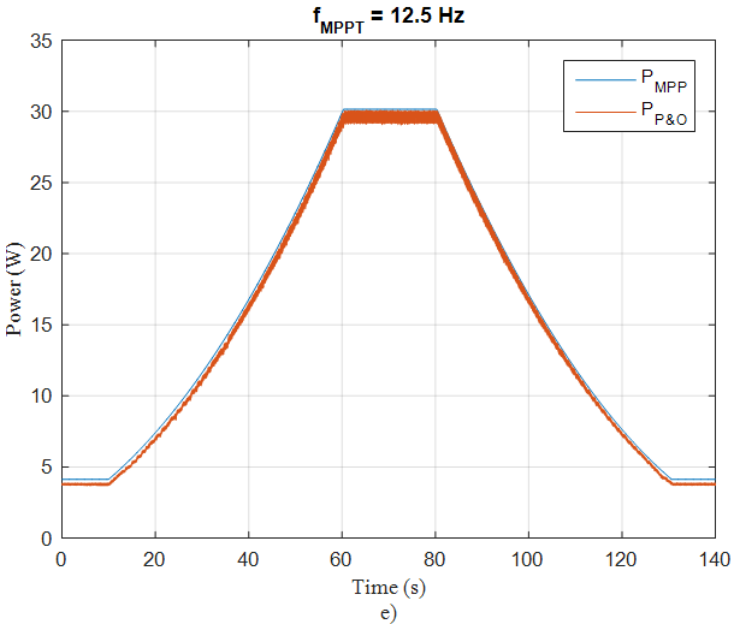

Figure 4-11 Ideal MPP power (blue) and TEG emulator output power (red) analyzed for f_{MPPT} a) 2.5Hz, b) 5Hz, c) 7.5Hz d) 10Hz, and e) 12.5Hz for ramp rate of 5°C/s.

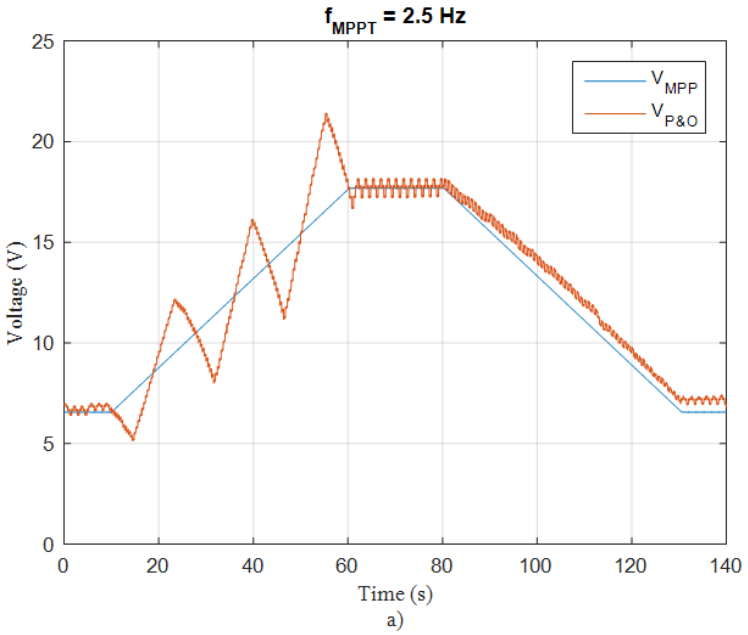
f_{MPPT} = 2.5 Hz
V_{MPP}
$V_{P\&O}$
Voltage (V)
Time (s)
0
5
10
15
20
25
0
20
40
60
80
100
120
140

a)

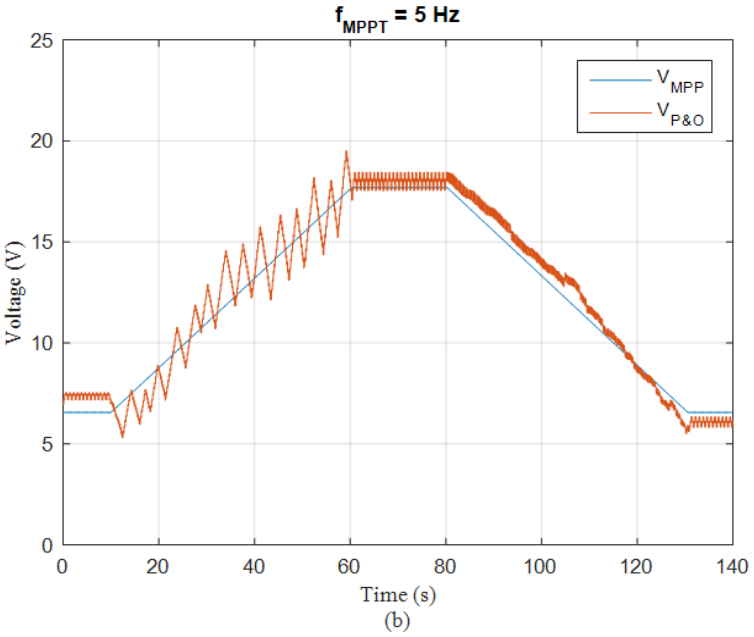
f_{MPPT} = 5 Hz
V_{MPP}
$V_{P\&O}$
Voltage (V)
Time (s)
0
5
10
15
20
25
0
20
40
60
80
100
120
140

(b)

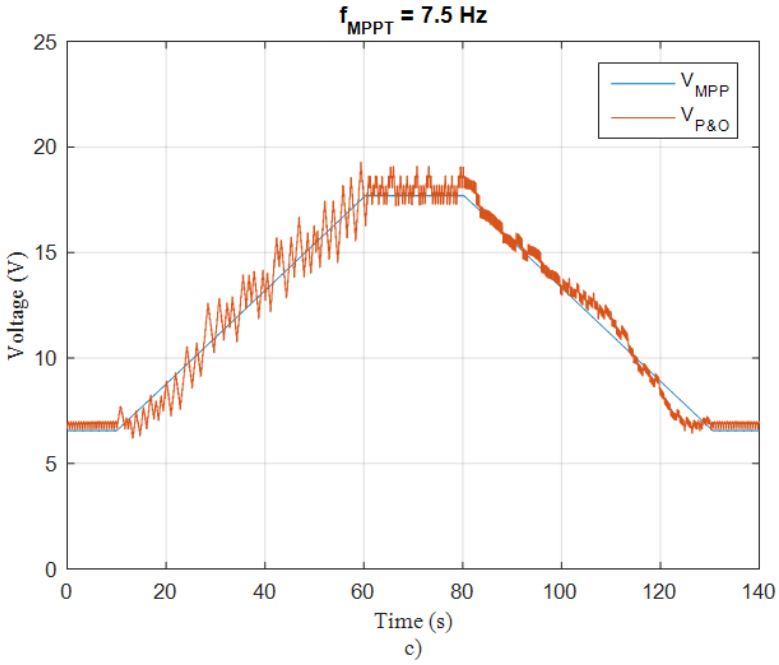
f_{MPPT} = 7.5 Hz
V_{MPP}
$V_{P\&O}$
Voltage (V)
Time (s)
0
5
10
15
20
25
0
20
40
60
80
100
120
140

c)

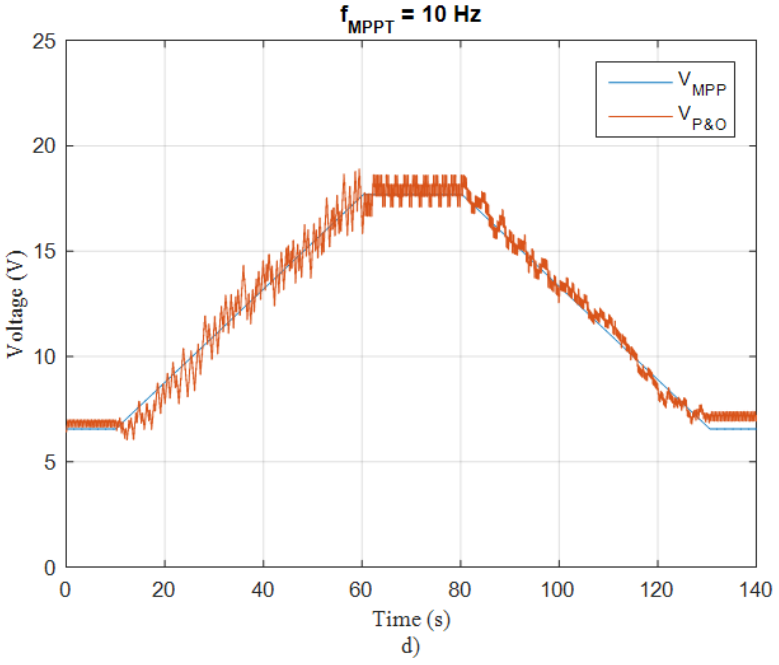
f_{MPPT} = 10 Hz
V_{MPP}
$V_{P\&O}$
Voltage (V)
Time (s)
0
5
10
15
20
25
0
20
40
60
80
100
120
140

d)

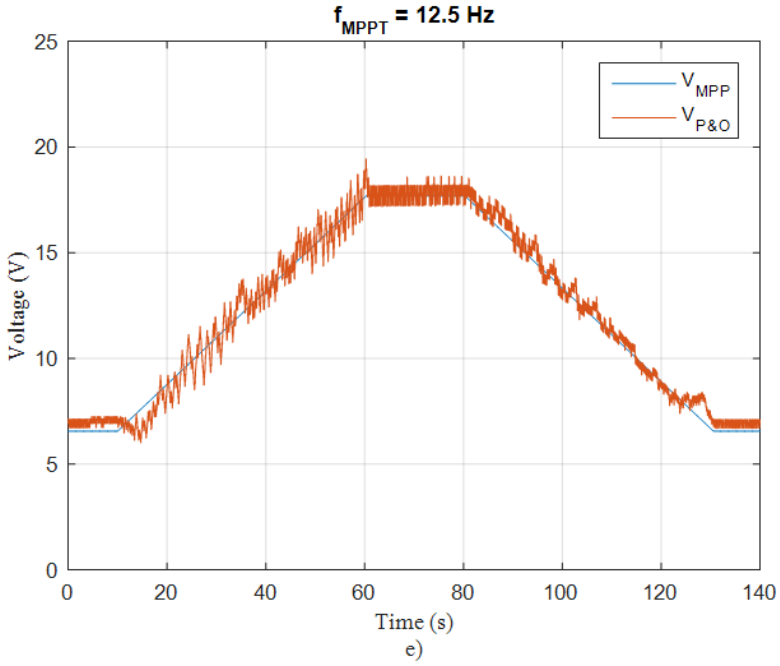

Figure 4-12 Ideal MPP voltage (blue) and TEG emulator output voltage (red) analyzed for f_{MPPT} a) 2.5Hz, b) 5Hz, c) 7.5Hz d) 10Hz and e)12.5 Hz.

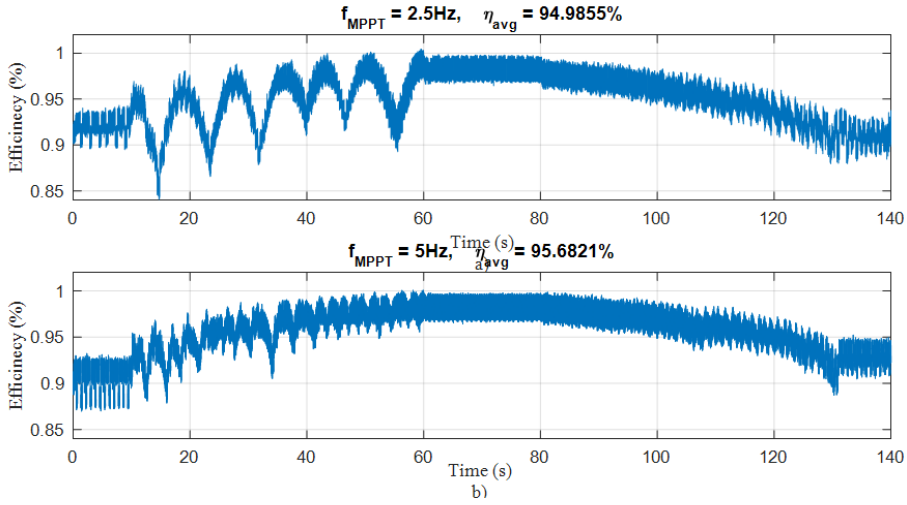

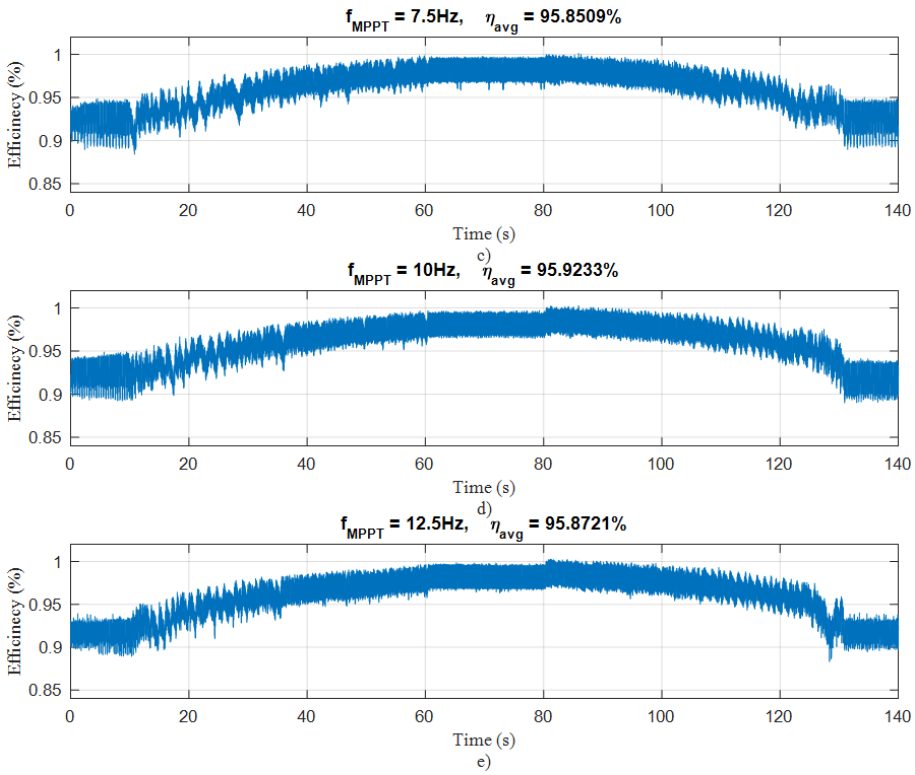

Figure 4-13 Instantaneous P&O efficiencies for f_{MPPT} a) 2.5Hz, b) 5Hz, c) 7.5Hz d) 10Hz and e) 12.5Hz.

Overall, the most significant tracking issues of P&O are during ramped increase in the temperature input and, as expected, the results validate this assumption. If the MPPT frequency is too small (*i.e.* 2.5 Hz), then the P&O will oscillate far away from the actual MPP causing a significant efficiency drop than can be seen in the instantaneous efficiency plot in Figure 4-13a). The average efficiency results from Table 4-6 show that the lowest efficiencies are achieved for the temperature sequence 1. This effect was also expected, as the P&O has more tracking difficulties the higher the dynamics of the temperature and sequence 1 has the fastest slope (5°C/s).

In case the temperature profile of a TEG application is similar to a sequence of trapezoidal-like pattern, the high drop in the instantaneous efficiency on the rising temperature parts could lead to a serious drop in the average MPPT efficiency. However, this issue is generally improved by optimizing the MPPT algorithm specific to particular system and application.

For all the temperature sequences, the highest efficiency values are found at a MPPT sampling frequency of 10Hz. To increase the MPPT efficiency, a PI controller needs to be used instead of the proportional one to eliminate the steady state error.

To assess the repeatability of the results, three extra tests were carried for f_{MPPT} = *2.5Hz*. The P&O efficiencies were 95.6215%, 95.7535% and 95.7181% respectively which means a maximum deviation of 0.132%.

Using the low resolution option and the fastest temperature sequence (5°C/s slope), the P&O loses its tracking ability below 2.5Hz. At high resolution, the MPPT was still able to track at a frequency of 1Hz. This option may be more useful for TEG applications where the temperature changes less than 5°C/s so a smaller frequency for the MPPT method can be chosen and tracking accuracy can be improved. However, because the SAS in high resolution option limits the temperature change at 2.85Hz (equivalent to 350ms), only MPPT frequency lower than this value can be used to still emulate dynamic operation.

4.5. CONCLUSIONS

Thermoelectric technology is still at its beginning stage and further work is necessary for this technology to become mature and competitive. For example there is still no standard way of acquiring the characteristics of TEG modules or specific requirements for testing the TEG systems like the EN 50530 standard for PV systems.

This chapter has presented the commercial mechanical apparatus used to test a TEG module. The electrical characterization of a calcium-manganese oxide module was performed at various temperatures. These data were then used to define the parameters of a 30W TEG array assured to be isothermal. Such characterizations are useful for testing MPPT converters were having an actual module is optional.

Further, the chapter described an approach to design and model a TEG emulator for static and dynamic MPPT testing of TEG system with the present available devices for PV systems. The designed TEG emulator can facilitate the extra dynamic MPPT efficiency investigation that was so far limited when the power electronics of a TEG system were experimentally tested using a DC supply in series with a fixed resistor instead of the actual TEG.

Three popular control methods were investigated: P&O, INC and *fractional* V_{OC}. P&O tracks in a similar hill-climbing way like INC, but it is easier to be digitally implemented. Compared to *fractional* V_{OC}, P&O algorithm does not disconnect the converter from the TEG hence it does not interrupt the energy transfer between the

two. Therefore, the standard P&O was chosen for efficiency testing using the TEG emulator.

The EN 50530 standard for PVs was used as reference to propose the trapezoidal temperature sequence for the dynamic analysis and the equations for the efficiency calculations. Different power levels were used to investigate the static P&O performance. For dynamic MPPT testing, three trapezoidal sequences with different slopes were used. Results validate the expected poor tracking of the P&O at low frequencies (2.5Hz) and fast changing temperature conditions (5°C/s slope). However, the target of designing a TEG emulator for controlled power electronics testing was achieved and validated. Moreover, it has been established that the TEG emulator system can achieve repeatability of the results.

Nevertheless, the programmable power supply used in the TEG emulator design is individual to solar panels. This means that it presents a series of restrictions when used as a TEG. The SAS limitations were identified and suggestions were given how to adapt the apparatus for various TEG application requirements (*e.g.* table and SAS mode for limited temperature range testing or table mode with offsets for unlimited temperature range testing).

Dynamic efficiency is yet a difficult parameter to calculate because the MPP of a TEG system operates most of the times differs from the predicted theoretical one. However, the TEG simulator was able to generate the theoretical MPP with a relative error of less than 0.25%. This means that the apparatus could be successfully used to predict TEG system performance, but similar to the PV programmable supply, a device should be constructed for TEG system with the appropriate equations. The thermal interactions between the components of the TEG system could be included by the user in the MATLAB program that runs the simulator.

CHAPTER 5. CONSTANT HEAT CHARACTERIZATION OF TE MODULES

This chapter first presents the experimental electrical and thermal parameter characterization of the TE device in constant heat corresponding to the conditions present in practical TEG systems. The experimental validation was then performed to show that manipulation of the Peltier effect can have a positive impact on the performance of TEGs relative to the performance set by the maximum power transfer theorem.

5.1. THEORETICAL ANALYSIS OF THE MPP IN TEG SYSTEMS

The *maximum power transfer theorem* states that the MPP for a TE module is reached when the load resistance is matched to that of the TE device. This equality is achieved when the load voltage is equal to half of the V_{OC} of the TEG. The work carried out in this chapter will show that there is a missing condition for the theorem to be also true at the system level. The "theoretical" MPP according to the *maximum power transfer theorem* is the same as the "real" MPP *only* when the TEG system is operated under *constant temperature* condition. This means that the system runs with an unlimited heat source available, and the gradient across the device is kept constant, independent of the Peltier effect due to current changes though the system modifying the module's thermal conductivity.

In practical TEG applications, the available heat is limited. This means the TEG system is operating at constant thermal input rather than constant temperature, referred to as *constant heat*. In this case the Peltier effect can cause significant changes in temperature gradient which further affect the power generated by the TEG and hence, the MPP.

5.2. MAXIMIZING POWER GENERATION THROUGH PELTIER EFFECT

To date, little research effort has focused on the constant heat operation of a TEG system. Most of those concentrated on assessing the existing parameter characterization of modules or developing new methods (84,121). The MPPT control in the TEG system is still performed with the algorithms developed for PV systems (i.e. P&O, INC, *fractional* V_{OC}). These algorithms completely disregard the

slow system impact of the Peltier effect that appears almost instantaneous when current starts flowing through the TE module. Standard algorithms are designed to track the MPP at a minimum time period of ~1 second whereas the Peltier effect may need many minutes for the system to reach steady-state. By iteratively searching or setting the MPP voltage at half of the V_{OC}, the algorithms do not allow the Peltier effect to cause relevant changes in the system. However, the Peltier effect can cause a positive or negative outcome on the power generation of the system depending on how it is manipulated. The Peltier effect is manipulated by adjusting the current that flows through the TE module, usually by selecting an operation voltage that does not correspond to $V_{OC}/2$.

Montecucco *et al.* (117) investigated through simulation a TEG system operating at constant heat. They reduced the Peltier effect to introduce a positive effect in the system by making the TEG operate at lower current and better thermal efficiency than the constant temperature MPP. The reduced Peltier effect caused a temperature gradient increase across the module which in turn led to an increase in the power generated by the device and therefore a new MPP, referred to as the *real* MPP. The reason for this behaviour is that the TEG power output varies proportionally to V^2 whereas the current varies linearly with V (as explained in 2.3.4). At different values in thermal input power to the TEG system, the corresponding voltage fraction at the MPP was found to be at different percentage of the V_{OC}.

Presently in the literature, there is no clear information on the exact percentage of V_{OC} the TEG should operate at to reach the real MPP, or experimental validation of the real MPP. Hence, the potential of the Peltier effect to influence the power generation of a TEG system operating in constant heat was investigated using test apparatus developed at The University of Glasgow (83).

5.3. DESCRIPTION OF THE TEST SETUP

The TEG measuring system used for the experimental characterization is shown in Figure 5-1 and it is able to test one TE module at a time. To better understand the TEG fixture side, the block diagram of its architecture is presented in Figure 5-2. The mechanical, thermal and electrical features of the setup will be further explained in detail.

5.3.1. MECHANICAL STRUCTURE

The system has a stationary heat sink block positioned above the heater block and a separate mobile mechanical structure that can be adjusted up to 50 mm vertically. This means that the module positioned on top of the heater and the heater block are brought towards the cold block.

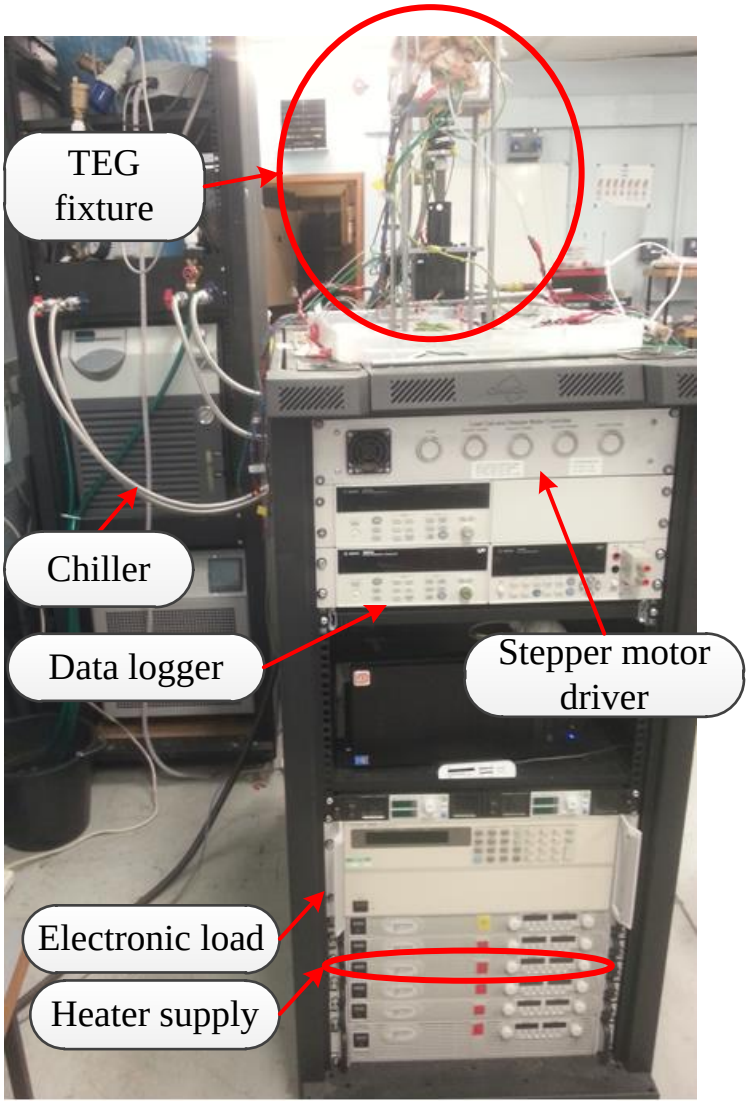

Figure 5-1 TEG measuring system

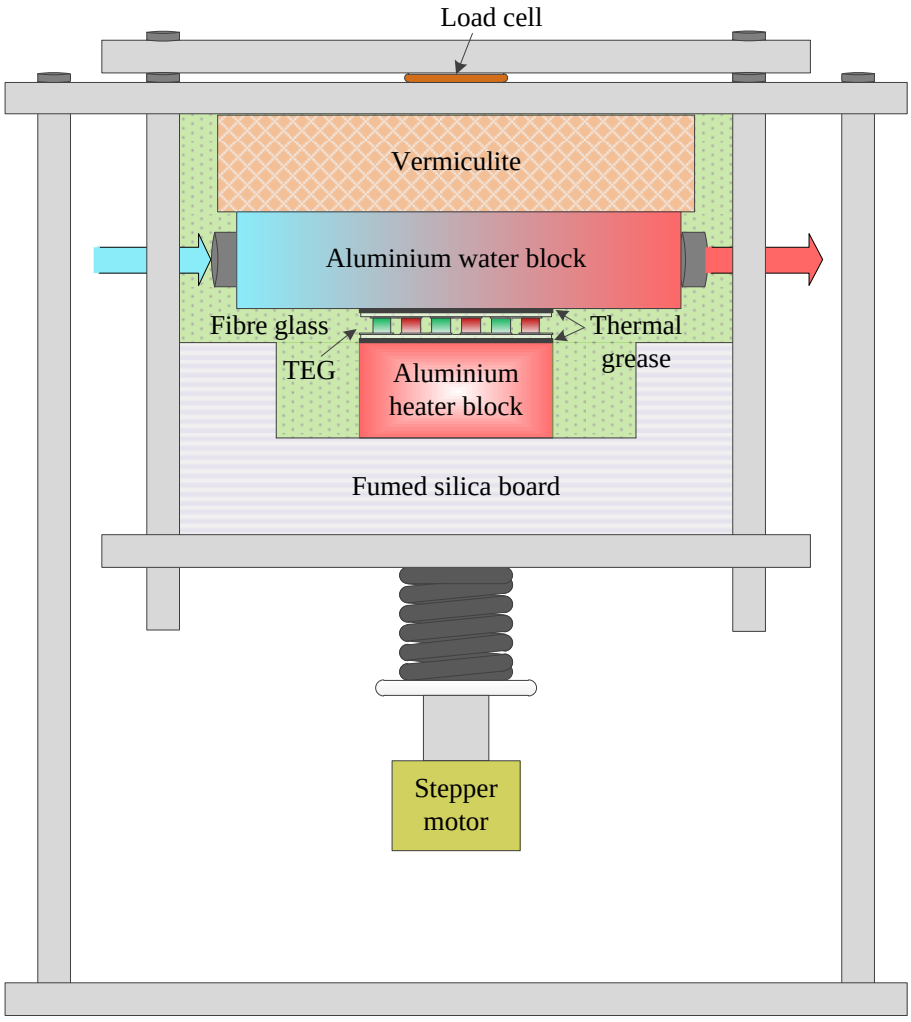

Figure 5-2 Diagram of the test setup used for TE module characterization.

The hot side is composed of an aluminium heater block with size 40mm x 40mm x 25mm and thermal conductivity of κ_{Al} = 205W/mK. The block is heated using a silicon nitride igniter (Glo120-400-370URF) rated at 500W(550°C) and connected to a 750W DC power supply unit (Agilent N5750A). The area of the heater was chosen to match that of the TE module used for the tests. A larger area heater compared to the module would increase losses in the system and a smaller heater would not provide temperature uniformity across the TEG. The temperature at the interface between the heater and any object (*e.g.* TE module) is sensed by two symmetric thermocouples inserted through the aluminium block and positioned as in

Figure 5-3. This way, the temperature distribution across the hot side of the TE module could be evaluated[10]. Because the temperature of the heater may influence the temperature reading at the interface between the heater and the module, the diameter of the hole (3mm) was made larger than that of the thermocouple (1mm). Therefore, the thermocouple did not touch the aluminium block, but only the interfaced object.

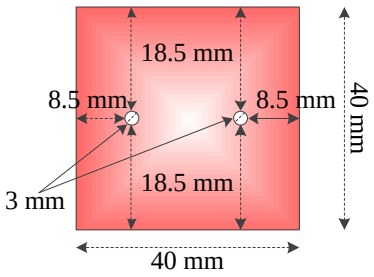

Figure 5-3 Top view of the aluminium heater block and the position of the two hot side thermocouples.

An aluminium water-cooled heat sink block with size 80mm x 80mm x 25mm and thermal conductivity of κ_{Al} = 205W/mK served as the cold side. The temperature at the interface between the heat sink and the TE module was sensed by one thermocouple positioned in the middle of the block and inserted through the lateral side of the block. Similarly to the hot side, the diameter of the hole in the heat sink block was made larger than that of the thermocouple. A chiller unit (Thermal Exchange CS-10) regulated the water flow temperature to reach a value set by the user between 10°C – 25°C and it was capable of removing 1.3 kW of heat power. The water flow was measured by a flow meter and the water temperature was sensed at the entry and exit of the heat sink block. All the thermocouples used were K-type (TC Direct).

The system components were supported by a fixed mechanical structure composed of top and bottom steel plates connected by four columns (47cm height). A separate mobile structure consisting of two steel plates and two columns (32cm height) was used for the clamping mechanism. The top steel plate of the mobile structure was fixed and the bottom one was mobile. A load cell was positioned between the mobile and the stationary structured to measure the clamping pressure applied to the TEG. Below the bottom plate, a 179 N/mm spring was placed, connected to a stepper-motor. The mobile plate that holds the heater and the TE device is brought

[10] During the tests, the temperature difference between the two hot side thermocouple readings was <1.2 °C. All calculations were made with the hot side temperature as the average temperature between the two hot side temperature measurements.

towards the heat sink by the stepper motor. This mobile structure is able to regulate the clamping pressure to a value set by user but it can also automatically compensate for pressure variations during tests when thermal expansion and contraction occur. The pressure feedback control was based on the load cell measurements.

5.3.2. HEAT ISOLATION

Between the hot aluminium block and the bottom mobile steel plate, a fumed silica board ($\kappa_{MSilica}$ = 0.02W/mK) was used to insulate the heater and to minimize the heat conducted through the steel columns. The fumed silica board only partially insulated the heater because initially, it was shaped for a larger copper heater block (85mm x 75mm x 30mm). Therefore, additional insulation was necessary and fibre glass (κ_{Fibre} = 0.04W/mK) was used as shown in Figure 5-2. A vermiculite block with thermal conductivity of κ_{Verm} = 0.07W/mK was used to provide insulation between the water block and the top steel plate. Thermal grease (Electrolube HTC02S) with $\kappa_{Thermal\_grease}$ = 0.9W/mK was used on both sides of the module to reduce the contact thermal resistance.

5.3.3. ELECTRICAL AND CONTROL STRUCTURES

The thermocouples, the load cell and the flow meter were connected to a data logger unit (Agilent 34972A). The module was connected to an electronic load (Agilent N3300A) and the heater was controlled by a DC power supply unit. All instruments were connected to a computer either through a general-purpose interface bus (GPIB) or a universal serial bus (USB). The instruments were controlled by a VEE Pro (Agilent) software program and the measurements were automatically recorded to a Microsoft Excel sheet.

The test rig is able to accommodate both constant heat and constant temperature operating conditions. To achieve constant heat, the VEE Pro program needs as feedback the heater power readings to maintain it to the value set by the user. On the other hand, the constant temperature operation is fulfilled based on feedback temperature measurements of the hot and cold sides of the module. In both cases, a PI control was used to regulate the heater power or the temperature gradient across the module. The flow diagram and description of the constant temperature Agilent VEE Pro control program can be found in (83). The constant heat program will be described in more detail in 5.5.

5.4. HEAT LOSSES CHARACTERIZATION

In every TEG system there exist heat losses, no matter how it is insulated. This means that not all the heat provided by the heater block is transferred through the

TEG, because a part of it is lost to the ambient. To minimize the heat loss to ambient, thermal insulating materials can be used around the TEG system (*e.g.* fibre glass, vermiculite). Even so, there still remain losses in the system. To ensure a constant heat through a TEG, these residual heat losses need to be known and compensated for by the heater. The amount of heat lost varies in a non-linear way with the difference in temperature between the heater and the external boundary of the heater system. The apparatus described in Figure 5-2 was modified to perform the characterization of losses as shown in Figure 5-4.

The TE module was replaced by a 40mm x 40mm x 25mm vermiculite block. Two thermocouples were placed on the hot side and one thermocouple was placed on the cold side of the vermiculite block, at the interfaces with the heater and heat sink respectively, to provide measurements of these temperatures. Using knowledge of the thermal conductivity of the vermiculite, the heat conducted from the heater to the heat sink through the vermiculite was calculated using (5-1). The system heat loss Q_{loss} was characterized as the difference between the heater power and the heat flow through the vermiculite block.

$$Q_{loss} = P_{heater} - Q_{vermiculite} = P_{heater} - \kappa_{Verm} A_{Verm} \frac{T_h - T_c}{l_{Verm}} \qquad (5\text{-}1)$$

Where κ_{Verm} = 0.07W/mK, the thermal conductivity of the vermiculite; A_{Verm} = 0.0016m^2, the area of the vermiculite block; l_{Verm} = 0.025m, the height of the vermiculite block; T_h is the temperature measured between the vermiculite block and heater; and T_c is the temperature measured between the vermiculite and water block.

The losses were first characterized for a heater input power range of 2W to 10W with 2W increment. The upper limit for the heater power was set to 10W because the equivalent heater temperature was recorded as 240°C. The heat loss characterization was performed in the temperature range corresponding to the commercial Bi_2Te_3 module chosen to be later tested. The chiller temperature $T_{chiller}$ was set to 25°C to match the ambient temperature. All measurements were recorded after the system reached thermal equilibrium for every set heater power. This condition was reached when the difference between the maximum and minimum of 50 consecutive hot side temperature measurements was <0.1°C. The temperatures at the interface between the vermiculite and the heater and heat sink were monitored to calculate the heat losses. For each set heater value from 2W to 10W, the measurements were recorded after the system reached thermal equilibrium. This test is henceforth referred to as *Test 1*. As the power to the heater increased, more heat was transferred through the vermiculite block, therefore both T_h and T_c rose as shown in Table 5-1.

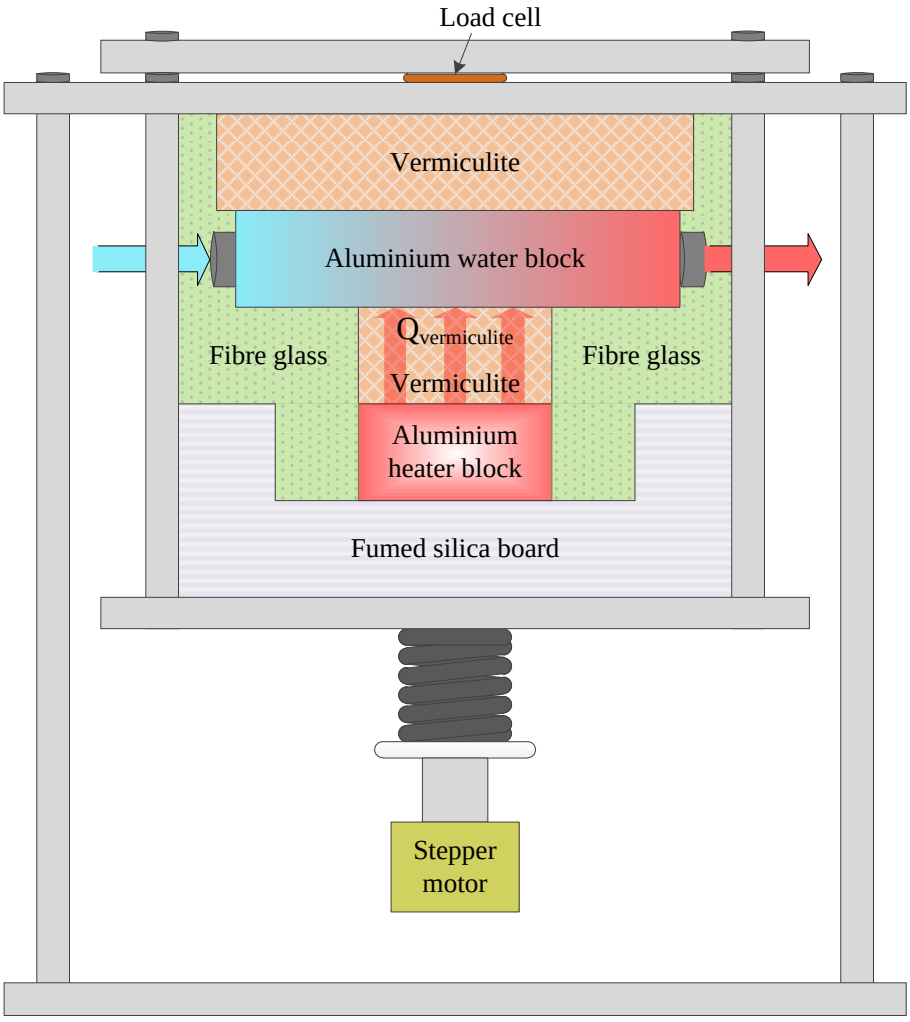

Figure 5-4 Diagram of the laboratory setup for characterization of heat losses in constant heat operation.

A second test, *Test 2*, was performed to investigate the influence of T_c on the system heat losses. For this test, the chiller temperature was set to 12°C. In this case, for a fixed power to the heater, more heat was removed by the heat sink compared to the $T_{chiller}$ = 25°C case, resulting in a slight decrease of T_h. At the same time T_c dropped significantly, equivalent to the chiller temperature change. The absolute heat loss deviation between *Test1* and *Test2* results remains constant at ~0.04W as the power to the heater is changed from 2W to 10W in steps of 2W. However, the relative error of the heat losses between the two test cases was 2.2 % at 2 W input and decreased

to 0.5% at 10W as shown in Figure 5-5. The heat loss deviation and the relative error were calculated using equation (5-2) and (5-3) respectively.

$$deviation_{Q_{loss}\_Test1,Test2} = \left| Q_{loss\_Test1} - Q_{loss\_Test2} \right| \qquad (5\text{-}2)$$

$$err_{Q_{loss}} = \frac{\left| Q_{loss\_Test1} - Q_{loss\_Test2} \right|}{Q_{loss\_Test1}} \cdot 100 \qquad (5\text{-}3)$$

If the power losses were to be analytically calculated based on the temperature difference $(T_h - T_c)$, this would give two different equations because of the significant change in the chiller temperature as shown in Figure 5-6. To compensate for heat losses in an actual TEG system with multiple equations for every T_c change would be impractical. However, it can be observed from Table 5-1 and Figure 5-7 that T_h was only slightly influenced by the change in the chiller temperature from 25 °C to 12 °C. Due to the small difference between the heat losses in the two tests and the small dependency of T_h on large changes of T_c, a heat losses equation was derived based only on T_h. The influence of T_c was considered negligible, at least for the values of T_c likely to be encountered in the laboratory. The losses were thus fitted according to T_h using a second order polynomial:

$$Q_{losses\_fit} = 3 \cdot 10^{-5} \cdot T_h^2 + 0.0357 \cdot T_h \qquad (5\text{-}4)$$

The heat loss measurements plotted against T_h are shown in Figure 5-8 and the points were mathematically fitted using equation (5-4). The use of (5-4) is necessary for operating the TEG in constant heat operation. In order to maintain a constant heat flux through the module despite any temperature changes introduced by the Peltier effect, the heater power needs to include compensation for the thermal losses associated with a change in the temperature of the whole apparatus. Equation (5-4) will be integrated in the control program that regulates the heater power by calculating the compensation required to maintain the desired constant heat flux through the TE module.

The operating temperature range of the chiller used in the experimental setup is limited to between 10°C and 25°C. It was found that over this range the relative error of the heat loss is less than 2.3%. In practical TEG applications the coolant can reach significantly higher temperatures (*e.g.* the cold side (coolant) temperature for car exhaust applications is between 50°C and 90°C, depending on which side of the radiator the coolant flow is connected to). Due to the limitation on the chiller temperature range, these higher values could not be investigated.

Table 5-1 Characterization of the heat losses for two cases of the chiller temperature (Test 1 with $T_{chiller}$ = 25°C and Test 2 with $T_{chiller}$ = 12°C).

P_{heater} (W)	**T_h (°C)**		**T_c (°C)**		**ΔT (°C)**		**Q_{loss} (W)**		**err_{Qloss} (%)**
	Test 1	***Test 2***	***Test 1***	***Test 2***	***Test 1***	***Test 2***	***Test 1***	***Test 2***	
2	71.05	67.78	24.95	12.75	46.1	55.03	1.794	1.753	2.2854
4	118.5	115.3	25.22	13.13	93.28	102.17	3.583	3.542	1.1443
6	162.9	160	25.52	13.37	137.38	146.63	5.385	5.343	0.7799
8	204.2	201.4	25.79	13.64	178.41	187.76	7.201	7.159	0.5832
10	242.8	240.6	26.07	13.93	216.73	226.67	9.031	8.985	0.5093

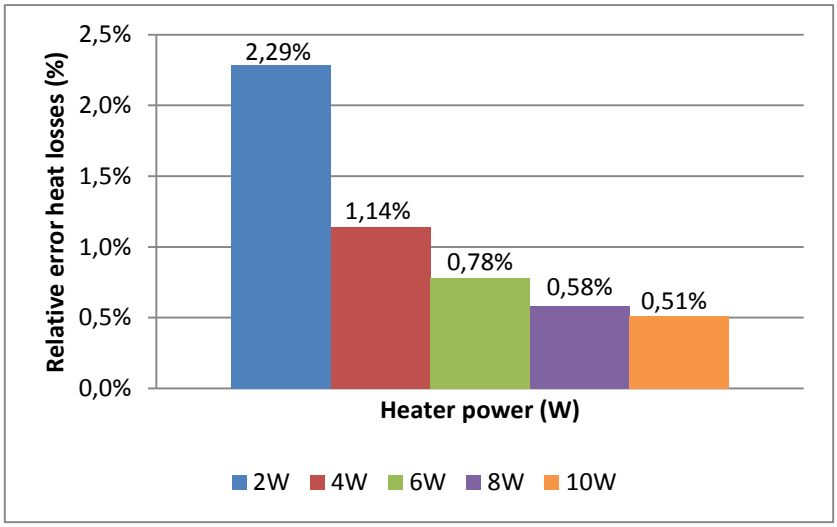

Figure 5-5 Relative error of the heat losses between the two test cases $T_{chiller}$ = 12°C and $T_{chiller}$ = 25°C for heater power range from 2W to 10W.

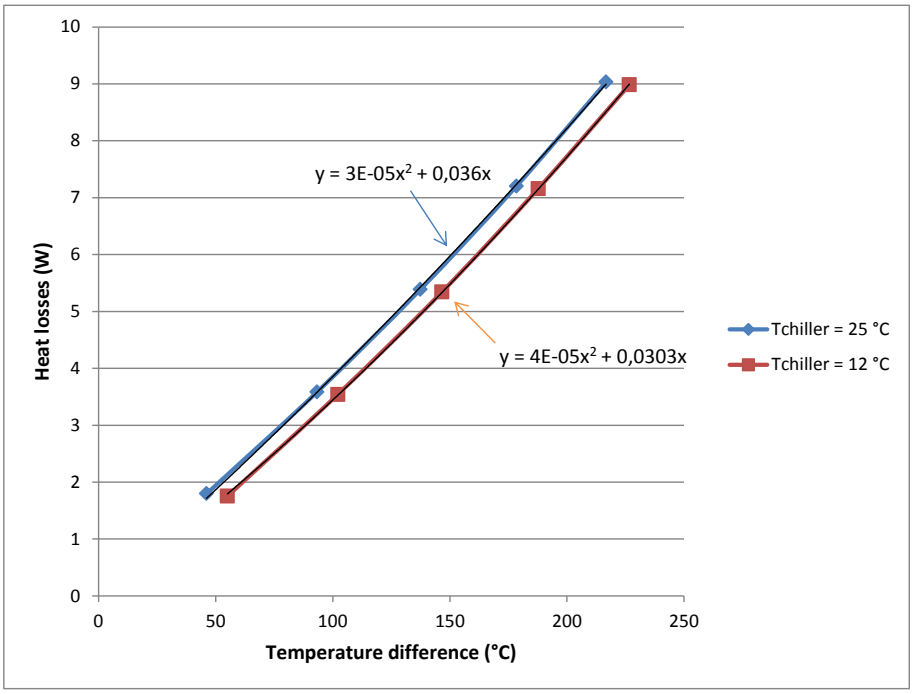

Figure 5-6 Heat losses plotted against temperature difference for the two test cases $T_{chiller}$ = 12°C and $T_{chiller}$ = 25°C.

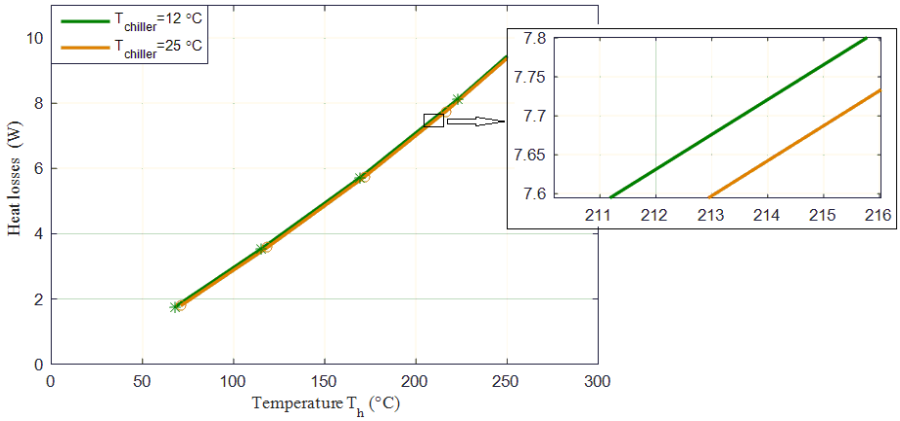

Figure 5-7 Comparison of the heat losses plotted against T_h for the two test cases $T_{chiller}$ = 12°C and $T_{chiller}$ = 25°C.

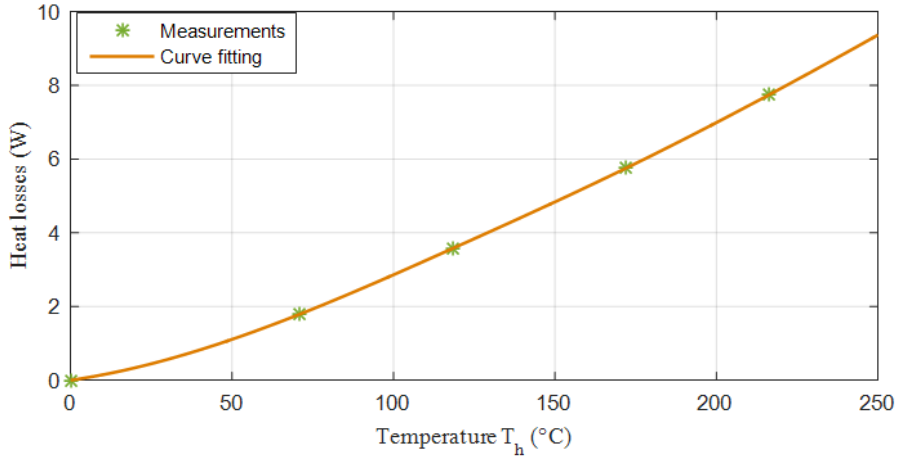

Figure 5-8 Heat losses characterization plotted against T_h with chiller temperature set to 25°C.

5.5. TEG CHARACTERIZATION IN CONSTANT HEAT OPERATION

The experimental setup from Figure 5-4 was changed to accommodate TEG parameter characterization by removing the vermiculite block and replacing it with a 40mm x 40mm TE module as shown in Figure 5-2. Two Bi_2Te_3 modules with

different pellet sizes were chosen for the experimental tests: GM250-241-10-12 (l_{pellet} = 1.2mm) and GM250-241-10-16 (l_{pellet} = 1.6mm).

At the present, the accepted method of characterizing TE modules and predicting their behaviour when integrated into an application is by obtaining their electrical and thermal characteristics with experimental setups that operate in constant temperature. Typically the module is placed between a temperature controlled heater and a water- or air-cooled heat sink. The equipment typically enables the components to be compressed at a fixed or variable set pressure for improved thermal contact. The results produced usually consist of steady-state *I-V* and *P-V* characteristics of the TEGs at several temperatures from which the full behaviour of the TE device for the application specific temperatures can be extrapolated.

Using this technique, the temperature difference across the module is kept constant while it is characterized at a specific temperature and variable load current (*i.e.* open-circuit to short-circuit conditions). This method is primarily focused on maintaining a constant temperature difference. The amount of heat input is usually not monitored or a parameter of interest although occasionally a manufacturer may provide the module's efficiency.

This TEG characterization approach is of limited utility to the system designer: it does not correlate with the actual operating conditions of the TEG in its intended application. The distinct characteristic of processes that release waste heat and are compatible with TEG integration is the limited thermal flux available. Under such conditions, only the thermal energy would remain constant and not the module temperature. For example, Pu-238 used for RTGs in space applications generates a constant 0.39 W/g of heat as the thermal source for the TE devices. The heat generation is affected by the degradation of the Pu-238 during its half-life but it is independent of the load current change in the TEG system. This feature is specific but universal to TEG applications used in waste heat recovery.

A TE module operating as a generator in constant heat is significantly influenced by the magnitude of the Peltier effect. To illustrate this effect, a constant heat characterization was performed on the two Bi_2Te_3 modules (GM250-241-10-12, GM250-241-10-16[11]) and the results are presented in Figure 5-9.

The maximum heat flux through the GM250-241-10-16 module that gives ~250°C on the hot side is ~110W and therefore it was chosen as the limit. Because the GM250-241-10-12 has lower pellet length and therefore higher thermal conductivity, the heat flux through this module was limited at 130W.

[11] European Thermodynamics Ltd.

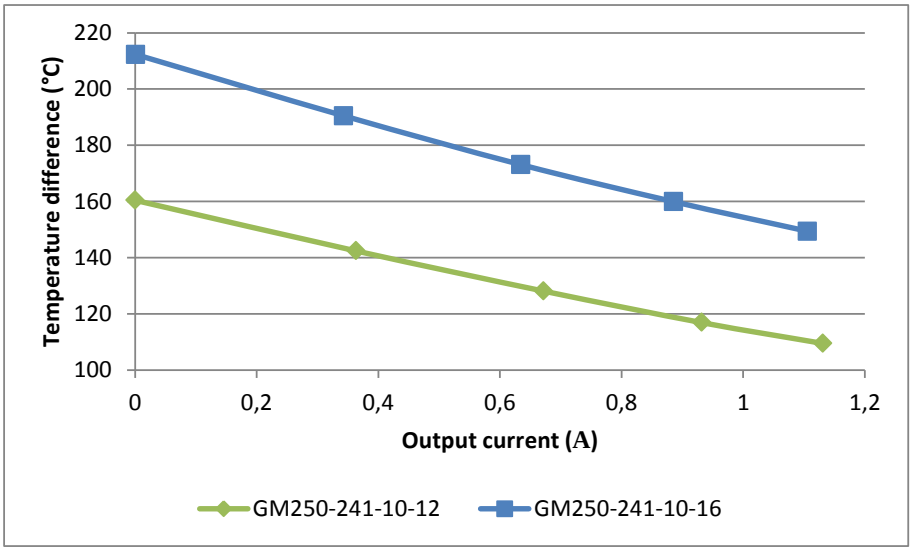

Figure 5-9 Temperature difference change from open-circuit to short-circuit test for 110W constant power to the TEG.

Both modules were first tested at 110W constant heat flow and the electrical load conditions were varied from open-circuit to short-circuit. For each load current change, the system was left to reach thermal equilibrium before the temperature measurements were recorded. In this way, the variable influence of the Peltier effect was observed.

Initially, no current was flowing through the device and the temperature gradient across the TEG was measured at 160.4°C (GM250-241-10-12) and 212.3°C (GM250-241-10-16). The load voltage was then fixed at 75%, 50% and 25% of the initial V_{OC} reading. Finally, the modules were short-circuited and the temperature difference across the devices corresponding to short-circuit condition was 109.4°C (GM250-241-10-12) and 149.4°C (GM250-241-10-16). In other words, a change from no load current to full load current caused a drop in the temperature difference across the modules of 51°C (GM250-241-10-12) and 62.9°C (GM250-241-10-16). The results clearly show the substantial influence of the load current value on the thermal efficiency of the TEG system.

To obtain the constant heat *P-V* and *I-V* characteristics of the modules, a control program was developed in Agilent VEE Pro and its flow diagram is shown in Figure 5-10.

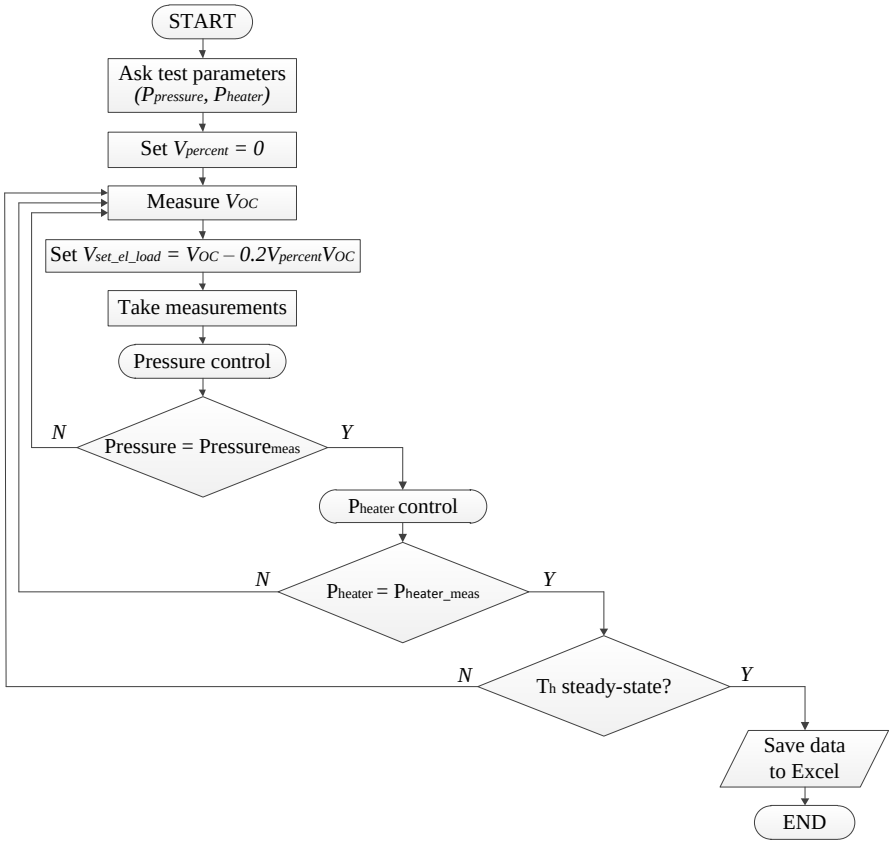

Figure 5-10 Flow diagram of the Agilent VEE Pro program to obtain the I-V and P-V characteristics in constant heat operation

At the beginning, the program asks the user to set the values of the desired clamping pressure *($P_{pressure}$)* and the heater power *(P_{heater})*. The variable that aids in setting the voltage of the electronic load $V_{percent}$ is initialized to zero. The load value is changed based on a V_{OC} measurement, the variable $V_{percent}$ and the following equation in the program:

$$V_{set\_el\_load} = V_{OC} - 0.2 \cdot V_{percent} \cdot V_{OC} \qquad (5\text{-}5)$$

The V_{OC} is measured and the voltage of the electronic load is set according to (5-5). In the first cycle, $V_{percent} = 0$ which means that $V_{set\_el\_load} = V_{OC}$ corresponding to the open-circuit constant heat test at a specific constant heat input.

After the voltage to the electronic load is set, the program takes all the measurements from the data logger, the electronic load and the power supply. The

first parameter checked by the program is the clamping pressure. The measurement is compared to the value set at the beginning of the program and regulated accordingly using a PI controller. The heater power follows, and similarly, the measured value is compared to the set one and the difference is fed to a PI controller that minimizes the error between the two values.

Afterwards, the program checks if thermal equilibrium has been reached. This was programed to happen when the difference between the maximum and minimum of 50 consecutive hot side temperature measurements is <0.1°C. When this condition is met, the corresponding measurements are recorded into the Excel sheet.

After each cycle, $V_{percent}$ is increased with 1.25 until it reaches the value 5. This means that one constant heat *I-V* characteristic will be fitted based on five measured points taken at $V_{set\_el\_load} = \{V_{OC}, 75\% V_{OC}, 50\% V_{OC}, 25\% V_{OC}, 0\}$.

All tests were performed at a clamping pressure of 1MPa. In order to assess the amount by which the module ΔT varied with the heat flux through the device from open- to short-circuit, the heat flow through the TE device was varied from 30W to 130W for GM250-241-10-12 and to 110W for GM250-241-10-16 in steps of 20W to obtain the *P-V* and *I-V* characteristics.

The thermal transient due to the Peltier effect on the temperature gradient of the system is slow (*i.e.* minutes), and hence the system was left to reach steady-state and only after equilibrium was reached were the measurements recorded. The electrical *P-V* and *I-V* characteristics obtained from the TE modules in constant heat operation are shown in Figure 5-11a+b and Figure 5-12a+b (solid lines). In order to evaluate the repeatability of the measurements, the constant heat characterization for GM250-241-10-12 was repeated and the second set of results are shown in Figure 5-11a+b with dashed lines. The variance between the results from both tests was less than 2.5%; this was judged to show that the measurement system offers acceptable precision and consistency.

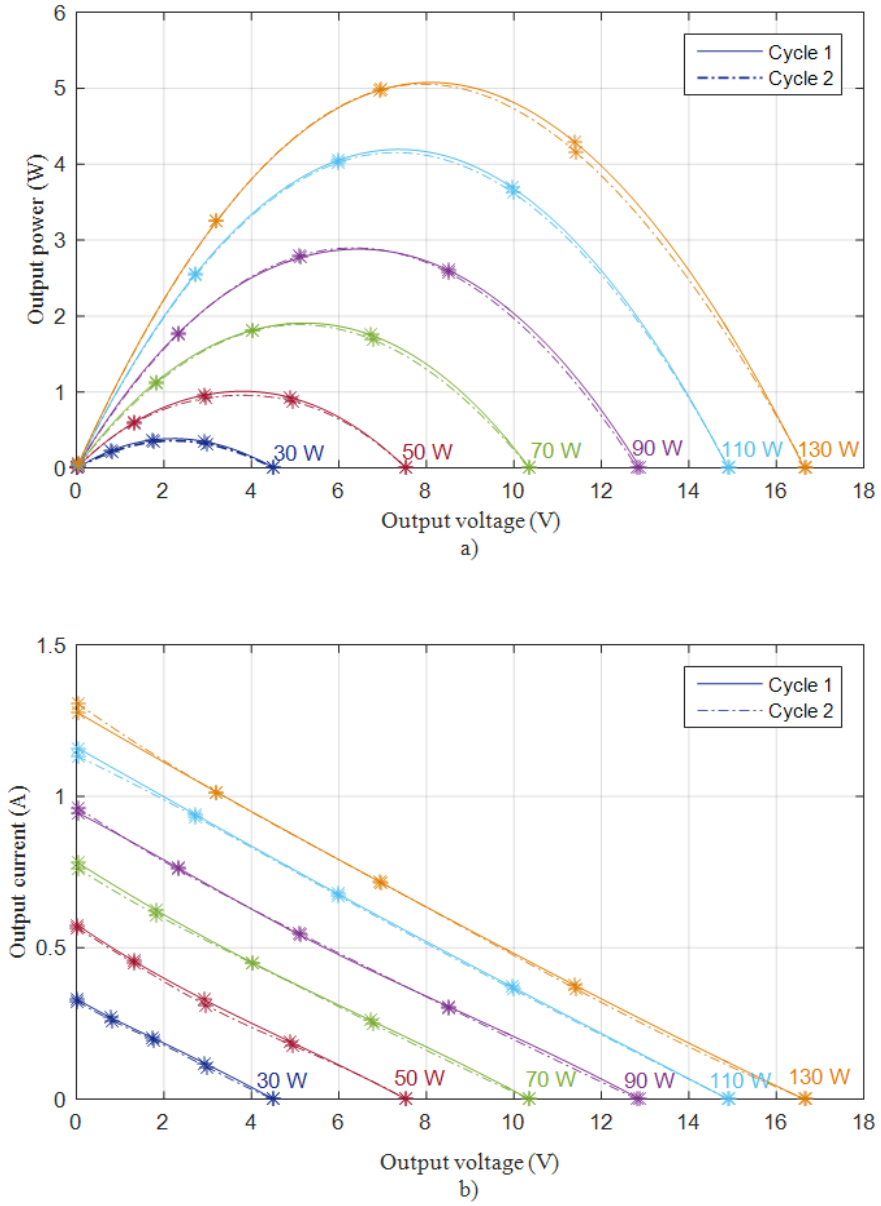

Figure 5-11 a) Output power versus output voltage and b) output current versus output voltage for GM250-241-10-12. The module was tested two times in constant heat starting at 30W to 130W with 20W increments (cycle 1 – solid line, cycle 2 – dashed line).

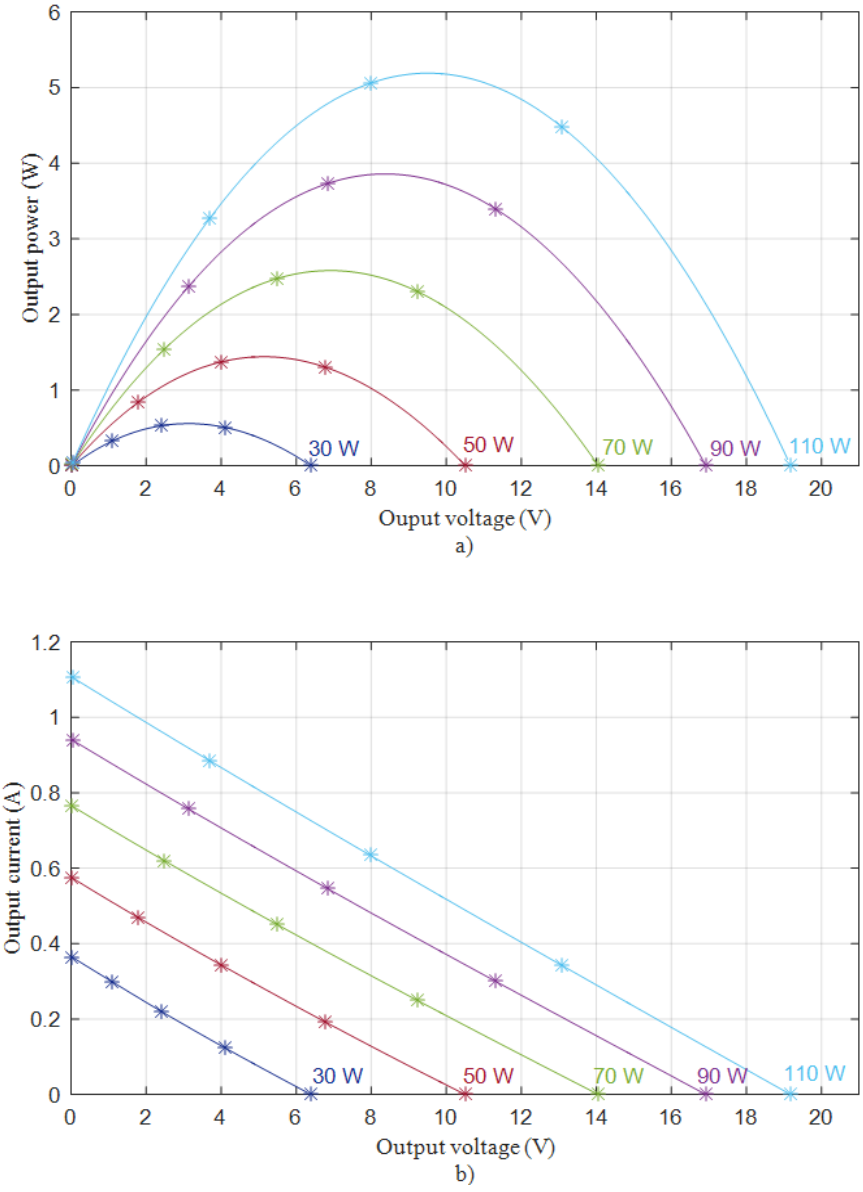

Figure 5-12 a) Output power versus output voltage and b) output current versus output voltage for GM250-241-10-16. The module was tested in constant heat starting at 30W to 110W with 20W increments.

Figure 5-13 shows the steady-state V_{OC} measurements and the ΔT variation with the heater power. In this case there is no current flowing through the module and hence no Peltier effect. For any fixed temperature difference, the V_{OC} value is similar for both modules. The small difference is cause by the likewise small difference in the Seebeck coefficient between the two modules (later shown in Figure 5-16).

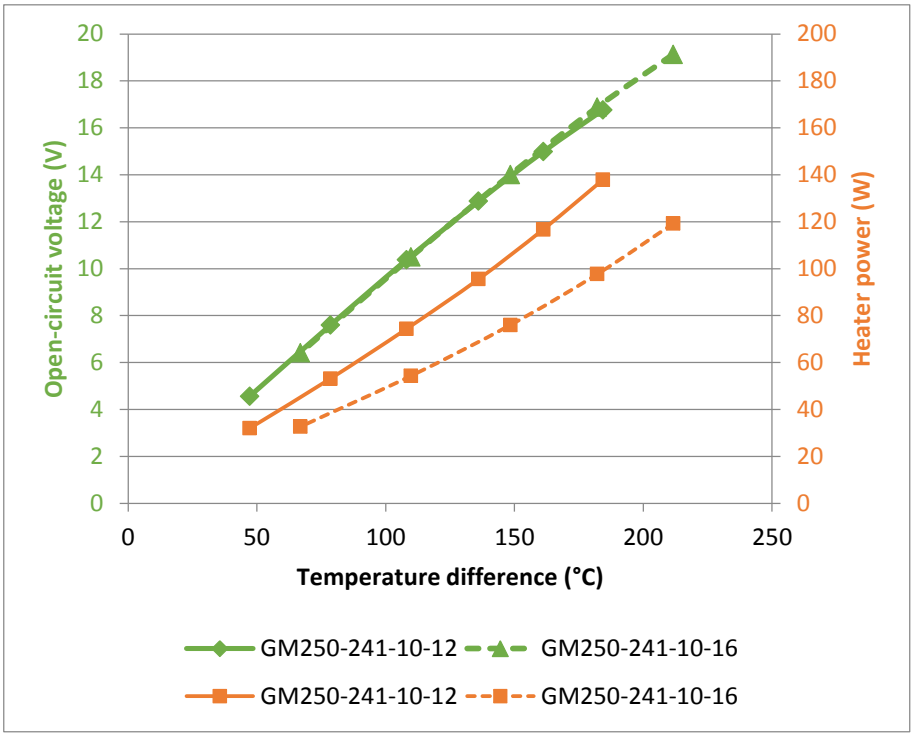

Figure 5-13 Open-circuit voltage for modules GM250-241-10-12 (solid line) and GM250-241-10-16 (dased line) in constant heat operation

The V_{OC} values were fitted based on the temperature gradient ΔT using a second order polynomial as shown in equation (5-6).

$$V_{OC\_fit} = -0.00009\Delta T^2 + 0.1096\Delta T - 0.4366 \qquad (5\text{-}6)$$

The mathematical fitting used for *(5-6)* is based on the temperature gradient range from the experimental measurements of the GM250-241-10-12 module (*i.e.* ΔT_{MIN} @ 30W= 47.22°C and ΔT_{MAX} @ 130W = 184.4°C). This allows an improved approximation of the V_{OC} values between these limits of 47.22°C and 184.4°C. However, below ΔT_{MIN}, the precision of the calculated V_{OC} decreases slightly (*e.g.*, at ΔT = 0°C, the predicted V_{OC} is -0.4366V whereas the real value is obviously 0V). Moreover, using (5-6), the differences between the measured values and those

acquired from the mathematical fitting were found to be less than 0.6% as illustrated in Figure 5-14. A second order polynomial (equation (5-7)) with zero intercept (*i.e.* $\Delta T = 0$°C and $V_{OC_fit} = 0$V) would results in overall larger differences between the measured and calculated V_{OC} values (Figure 5-15). Analysis of the V_{OC} values for the GM250-241-10-16 followed the same trend, therefore, equation (5-6) was used to calculate the V_{OC} values.

$$V_{OC\_fit} = -0.00006\Delta T^2 + 0.1016\Delta T \qquad (5\text{-}7)$$

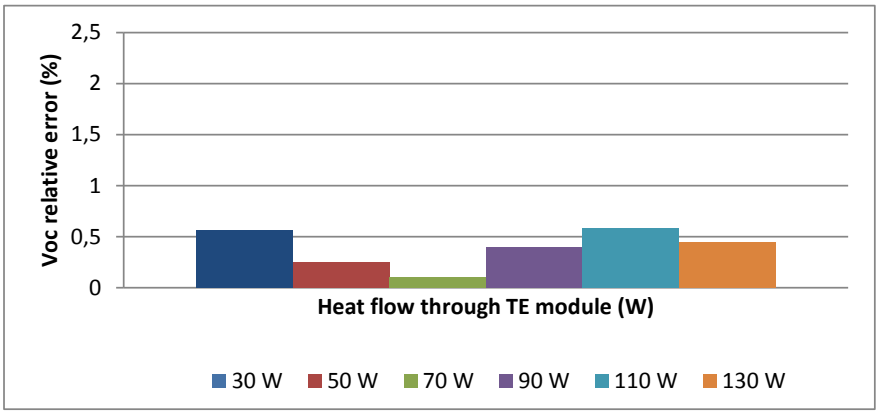

Figure 5-14 The relative error between measured V_{OC} and calculated V_{OC} based on mathematical fitting (equation (5-6)) at constant heat flow through the GM250-241-10-12 module from 30W to 130W.

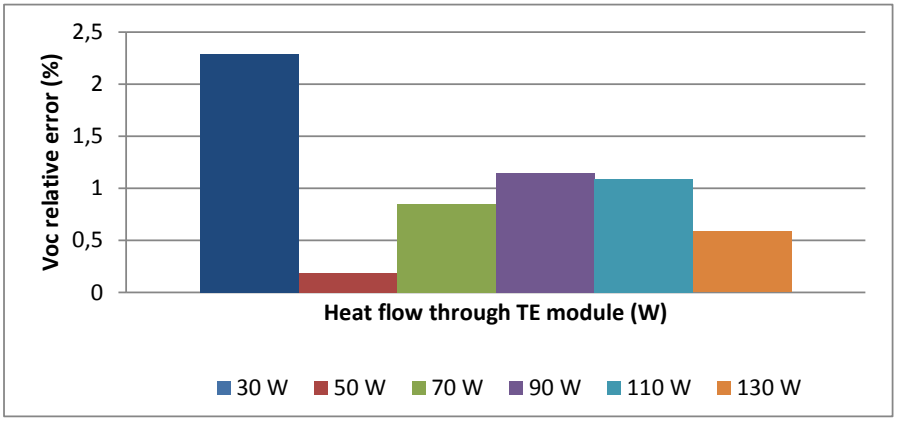

Figure 5-15 The relative error between measured V_{OC} and calculated V_{OC} based on mathematical fitting (equation (5-7)) at constant heat flow through the GM250-241-10-12 module from 30W to 130W.

Based on the constant heat measurements taken for the modules, various parameters can be determined. Using the V_{OC} readings, the composite (*p*- and *n*- combined) Seebeck coefficient variation with temperature of the modules can be estimated and is presented in Figure 5-16. The curve is typical of that for Bi_2Te_3. The variation in the internal resistance with temperature is plotted in Figure 5-17 and the thermal conductivity of the device was computed for both short-circuit and open-circuit cases shown in Figure 5-18. As expected, the module with higher pellet length has a higher internal resistance but lower thermal conductivity.

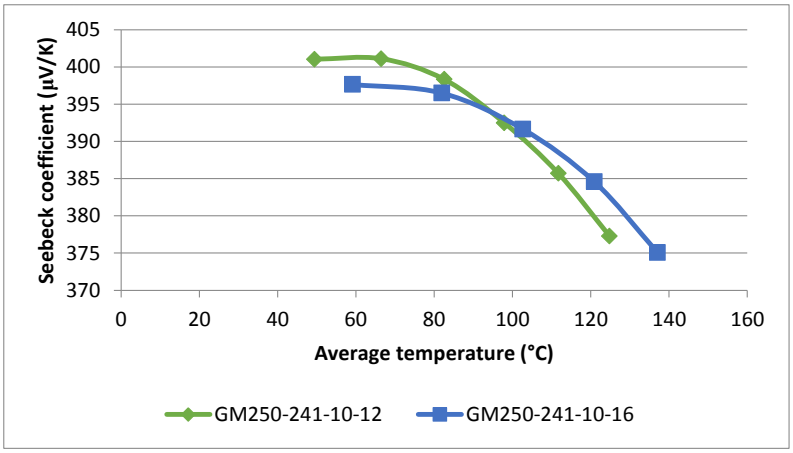

Figure 5-16 The Seebeck coefficient of the TE modules GM250-241-10-12 and GM250-241-10-16.

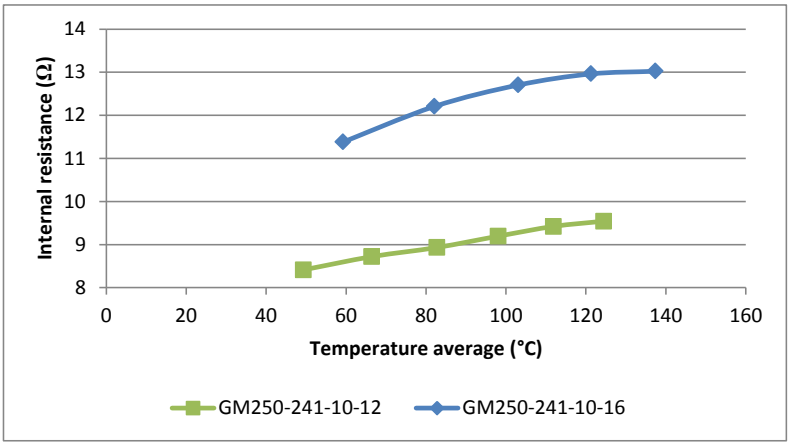

Figure 5-17 The internal resistance of the TE modules GM250-241-10-12 and GM250-241-10-16 in constant heat operation.

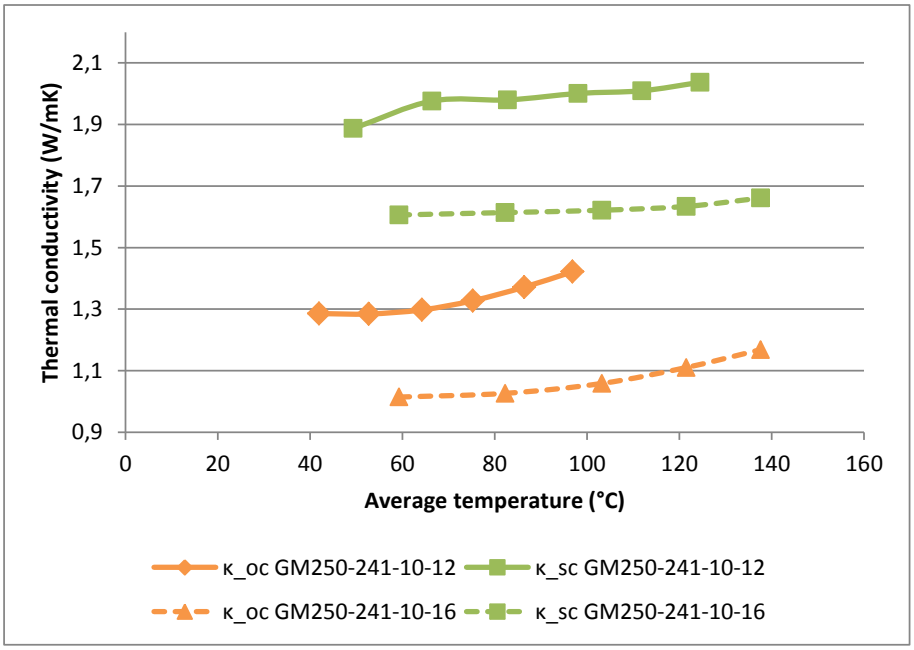

Figure 5-18 Thermal conductivity of the GM250-241-10-12 and GM250-241-10-16 modules for open- and short-circuit conditions and constant heat operation.

The experimentally obtained values of the thermal conductivity in open- and short circuit are presented in Table 5-2 for GM250-241-10-12 and Table 5-3 for GM250-241-10-16.

Table 5-2 The variance in the thermal conductivity at open- and short-circuit for the GM250-241-10-12.

Q_{TEG} (W)	Open-circuit			Short-circuit		
	T_{avg_oc} (°C)	T_{c_oc} (°C)	κ_{oc} (W/mK)	T_{avg_sc} (°C)	T_{c_sc} (°C)	κ_{sc} (W/mK)
30	49.28	25.95	1.285485	41.89	26	1.886792
50	66.39	27.45	1.284117	52.68	27.38	1.976187
70	82.76	28.81	1.297456	64.19	28.84	1.97975
90	98.08	30.27	1.327272	75.23	30.25	2.000811
110	111.86	31.66	1.371537	86.39	31.65	2.009527
130	124.45	33	1.421604	96.86	33	2.036772

Table 5-3 The variance in the thermal conductivity at open- and short-circuit for the GM250-241-10-16.

Q_{TEG} (W)	Open-circuit			Short-circuit		
	T_{avg_oc} (°C)	T_{c_oc} (°C)	κ_{oc} (W/mK)	T_{avg_sc} (°C)	T_{c_sc} (°C)	κ_{sc} (W/mK)
30	59.23	25.95	1.014138	47	26	1.605938
50	82.26	27.45	1.02623	62.24	27.38	1.613713
70	103.20	28.81	1.058464	77.41	28.84	1.621304
90	121.48	30.27	1.110085	92.22	30.25	1.633677
110	137.60	31.66	1.16815	106.16	31.65	1.660946

Often in TEG simulations, the thermal conductivity is considered variable with the average temperature and the measurements are taken from a constant temperature test. Table 5-2 and Table 5-3 present experimental values for the thermal conductivity in both open- and short-circuit cases at various heat flow values for two Bi_2Te_3 with different pellet size. These values can be used to extrapolate more accurate value of the thermal conductivity for any test-case simulations. The *I-V* and *P-V* characteristics of a TE device along with experimental measurements of the Seebeck coefficient, internal resistance and thermal conductivity provide essential information to system designers on the performance of a TE device integrated into applications.

5.6. MPP IN CONSTANT HEAT OPERATION

Performing a constant temperature characterization on a TE module requires maintaining the temperature gradient across the device fixed at a specific value, independent of the load variation. Figure 5-19 shows such a characterization using the GM250-241-10-12 module at $\Delta T = 154°C$. In constant temperature conditions, the MPP is reached when the load voltage is set as half of the V_{OC} as stated by the *maximum power transfer theorem*. During such a TEG performance characterization, the heat flux through the TEG system varies as the load conditions are changing from open- to short-circuit as shown in Figure 5-20. When performing the measurements, first, the power to the heater is automatically set to 120W to maintain $\Delta T = 154°C$ in open-circuit condition. As the current through the system increases, the heater power increases as well to compensate for the additional heat pumped through the module due to the Peltier effect. At short-circuit, the heater power reaches 160W. In waste heat applications, the amount of the available heat is limited and therefore, as previously discussed, it would not change sufficiently to maintain a constant temperature gradient across the TEG module(s) in an integrated system. In order to properly investigate actual performance in a practical system, a

TE module needs to be characterized under constant heat conditions rather than the more usual constant temperature conditions.

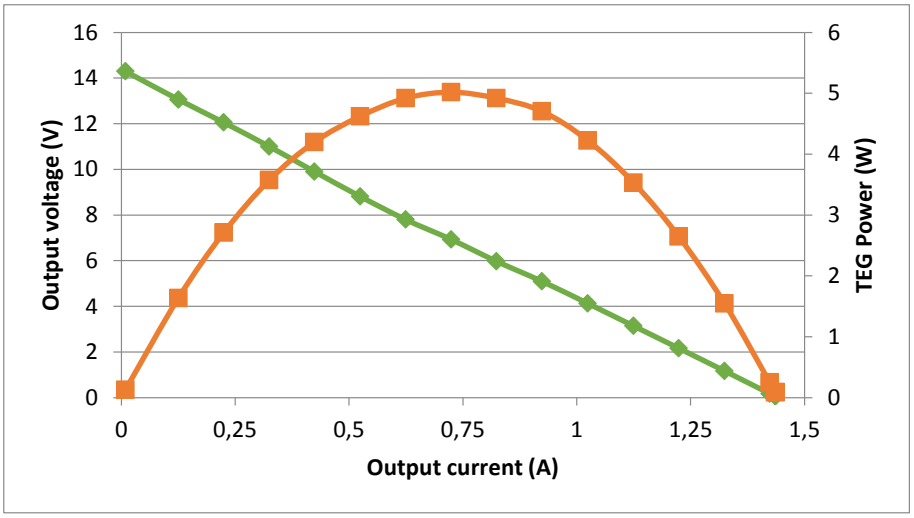

Figure 5-19 P-V and I-V curves for the GM250-241-10-12 module in constant temperature condition at ΔT = 154°C.

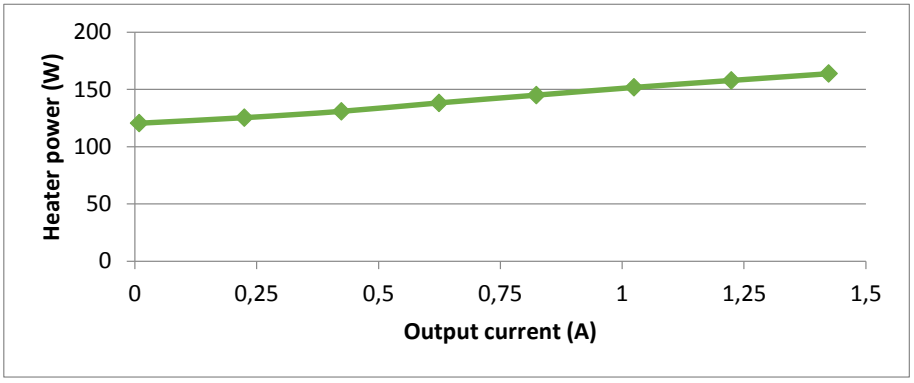

Figure 5-20 Heater power variation with output current value change for the GM250-241-10-12 module in constant temperature condition at ΔT = 154°C.

Figure 5-21 shows a) output power versus the temperature gradient at 130W constant heat and b) output current versus output voltage at constant temperature. The graphs will be used to better explain the influence of the Peltier effect on the TEG system and its MPP. The theoretical MPP according to the *maximum power transfer theorem* was first analysed. The heat flow through the TEG was maintained at 130 W and the voltage was set accordingly ($\beta_1 = V_1/V_{OC1} = 0.5$). At thermal equilibrium, the output power was recorded as $P_{MPP\_1} = 4.98W$ and the temperature

gradient across the module was $\Delta T_1 = 150.5°C$. This point is plotted on the power curve of the module in Figure 5-21a) with green. The equivalent constant temperature *I-V* characteristic of the MPP at $\Delta T_1 = 150.5°C$ is plotted in Figure 5-21b) with green. Looking at the power curve, it can be clearly seen that $P_{MPP\_1} = 4.98W$ is not the MPP. The real MPP was found at $P_{MPP\_1} = 5.08W$ and corresponding to $\Delta T_2 = 154.7°C$ (magenta in Figure 5-21). The MPP condition for 130 W constant heat coincides to $\beta_2 = V_2/V_{OC2} = 0.56$.

The main difference between the two conditions $\beta_1 = 0.5$ and $\beta_2 = 0.56$ is the value of the current flowing though the module. By continuously setting $\beta_2 = 0.56$, the value of the voltage will always be higher than in the case of $\beta_1 = 0.5$. This also means, the current value is smaller when $\beta_2 = 0.56$ compared to $\beta_1 = 0.5$. As explained by Montecucco *et. al* (48,117), when a TEG is operating at a smaller current than $I_{SC}/2$, the Peltier effect decreases and the thermal efficiency of the system increases. The overall outcome is a larger temperature gradient across the module and hence a different MPP compared to the case when $\beta_1 = 0.5$.

Similarly, the MPP of all the constant heat measurements shown in section 5.5 were analysed. Results show that the fraction between the optimum voltage and V_{OC} (β) varies with the heat flow through the module in a non-linear way as presented in Figure 5-22. At small heat flow through the module (*i.e.* 30W), $\beta = 0.61$ and as the heater power increases, β slowly decreases towards the theoretical $\beta = 0.5$. The GM250-241-10-12 module is limited at 250°C which corresponds to 150W heat ($\beta \approx 0.56$) and for this reason the device cannot be experimentally tested to investigate at which heat value β converges to 0.5.

The β values for the GM250-241-10-16 module were experimentally obtained and plotted in Figure 5-23. Figure 5-22 and Figure 5-23 show that the β values are similar for both modules and follow the same non-linear trend: higher β value at low heat flux values through the TEG (Q_{TEG}) and lower β value at large Q_{TEG}.

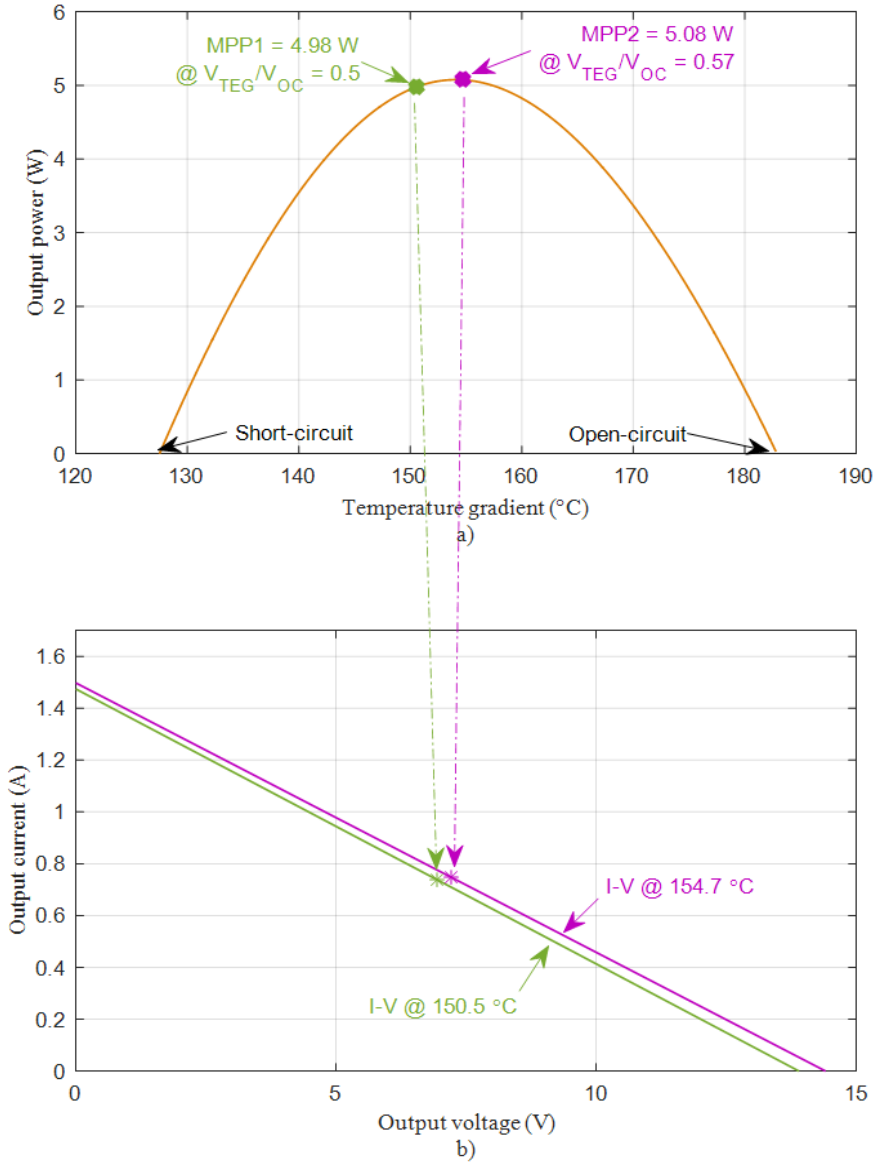

Figure 5-21a) Output power versus temperature gradient (constant heat) and b)output current versus output voltage (constant temperature). The green "theoretical" MPP1 point corresponds to the green I-V curve plotted for the condition when the output voltage is half of V_{OC}. The magenta MPP2 point corresponding to the magenta I-V curve is the real MPP point at 130W.

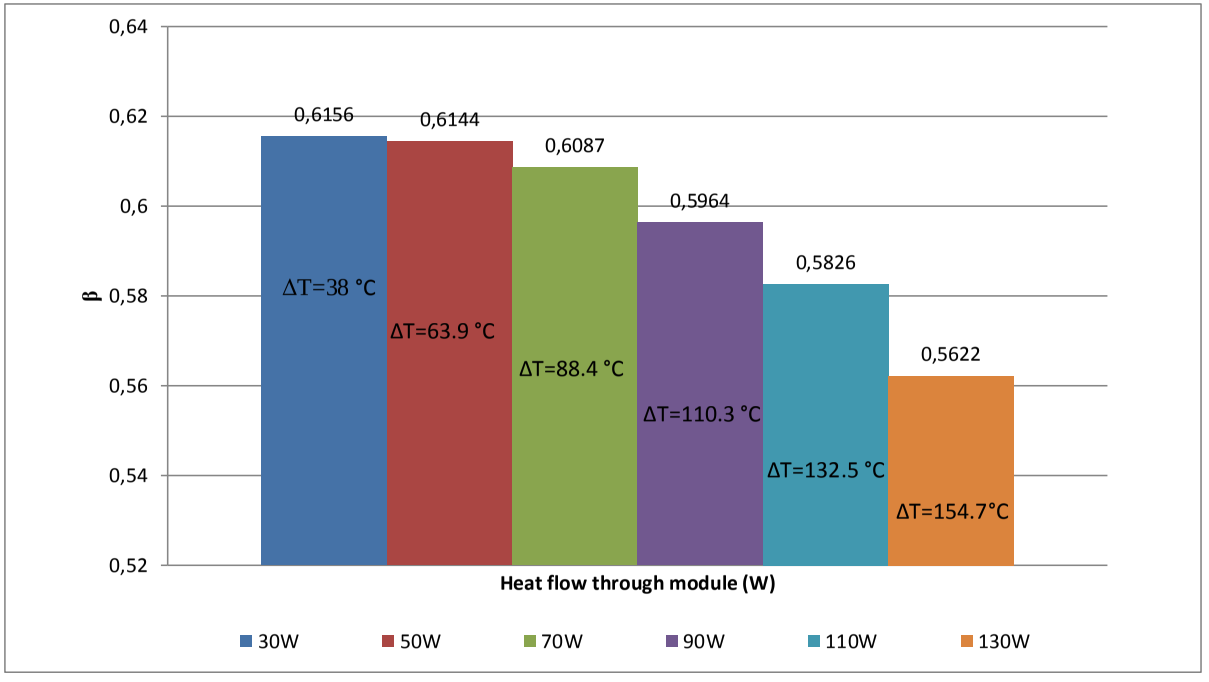

Figure 5-22 The fraction between the voltage and V_{OC} (β) that sets the conditions to achieve MPP in constant heat operation for the GM250-241-10-12 module. The β values are calculated for the heat flow range of 30W to 130W. Each bar displays the corresponding temperature gradient across the module at thermal equilibrium.

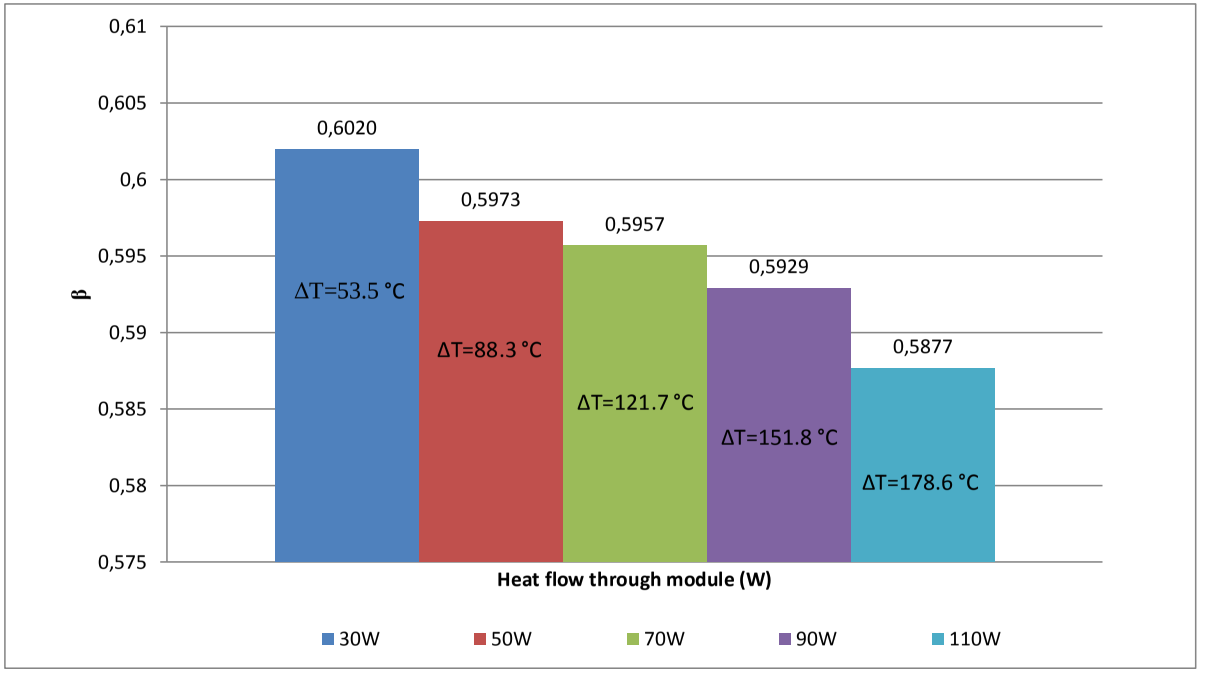

Figure 5-23 The fraction between the voltage and V_{OC} (β) that sets the conditions to achieve MPP in constant heat operation for the GM250-241-10-16 module. The β values are calculated for the heat flow range of 30W to 110W. Each bar displays the corresponding temperature gradient across the module at thermal equilibrium.

Figure 5-24 shows the a) *I-V*, b) *P-V* and c) *ΔT-V* curves obtained at 130W constant heat through the GM250-241-10-12 module. MPPT control algorithms in TEG systems such as *fractional* V_{OC} repeatedly measure the open-circuit voltage and set the optimum voltage at $\beta_1 = 0.5$ as being the optimal operating condition for the TEG. Looking at Figure 5-24a), "Point 1" corresponds to the $V_{OC} = 16.67V$ measurement at $\Delta T = 182.89°C$. The *fractional* V_{OC} method would first set the voltage to $V_{set} = 8.335$ V, *i.e.* half of V_{OC}. At the same time, current will start flowing through the module and the Peltier effect would slowly cause a temperature gradient drop across the device. The MPPT would continue to set the voltage as half of the V_{OC}, but because the temperature gradient is decreasing, the instantaneous V_{OC} will follow the same trend. "Point 2" is equivalent to the voltage ($V_{set} = 6.95V$) set by the MPPT when the system reaches thermal equilibrium which gives $P_{MPP} = 4.98W$. "Point 3" is the instantaneous V_{OC} reading of the set voltage from "Point 2".

As previously shown, using only the voltage condition of the *maximum power transfer theorem* is not sufficient to reach the optimum operating point of a TEG system. Starting from the same "Point 1" and repeatedly setting the voltage as $V_{set} = 0.56V_{OC}$, the steady-state "Point 4" would give the actual optimum power $P_{MPP} = 5.08W$ that the TE device can generate. "Point 5" is the instantaneous V_{OC} reading corresponding to "Point 4".

Hill-climbing algorithms such as P&O or INC would oscillate around "Point 2". In a practical TEG system these control methods usually regulate the voltage at least once per second. This short time would not be sufficient for the Peltier effect to have a noticeable impact on the temperature gradient across the module and the hot- and cold side heat exchangers. Due to the iterative positive – negative oscillations every two consecutive perturbations, the small Peltier effect would be effectively cancelled out. Therefore, the hill-climbing MPPTs in TEG systems would never reach the real MPP potential *i.e.* "Point 4".

Because the theoretical MPP given by the *maximum power transfer theorem* has been taken as reference, there are presently no available MPPT algorithms that search for the real MPP in TEG systems. Development of MPPT algorithms that take into consideration the actual behaviour of the heat flow in the system (*i.e.* limited heat) are necessary to improve the power extraction from TEGs. In this chapter, it was demonstrated that in the case of 130W constant heat, setting the module at $\beta = 0.56$ instead of $\beta = 0.5$ gives a 1.91% increase in the power generated by a single TEG module.

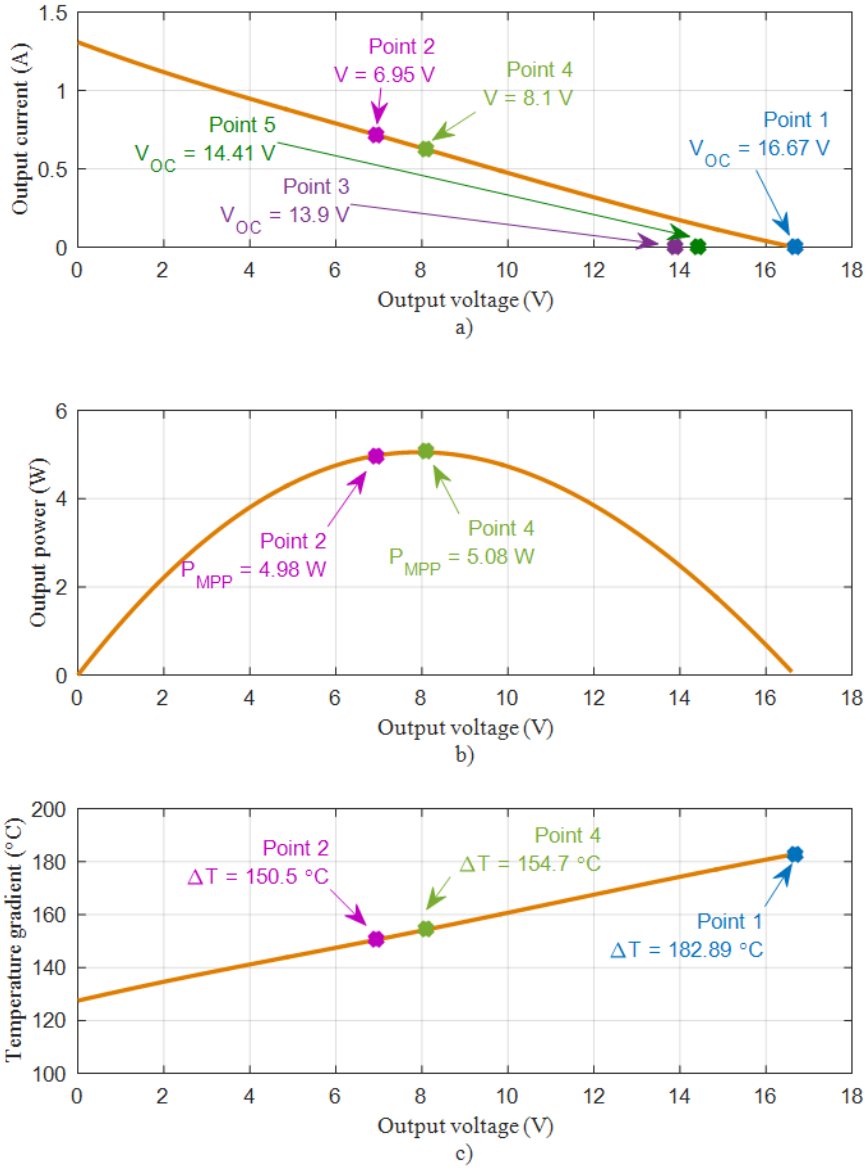

Figure 5-24 a) I-V, b) P-V and c) ΔT-V constant heat characteristics of the module that show the MPP (Point 2 - magenta) set by β = 0.5 and the MPP (Point 4 - green) set by β = 0.56.

The conversion efficiency of both modules operating at the real MPP (*i.e.* β values from Figure 5-22 and Figure 5-23), calculated using equation *(2-20)*, is shown in Figure 5-25.

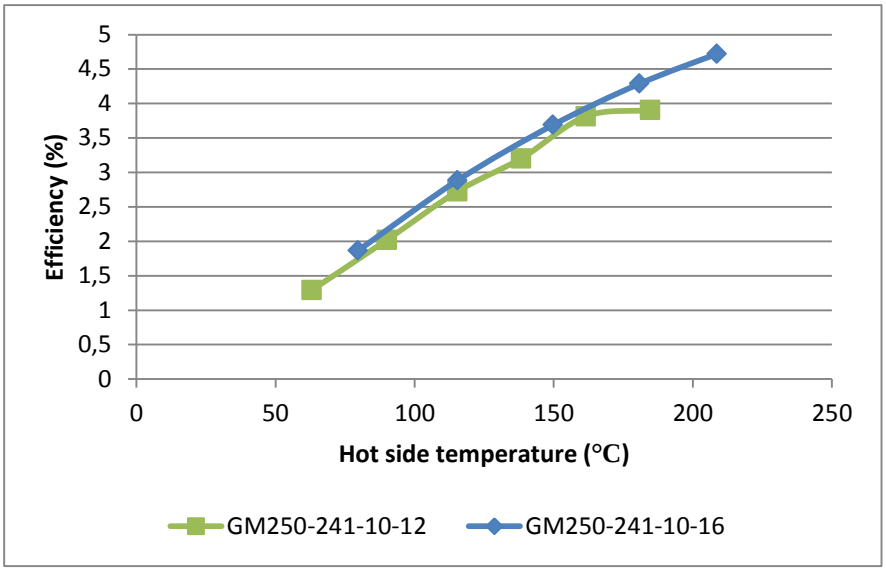

Figure 5-25 Conversion efficiency of the GM250-241-10-12 and GM250-241-1016 modules.

Table 5-4 contains, for 30W to 130W constant heat flow (GM250-241-10-12) and to 110W (GM250-241-10-16), the calculated percentage of the additional power than can be generated by the TE modules if the thermal conductivity is manipulated accordingly ($\beta \neq 0.5$). Results show between 1.91% and up to 5.31% extra power can be generated by the TEGs compared to the conditions set by the *maximum power transfer theorem*.

Table 5-4 Comparison between the power generated with the conditions from the maximum power transfer theorem ($\beta = 0.5$) and the power generated using the Peltier effect to decrease the thermal conductivity of the module ($\beta \neq 0.5$) for 30W to 130W constant heat flow.

Q_{TEG} (W)	GM250-241-10-12			GM250-241-10-16		
	$P_{MPP,\beta=0.5}$ (W)	$P_{MPP,\beta\neq0.5}$ (W)	err_{PMPP} (%)	$P_{MPP,\beta=0.5}$ (W)	$P_{MPP,\beta\neq0.5}$ (W)	err_{PMPP} (%)
30	0.3699	0.3875	4.77	0.5307	0.5583	5.20
50	0.9591	1.0101	5.31	1.3736	1.4421	4.98
70	1.8138	1.9081	5.19	2.4766	2.5813	4.22
90	2.7708	2.8827	4.03	3.7312	3.8584	3.41
110	4.0509	4.1947	3.54	5.0577	5.1911	2.63
130	4.9816	5.0769	1.91	-	-	-

5.7. CONCLUSIONS

The prevailing practise of academia and industry to match TE module parameter characterization conditions to those available in practical TEG systems can lead to major discrepancies in predicting the system performance.

The standard constant temperature TEG parameter characterization completely disregards the variation of the heat flow with the load current. In this chapter it was shown that using such a characterization method, the heat flow though the TEG system increased 33% (120W to 160 W) to maintain a constant temperature across the TE device when changing from open-circuit to short-circuit conditions. If these conditions were compared to a TEG system, then that 33% increase would not naturally happen just because the current through the system changed. Instead, because of the increased current and the Peltier effect, more heat would be pumped from the hot to the cold side and therefore the temperature gradient across the module would decrease. It was shown that at 110W constant heat flow, the Peltier effect can cause a significant 51°C or 62.9°C temperature drop across a TE module (depending on the pellet length).

This chapter offers a TEG constant heat characterization that complies with the practical behaviour of TEG system (*i.e.* limited heat). To date, the standard MPPT control methods (i.e., P&O, *fractional* V_{OC} etc.) have been used in TEG systems.

However, the algorithms were designed and tested for constant temperature conditions corresponding to the *maximum power transfer theorem* and with no allowance made for the influence of the Peltier effect. It was experimentally demonstrated that the performance of the TEG systems can be improved by manipulating the Peltier effect to have a positive impact on the overall thermal efficiency of the system. Results showed between 1.91% and 5.31% system output power increase when operated at the real MPP rather than the theoretical MPP.

CHAPTER 6. MPP IN CONSTANT HEAT SYSTEMS

This chapter describes the developed hot air system with features similar to potential TEG applications and is intended to test TE modules in constant heat operation. Moreover, experimental results are shown to validate the hypothesis that the TEG system can generate more power when operated with different conditions than that predicted by the maximum power transfer theorem.

6.1. HOT GAS TEG SYSTEM

To properly asses the influence of the Peltier effect on the possible maximization of a TEG system power output, an apparatus able to reproduce the operating conditions of TEGs integrated into an application is necessary. Such a system was constructed at the University of Glasgow and is shown in Figure 6-1. The system is able to reproduce the operating conditions of a TEG application with hot air as the equivalent of the heat source.

The general concept behind the hot air system is that the heat source for the TE modules is obtained by using an inlet fan operating at a set frequency, blowing ambient air into a *heater plate* with electrical heaters attached. The air flows through the heater plate holes and the blow-though heaters attached to the plate. The role of this plate is to heat the ambient air flowing from the fan towards the TEG heat exchanger. The hot air heats the aluminium heat exchanger where the TE modules are placed. Downstream of the heat exchanger the air is exhausted to the laboratory.

6.2. MECHANICAL SIDE

The mechanical structure for the hot air flow path is formed from standard stainless steel insulated chimney sections into which are inserted a pair of circular- to square-section cone pieces that mate with an anodized aluminium heat exchanger. The TE modules are placed on this heat exchanger. The chimney sections consist of smaller inner cylinder shaped plates (175mm diameter) and larger outer plates (225mm diameter). The gap between the inner and outer plates was filled with Rockwool insulation ($\kappa_{Rockwool}$ = 0.033W/mK) to minimize the heat losses.

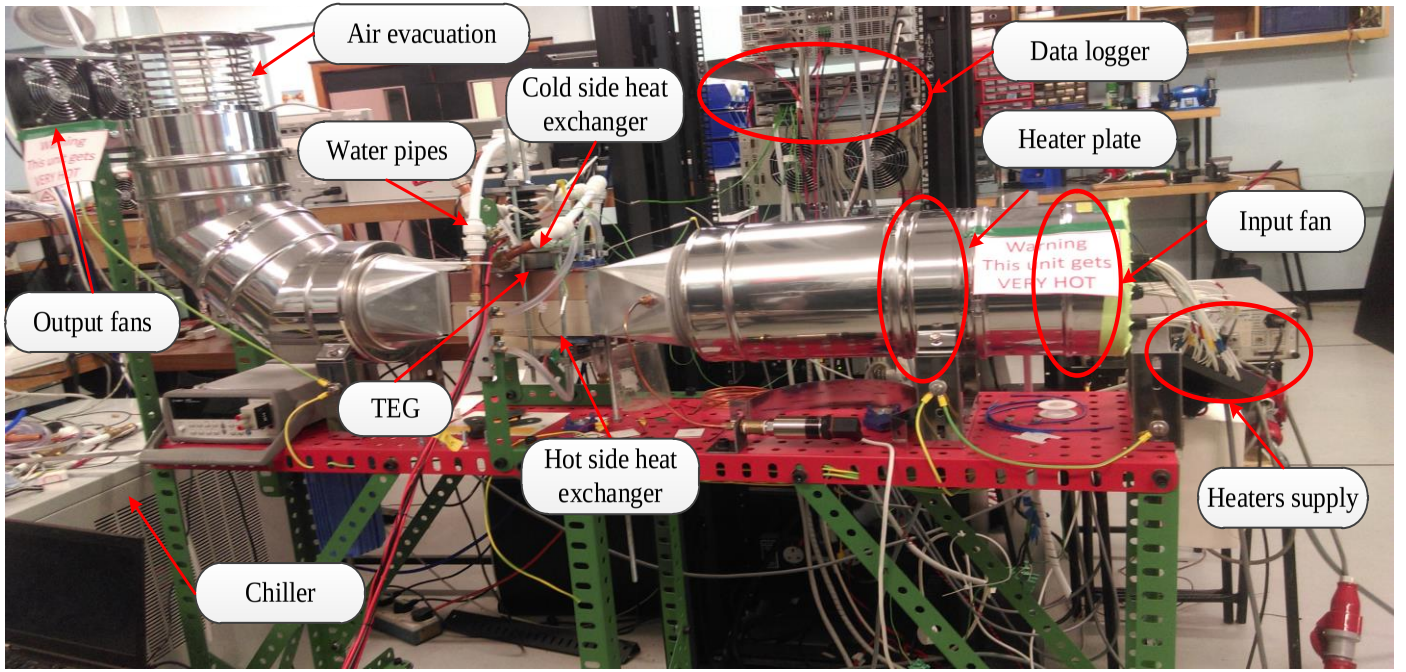

Figure 6-1 The hot air system used for measurements in constant heat operation.

The diagram of the heater side of the hot gas system is shown in Figure 6-2. A 12V PWM-controlled inlet fan (OD1238-12HB-VXC from Orion) provides the variable air flow to the system. The air is blown into a 100mm-long cylinder-shaped plenum which establishes a uniform positive pressure behind the heater plate. Air then passes through a set of 27 hollow metalized alumina igniters (PSx-6-240-B from FKK Co.,Ltd.) into a 400mm-long mixing region. Each igniter is rated at ~300W (1050°C) and are held horizontally in a 6.35mm-thick aluminium heater plate using ¼" BSP brass bushes, as shown in the photos of Figure 6-3. Initial testing of the heater unit (Figure 6-4) revealed a tendency of the heater plate to over-heat. Therefore, 31 additional holes where made in the plate, of which 27 holes are to allow air flow through the plate to prevent it from over-heating and 4 for mounting mineral-insulated stainless steel thermocouples. The thermocouples measure the temperature of the mounting plate and the temperature of the hot air positioned at 250mm, 400mm and 570mm from the heaters. The last was positioned to measure the hot air temperature at the entry of the aluminium heat exchanger. A fifth thermocouple is fitted in the incoming air stream to measure the ambient temperature. The heaters were supplied from a 415V / 3-phase star-connected supply with 9 igniters connected per phase and controlled using three commercial phase controller modules (Crydom MCPC2425C). The load on each phase is monitored using Murata digital power meters.

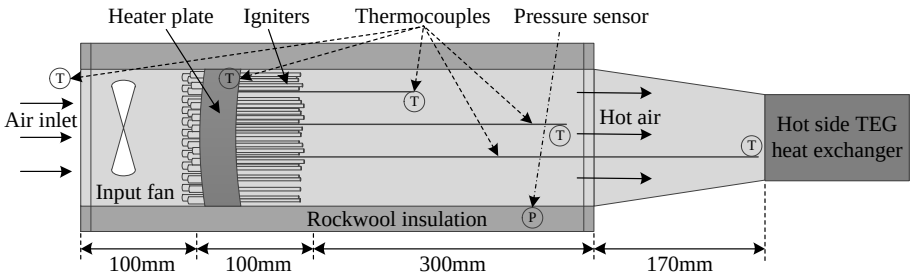

Figure 6-2 Schematic of the heater side of the hot gas system where the ambient air is heated.

The hot air exits from the 250mm x 120mm anodised aluminium (hot-side) heat exchanger and is exhausted through a standard chimney bird guard cowl placed after a 90° bend. Air emerging from the system is dispersed by two 12V / 120mm 4 wire PWM fans to avoid hot-spots on the ceiling above the apparatus. These fans conform to the Intel 4 wire fan specification and run continually at approx. ½ speed when the PWM control input is at 0%, ensuring there is always adequate dispersal of the hot air leaving the test rig.

The cold side heat exchanger of the TEG is composed of a 70mm x 70mm x 35mm aluminium water block with an internal labyrinth as shown in Figure 6-5.The labyrinth structure provides better water distribution and increased surface area in the heat exchanger to transfer the heat conducted through the TEG from the hot side

to the coolant. The temperature of the water entering the system is maintained at 10°C–11°C by a chiller unit (Thermal Exchange CS-45) capable of removing up to 4.3kW of heat.

a) **b)**

Figure 6-3 a)Front view and b) side view of the heater plate with blowing-air type igniters attached.

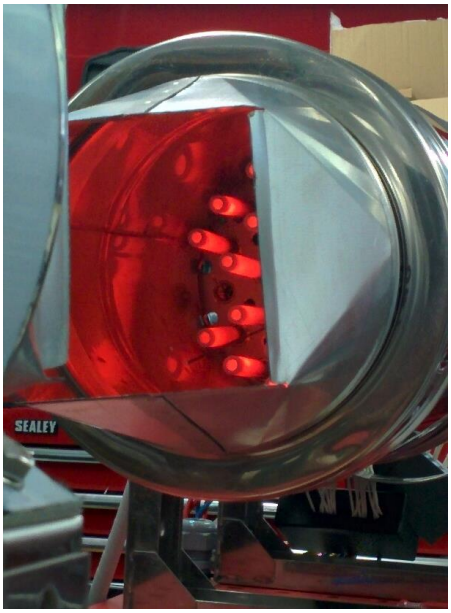

Figure 6-4 Initial testing of the heaters and the additional holes made to the heater plate from Figure 6-3 to prevent from over-heating.

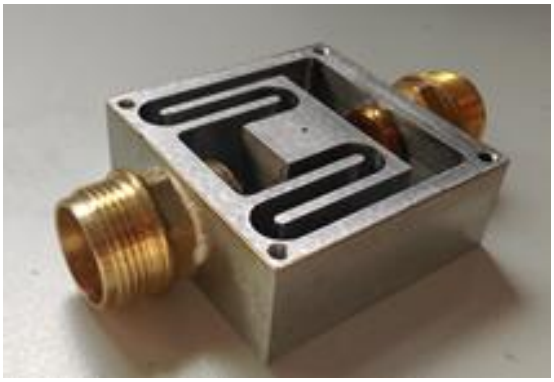

Figure 6-5 TEG cold side heat exchanger with labyrinth view for water path.

6.3. ELECTRICAL AND CONTROL SIDE

In order to control and monitor the hot gas system an electronic controller has been built to interface the Agilent 34980A data acquisition and control (DAQ) unit (Figure 6-6) to the power electronics. The unit includes the following functions:

1. Voltage to duty cycle conversion for the inlet fan. A voltage provided by the DAQ is used to modulate the duty cycle of a 25kHz TTL-compatible signal. This PWM signal in turn controls the rotation speed of the fan from 0Hz to 168Hz.
2. A watchdog timer is connected to the tacho output of the inlet fan. In the event pulses are not measured from the fan the unit assumes a fault and cuts power to the heater phase controllers. The DAQ also reads the tacho.
3. A second voltage to duty cycle conversion for the exhaust dispersal fans. These fans conform to the Intel 4 wire fan specification. The DAQ can set the PWM duty cycle and read back the fans' tacho frequencies, which are averages in the DAQ control program.
4. Phase control of each bank of 9 heaters. The DAQ sets a control voltage which modulates the half-sine conduction angle of solid state control relays. Each phase is separately switched from a common modulation signal and a Murata power meter is connected to each phase to show the power being supplied to the heaters.

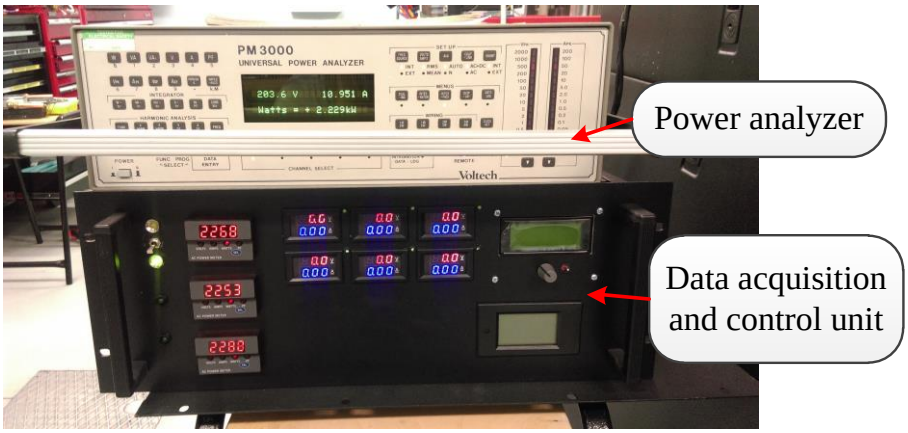

Figure 6-6 The data acquisition and control unit of the hot gas system.

There are a total of 10 K-type thermocouples placed around the hot air system to measure and monitor specific spot temperatures. All are connected to the DAQ. The thermocouples are positioned as follows:

- At the inlet of the system's input fan to measure the ambient temperature.
- Four thermocouples inside the plenum measure the temperatures of the heater plate, at 250mm, 400mm and 570mm away from the heater plate. The latter is positioned at the inlet of the TEG hot-side heat exchanger.
- Inside the metal of the hot heat exchanger immediately upstream of the area where the TE module was positioned.
- Inside the metal of the hot heat exchanger immediately downstream of the area where TE module was positioned.
- To measure the air temperature at the outlet of the hot heat exchanger.
- The inlet and outlet temperature of the coolant water for the cold side.

The outputs of the TEG device were connected to an electronic load (Agilent N3300A). Both Agilent instruments are connected through GPIB to a PC and controlled by a VEE Pro program interfaced with Microsoft Excel to log the measurements.

The inlet and dispersal fan speed is PWM controlled based on a voltage input signal set by the user via the DAQ. This means that for each voltage reference value, the fan runs at an equivalent speed. A test was performed for both the inlet and dispersal fans to acquire the correlation between the set voltage and the frequency values from the fans' tacho outputs. The fans were connected to the data logger to perform the frequency measurements. The voltage was varied starting from 0V up to 8V which was found to be equivalent to the upper limit for the fan speed. The input voltage-output frequency results for the inlet and dispersal fans are shown in Figure 6-7 and

Figure 6-8 respectively. The measured data was mathematically fitted using second order polynomials: equation *(6-1)* corresponds to the inlet fan and equation *(6-2)* to the dispersal fans. Both equations were then integrated into the VEE control program of the hot air system therefore, instead of setting the voltage reference for the fan control, the user can set the desired fan frequency.

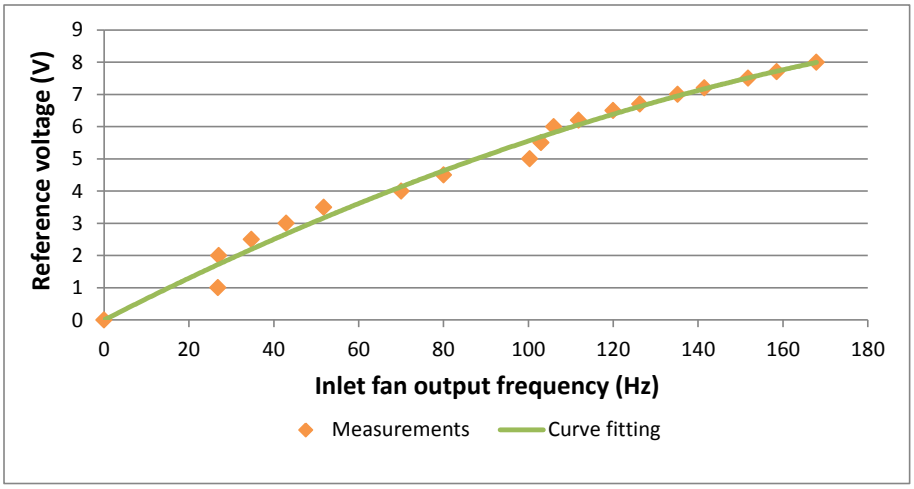

Figure 6-7 Inlet fan output frequency versus voltage reference of the PWM control (measurements and mathematical fitting).

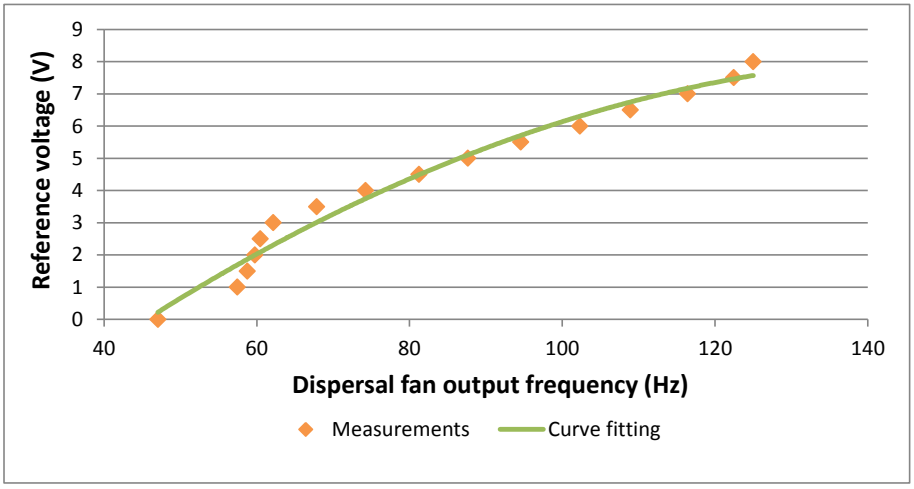

Figure 6-8 Dispersal fan output frequency versus voltage reference of the PWM control (measurements and mathematical fitting).

The dispersal fans were specifically chosen to have continuous operation. It can be seen from Figure 6-8 that even with no control signal, the fan is running at 50Hz.

The main reason of the fan choice was system protection *i.e.* to evacuate the hot air not to over-heat the heater place or the heat exchangers and to avoid hot-spots in the celling in case the system is malfunctioning.

$$V_{ref,inlet} = -0.0001 f_{fan,inlet}^2 + 0.0672 f_{fan,inlet} \quad (6\text{-}1)$$

$$V_{ref,dispersal} = -0.0007 f_{fan,dispersal}^2 + 0.2141 f_{fan,dispersal} - 8.3071 \quad (6\text{-}2)$$

The heaters were controlled using commercial microprocessor based phase angle controllers (Crydom MCPC2425C). The value of the heater power is calculated based on a control voltage set by the user. A set of tests was performed to investigate the heater power values corresponding to a control voltage range of 0V–11V for various inlet fan frequencies (20Hz to 160Hz in steps of 20Hz). During testing it was noticed that when the dispersal fans were operating at a higher speed, the evacuation of the hot air from the system was restricted due to increased backpressure at the chimney cowl. To avoid over-heating the system, the dispersal fan frequency was set to 60Hz. At lower inlet fan frequencies (*e.g.* 20Hz–40Hz), the heater plate reached ~300°C at a phase control voltage of 4V and 5V respectively. To avoid over-heating and damaging the heater plate, the control voltage range at lower input fan frequencies was limited depending on the temperature reading of the heater plate (maintained <300°C).

The power consumption of the igniters is dependent on the mains voltage value as described in the datasheet (345W@AC240V, 315W@AC230V, 295W@AC220V). Moreover, the power consumed by individual igniter may slightly vary due to manufacturing tolerances. No attempt was made to measure individual heater powers: visually observing the heater plate with the heaters at full power showed all were glowing at a similar brightness and colour – interpreted to mean the power being dissipated by each was also similar. The 3-phase power values were measured in two different ways: 1) using AC power meters (ACM20-2-AC1-R-C from Murata Power Solutions) fitted to the control unit and 2) with a universal three-phase power analyzer (PM300 from Voltech). The power measurements were logged only after the system reached thermal equilibrium *i.e.* the tolerance of the last 50 heater plate temperature readings was <1°C. For each fan frequency and control voltage settings, the heater power was recorded and the data is presented in Figure 6-9. The cosine component in the power transfer function due to the linear phase angle adjustment can be clearly seen. The maximum heater power reached was 8849W – display and 8821W power analyzer with $f_{fan,inlet}$ = 160Hz and $V_{heater,control}$ = 11V. The data set for each inlet fan frequency was mathematically fitted using second and third order polynomials, and the equations (*(6-3),(6-4)*) were integrated into the hot air system VEE control program. Therefore, the user can set the desired heater power directly and not by setting a control voltage value. The control program reads the inlet fan

setting and uses the corresponding heater power equation to calculate the equivalent voltage reference value.

$$V_{heater,control1} = a_1 \cdot P^2_{heaters,set} + a_2 \cdot P_{heaters,set} - a_3 \quad (6\text{-}3)$$

$$V_{heater,control2} = b_1 \cdot P^3_{heaters,set} + b_2 \cdot P^2_{heaters,set} + b_3 \cdot P_{heaters,set} - b_4 \quad (6\text{-}4)$$

The coefficient values corresponding to equation *(6-3)* and *(6-4)* are shown in Table 6-1and Table 6-2 respectively.

Table 6-1 Polynomial coefficient values of the second order fitting of the heater power against voltage control for inlet fan output frequency range 20Hz–100Hz.

Inlet fan output frequency (Hz)	**Polynomial coefficients**		
	a1	***a2***	***a3***
20	-0.0000002	0.0017	1.4628
40	-0.0000002	0.0017	1.3926
60	-0.0000001	0.0013	1.5655
80	-0.00000005	0.0011	1.6669
100	-0.00000001	0.0009	1.7347

Table 6-2 Polynomial coefficient values of the third order fitting of the heater power against voltage control for inlet fan output frequency range 100Hz–160Hz.

Inlet fan output frequency (Hz)	**Polynomial coefficients**			
	b1	***b2***	***b3***	***b4***
120	0.00000000001	-0.0000002	0.0013	1.5736
140	0.00000000004	-0.0000005	0.0021	1.0585
160	0.00000000003	-0.0000003	0.0018	1.2613

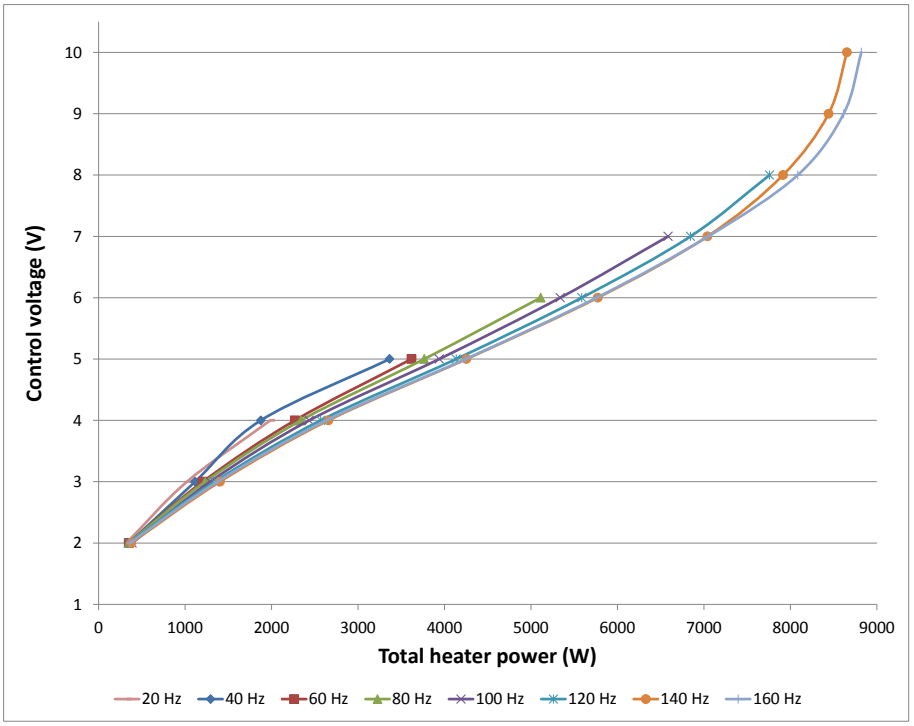

Figure 6-9 Total heater power against control voltage for the inlet fan output frequency range of 20Hz to 160Hz in steps of 20Hz.

6.4. TEST CONDITIONS

The operation of a practical TEG system at the real MPP described in Chapter 5 was further experimentally investigated using the hot gas system. As previously described in Chapter 5, the tests were performed using 40mm x 40mm modules: 1) GM250-241-10-16 rated at 7.3W electrical power output, 145W heat flow through module and 2) GM250-241-10-12 rated at 9.3W electrical power output, 185W heat flow through module. The test fixture was specifically designed to test only one TE module. Therefore, the size of the hot-side heat exchanger was chosen to be 40mm x 40mm and heated by only one igniter rated at 500W (550°C).

The hot-side heat exchanger integrated in the hot air system was designed at 250mm x 120mm x 120mm to provide enough space for multiple module integration and heated with 27 igniters each rated at 300W(1050°C). Because of the larger size of the heat exchanger in the hot air system compared to that of the test fixture described in Chapter 5, but also the different ratings and quantity of igniters used, more heat flux was designed to flow through the hot gas heat exchanger. Therefore,

the 62mm x 62mm GM250-127-28-10 module was chosen for further testing: it is rated at 28.3W electrical power output and capable of removing up to 560W of heat.

The module was placed between the aluminium heat exchanger heated by the hot gas system and a water-cooled aluminium heat sink, compressed by a 115mm (free length) spring with a rate of 135N per mm of compression to give a clamping pressure of 1MPa. The apparatus is shown in Figure 6-10.

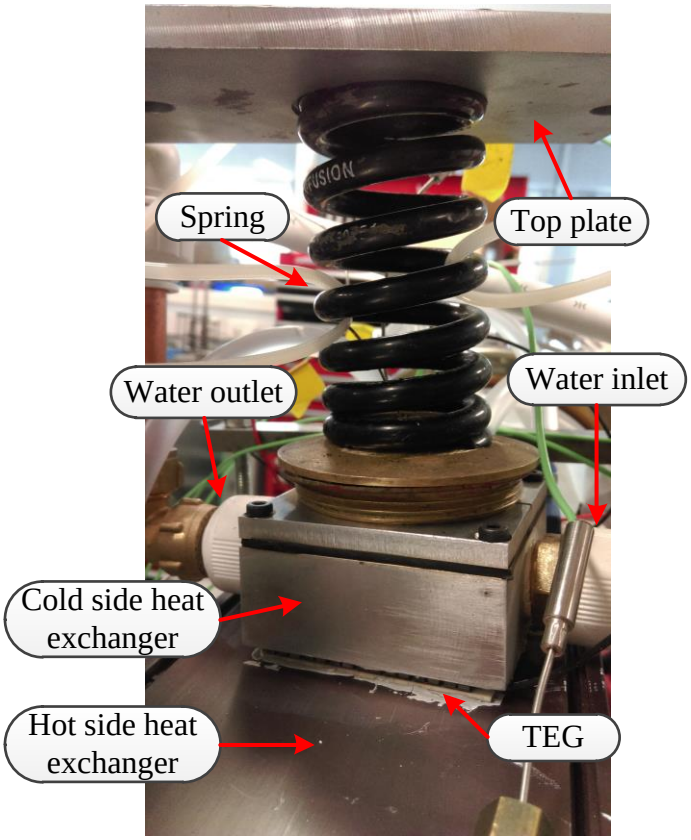

Figure 6-10 The TEG structure integrated into the hot air system's top side heat exchanger

A heat transfer paste with κ_{paste} = 10W/mK was used as thermal interface material between the module, the heat exchanger and the heat sink to improve the heat transfer. The water temperature was maintained at a nominal 10°C with a hysteresis of 0°C and +1°C. In other words, the chiller would operate until the water reached 10°C, at which point cooling would be turned off but the circulator pump would continue to run. Heat flux through the TEG would then cause the coolant to start to

warm up and when its temperature reached 11°C the chiller would restart and then cool the water back to 10°C, and so on.

To investigate the power generated by the TE device operating at different percentages of the V_{OC}, an electronic load was connected to the module (N3300A Agilent). The control of the hot gas system and the electronic load was performed using Agilent VEE. The flow diagram of the designed control program is shown in Figure 6-11.

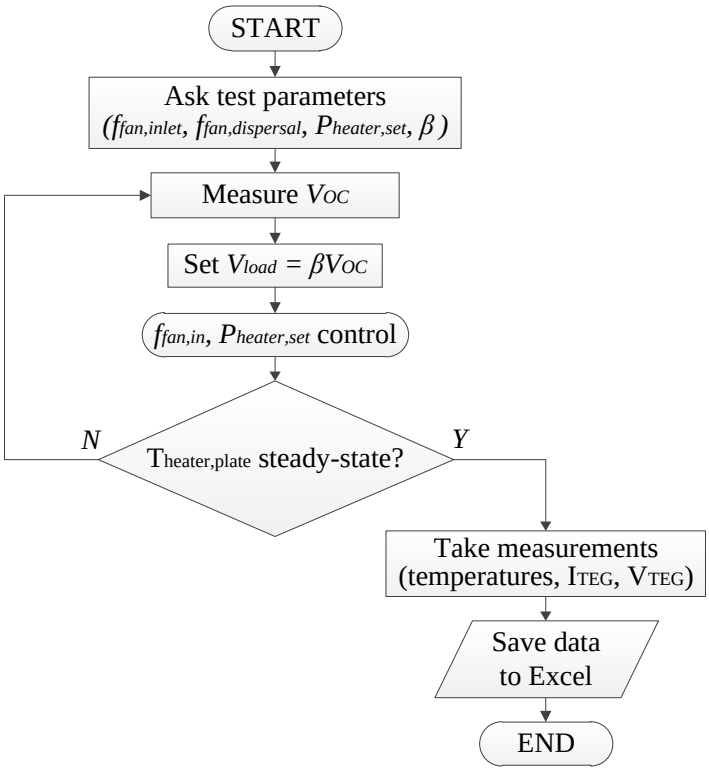

Figure 6-11 Flow diagram of the Agilent VEE Pro program that controls the hot air system

In addition to power measurement, the electronic load was also used to measure the output current and voltage. At T_h = 250°C and T_c = 30°C, the short-circuit current of the GM250-127-28-10 reaches 16.4A, as mentioned in the datasheet. Therefore, two paralleled 6 mm^2 40A wires were used to connect the module to the electronic load and their length was kept as short as possible (~2m). The current and voltage measurements were performed using 4-wire remote sensing to eliminate the effect of the voltage drop across the wires and achieve more accurate readings. The uncorrected voltage drop across the wires was 0.1V. At ΔT = 210°C and at MPP, the

GM250-127-28-10 module generated 6.37A and 24.23W. This means that 0.637W were lost in the wires that connect the module to the electronic load.

At programme initiation the Agilent VEE control program asks the user to set the desired inlet and dispersal fan frequencies ($f_{fan,inlet}$, $f_{fan,dispersal}$), the total power to the heaters (P_{heater}) and the β value, where β is the fraction of the open circuit voltage in the range $0 \leq \beta \leq 1$. Once running, the programme repeatedly measures the V_{OC} value, sets the operating voltage according to *(6-5)* and sends the voltage references for the fans and heaters which are calculated as explained in section 6.3. Thermal equilibrium in the heater is defined to be when the temperature of the heater plate reaches steady-state. After this, the TEG voltage and current are measured and the results are logged into an Excel sheet.

$$V_{set} = \beta \cdot V_{OC} \qquad (6\text{-}5)$$

6.5. EXPERIMENTAL VALIDATION OF THE REAL MPP IN TEG SYSTEMS

The tests carried on the hot gas system aim to evaluate the TE module power generation and the temperature variations of the hot-side heat exchanger by changing the value of β.

For the initial test, the main fan frequency was set to 80Hz to avoid over-heating the aluminium plate that holds the heaters and, at the same time, to reach ~250°C on the TEG heat exchanger. To meet these conditions, the corresponding total power to the heaters was set to 6.7kW. The measured total power to the heaters during the experiments was 6.695W±40W. The heaters present a low cold resistance at start-up (44.64Ω@AC240V) and to avoid large in-rush currents, the total power to the heaters was gradually increased to 6.7kW. The equivalent steady-state temperature of the heat exchanger (*i.e.*~230°C) was reached with the TEG open-circuited. Thermal equilibrium was considered reached when the difference between the maximum and the minimum of the previous 50 measurements was below 2°C.

The range of β was set between 0.5 and 0.6 with steps of 0.01. Afterwards, two additional TEG output power points were acquired for $\beta = 0.45$ and $\beta = 0.65$. The hot gas system temperature readings and the TEG output voltage and current measurements were acquired every 5s. The experiment duration for each β value was 1800s and sufficient to perform the measurements with the system in thermal equilibrium.

Because of the hysteresis in water temperature control between 10°C and 11°C, this 1°C temperature variation caused an equivalent change in the power generated by

the TE module (Figure 6-12). Therefore, the value of the TEG output power for each β was averaged over 800s out of 1800s as shown in Figure 6-12. This method excluded the power transient period after the β change from the averaging process.

Taking into consideration the TEG power analysis against β from section 5.6 (Figure 5-22 and Figure 5-23) and the set operating conditions, the TEG was expected to generate at its MPP between $0.5 < \beta < 0.56$. The average output power of the GM250-127-28-10 module plotted against β values are shown in Figure 6-13 (orange line – Test I). Results show that at $\beta = 0.5$ the power generated by the module is 24.4W. However, it can be observed that this is not the point when the module is producing the maximum power and the condition is met when $\beta = 0.53$ ($P_{teg} = 24.7W$).

The results from Test I, presented in Figure 6-13 with orange colour, show a power deviation from the expected trend at $\beta = 0.54$. The test for $\beta = 0.54$ was repeated with the same input conditions (*i.e.* $f_{fan,inlet} = 80Hz$ and $P_{heater} = 6.7kW$) and even though the temperature of the hot- and cold-side heat exchangers were maintain at the same values as the first test, the average power generated by the TE module varied. The expected average power concluded from the first test results with $\beta = 0.54$ was in the range 24.62W and 24.7W. The actual average power from the first test was 24.54W and from the second test 24.37W. Up to 25°C temperature variation was observed in the mixing region and ~4°C at the inlet of the heat exchanger between the two tests. However this temperature mismatch or other changes in the ambient environment[12] could have been sufficient to cause a variation in the power generated by the TE module.

Measurement anomalies are bound to occur especially in large systems with un-controlled parameters that can be easily influenced by changing ambient environmental conditions and the hot gas system used is no exception. In the case of the hot air system, only the power to the heaters and the fan frequency can be controlled by the user. The control of these parameters is useful not only to avoid the heater plate to over-heat, but also to achieve a desired temperature on the hot-side heat exchanger and maintain it at a lower values than the maximum limit imposed by the TE device. No feedback mechanism is employed to attempt to stabilize the air temperature in the apparatus to maintain the set point.

Moreover, because the heaters are grid-connected, the input power to the heaters is only maintained in a specific range around the desired value (*i.e.* $\pm 2\% P_{heaters\_set}$) dictated by the uncontrollable connection and disconnection of loads elsewhere on the 415V circuit in the building. Nor can phase voltage imbalance be compensated for. The mass flow rate in the plenum is not presently measured by the system

[12] The two tests were carried out on different days with different ambient temperature, atmospheric pressure and humidity.

although this may be added in the future. The hot air temperature inside the system is also uncontrolled (other than by the heater power set point) and can be influenced by ambient environmental changes *e.g.* air humidity and pressure.

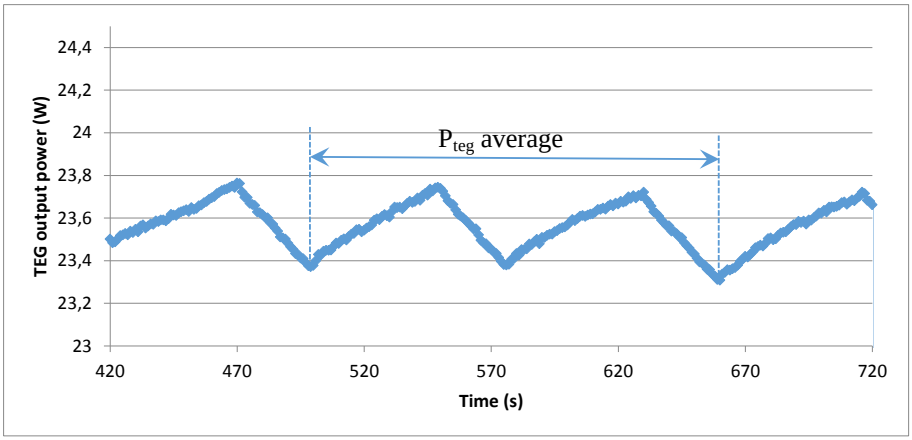

Figure 6-12 TEG output power variation caused by the hysteresis control of the chiller and the averaging process of the TEG output power.

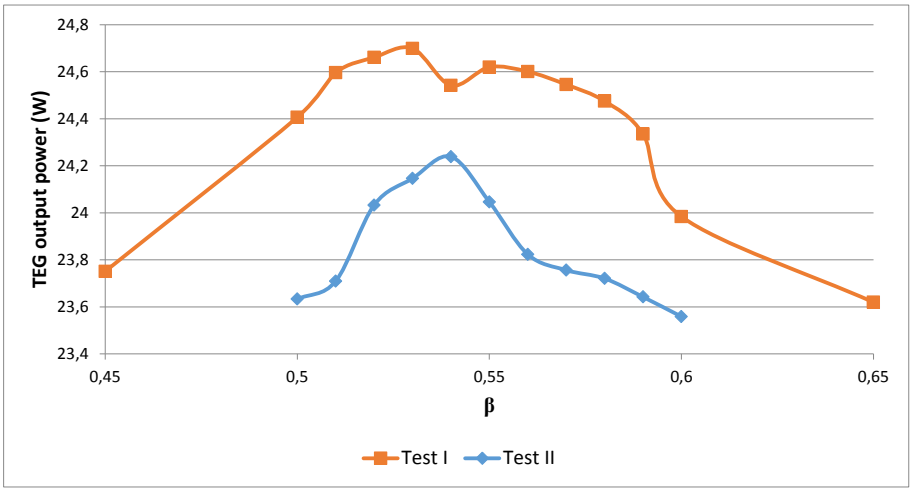

Figure 6-13 Average TEG output power against β with P_{heater} = 6.7kW, $f_{fan,inlet}$ = 80Hz and $f_{fan,dispersal}$ = 60Hz.

For example, the hot air system was operated in different days of the week with the same input conditions: $f_{fan,inlet}$ = 80Hz, $f_{fan,dispersal}$ = 60Hz and P_{set} = 6.7kW. Despite the unchanged conditions set by the user, a 70°C variation in the temperature of the hot air at the outlet of the heat exchanger was noticed. This temperature change was mainly attributed to the absolute atmospheric pressure (the effect of air density on

fan mass flow rate is well known), and the air humidity to a lesser extent. During the first test, the humidity level was below 20% and the hot gas temperature settled at 200°C whereas the next time the hot air was operated, the humidity level was 90% and the hot air reached 270°C. Therefore, the tests corresponded to a period of atmospheric "high" and "low" pressure respectively. This is the dominant effect in affecting the hot air temperature since there is a significant change in the mass flow rate through the system.

As explained in Chapter 5, when the electrical operating conditions of the module change (*i.e.* TEG current value), this means its thermal conductivity changes and therefore more or less heat is transferred through the module. A change in the amount of the heat removed from the hot heat exchanger would cause a temperature variation on the hot-side heat sink. During tests with the hot gas system, no significant variations were observed in the hot heat exchanger temperature when β was changed in steps of 0.01. In this case, the temperature stagnation is not necessarily an abnormality. The size of the heat exchanger used in the test fixture in Chapter 5 was 40mm x 40mm (for *one* module) whereas the size of the hot air heat exchanger was designed larger (250mm x 120mm) to accommodate up to 24 such modules. Moreover, only one TE device was used to remove heat from the hot air heat exchanger which is clearly not enough to cause significant changes in the temperature caused by its small thermal conductivity variation.

To further investigate the heat exchanger temperature issue a second test was performed. The input parameters remained unchanged, but before each β change, the module was maintained in open-circuit for 1800s. The TEG output power values against β are shown in Figure 6-13 with blue colour. The second set of results shows a similar trend in power variation with β compared to the results from the first test. The first test results reveal a TEG output power measurement issue at $\beta = 0.54$ and based on the initial results, the maximum power output was seen at $\beta = 0.53$. The second test showed that the actual MPP was achieved at $\beta = 0.54$ (P_{teg} = 24.24W).

Variations in the hot heat exchanger were observed in the second tests between open-circuit and at load conditions. During open-circuit the temperature varied between 231°C – 234°C whereas at load, the temperatures dropped in the range 225°C – 229°C. Accurate temperature measurements for the duration of a specific test are difficult to acquire in such large partially-controlled systems where the uncontrollable parameters can influence the readings. One reason the heat exchanger temperature at the beginning of the test was 231°C and 234°C at the end of the test was the ambient temperature in the laboratory which increased from 29°C to 34°C. Another cause for this variation can be attributed to the irregular change in the power to the heaters which are grid-connected.

In Chapter 5 (Figure 5-22 and Figure 5-23) it was shown the trend of the corresponding β values and the heat flux through the module to achieve system MPP operation. At lower heat flux values (*e.g.* 30W) the value of β for the GM250-241-10-12 module was higher (*i.e.* ~0.6) whereas for large heat flux (*e.g.* 130W) β had a value of 0.56. The maximum heat flow though the GM250-127-28-10 module stated in the datasheet is 566W and this value was achieved with the conditions set for Test I and Test II of Figure 6.12. The corresponding value of β at MPP was found to be 0.54 which validates the initial results from Figure 5-22 and Figure 5-23 taking into account the different heat flow limits of the modules (566W GM250-127-28-10, 186W GM250-241-10-12 and 145W GM250-241-10-16).

To further validate the concept of the variable β depending on the heat flux, a third test was performed with the following test conditions: $f_{fan,inlet}$ = 40Hz, $f_{fan,dispersal}$ = 60Hz and $P_{heaters}$ = 1kW. In this case, the hot heat exchanger temperature reached ~60°C and the heat flux through the module was calculated as ~150W. Because the value of β at MPP was expected to be >0.6, the TEG power was measured for the β range of 0.5 to 0.65 in steps of 0.01. For each β, the current, voltage and temperatures were measured each 5s over a period of 1800s. Between each β change, the module was open-circuited for 1800s. The results of Test III are presented in Figure 6-14. The maximum power output from the TEG is achieved when $\beta = 0.62$.

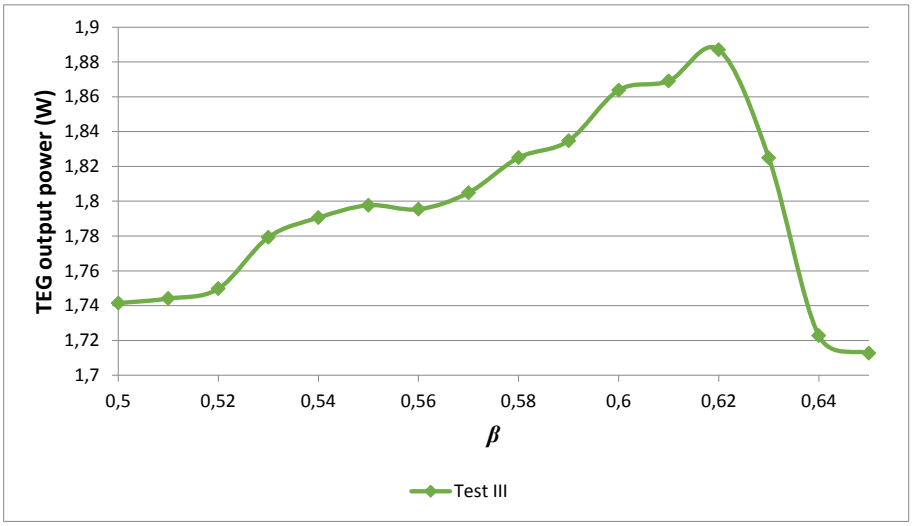

Figure 6-14 Average TEG output power against β with P_{heater} = 1kW, $f_{fan,inlet}$ = 40Hz and $f_{fan,dispersal}$ = 60Hz.

The predicted TEG output power increase with variable β over the standard conditions set by the *maximum power transfer theorem* was in the range 1.91% – 5.31% (Table 5-4). The result of Test II show a power increase of 2.56% i.e. from

23.63W at β = 0.5 to 24.24W at β = 0.54. Moreover, Test III presents an impressive 8.36% power increase from 1.74W at β = 0.5 to 1.89W at β = 0.62.

6.6. OPTIMAL RESISTANCE RATIO FOR CONSTANT HEAT OPERATION

Current studies (49,50) debate the fact that the maximum power conditions for TEG systems is in fact also when $R_{load}/R_{teg} = \sqrt{1+ZT}$. These affirmations are made based on TEG testing in constant temperature conditions. Min (121) investigated both constant temperature and constant heat cases. The following conclusions were reached: the two separate conditions hold in constant temperature and $R_{load}/R_{teg} = 1$ is valid for both maximum power and efficiency in constant heat operation.

As demonstrated in this thesis, the power generated by the TEG system can be increased by manipulating the Peltier effect and depending on the heat flux through the module, an optimal β value can be calculated. In what will follow, an attempt will be made to tie the current research affirmations regarding the maximum power condition to the data experimentally obtained throughout this thesis.

The ratio between R_{load} and R_{teg} can be calculated for the GM250-241-10-12 and GM250-241-10-16 modules based on the constant heat parametric characterization performed in Chapter 5 using the test fixture. The same can be done for the GM250-127-28-10 used on the hot gas system. The ratio can be calculated in two different ways: 1) mathematically based on the acquired β values and 2) from the measured current and voltage values.

First method implies that the optimum β value at the corresponding heat flux through the TEG is known. The measured load voltage V_{load} is the same as V_{set} and defined as:

$$V_{load} = \beta V_{OC} \tag{6-6}$$

The voltage drop across the internal resistance of the TEG V_{load} is described by the difference between the open-circuit voltage V_{OC} and V_{load}:

$$V_{teg} = V_{OC} - V_{load} \tag{6-7}$$

Inserting (6-6) into (6-7), it gives:

$$V_{teg} = (1-\beta)V_{OC} \tag{6-8}$$

From the electrical model of a TE module, it is known that the internal TEG resistance is modelled in series with the load resistance, therefore same current flows through both:

$$I = \frac{V_{teg}}{R_{teg}} = \frac{V_{load}}{R_{load}} \tag{6-9}$$

By replacing (6-6) and (6-8) into (6-9), the ratio between V_{load} and V_{teg} depending on the optimum β is established:

$$\frac{R_{load}}{R_{teg}} = \frac{\beta}{1-\beta} \tag{6-10}$$

The second method to calculate R_{load} /R_{teg} is based on the voltage and current measurements measured with the electronic load. The load resistance is first calculated by dividing the measured load voltage to the current value. The voltage drop across the internal resistance of the TEG equals the difference between V_{OC} and V_{load}. Therefore, R_{teg} is found by dividing V_{load} to the current value. The results for both methods are shown in Table 6-3 and are in good agreement among each other.

Table 6-3 Calculation of R_{load} /R_{teg} for GM250-241-10-12, GM250-241-10-16 and GM250-127-28-10 modules.

GM250-241-10-12									
Q_{tea} (W)	β	V_{load} (V)	V_{OC} (V)	I (A)	V_{tea} (V)	R_{load} (Ω)	R_{tea} (Ω)	R_{load}/R_{tea} Method 2	$\beta/(1-\beta)$ Method 1
30	0.6156	2.2	3.5739	0.1652	1.3739	13.3171	8.3168	1.6012	1.6014
50	0.6144	3.8	6.1848	0.2507	2.3848	15.1575	9.5128	1.5933	1.5933
70	0.6087	5.2	8.5434	0.3635	3.3434	14.3053	9.1978	1.5552	1.5555
90	0.5964	6.3	10.5434	0.4606	4.2641	13.6778	9.2577	1.4774	1.4777
110	0.5826	7.3	12.5292	0.5605	5.2292	13.024	9.3295	1.396	1.3957
130	0.5622	8.1	14.4085	0.6256	6.3085	12.9475	10.084	1.2839	1.2841
GM250-241-10-16									
Q_{tea} (W)	β	V_{load} (V)	V_{OC} (V)	I (A)	V_{tea} (V)	R_{load} (Ω)	R_{tea} (Ω)	R_{load}/R_{tea} Method 2	$\beta/(1-\beta)$ Method 1
30	0.602	3.1	5.1498	0.1801	2.0498	17.2126	11.3819	1.5122	1.5125
50	0.5973	5.1	8.5387	0.2828	3.4387	18.0339	12.1595	1.4831	1.4832
70	0.5957	6.9	11.5839	0.374	4.6839	18.4491	12.5238	1.4731	1.4734
90	0.5929	8.4	14.1679	0.4592	5.7679	18.2926	12.5608	1.4563	1.4564
110	0.5877	9.6	16.3359	0.5407	6.7359	17.7576	12.4579	1.4251	1.4254
GM250-127-28-10									
$Q_{heaters}$ (W)	β	V_{load} (V)	V_{OC} (V)	I (A)	V_{teg} (V)	R_{load} (Ω)	R_{teg} (Ω)	R_{load}/R_{teg} Method 2	$\beta/(1-\beta)$ Method 1
1000	0.62	1.0665	1.7564	1.7691	0.6899	0.6028	0.3899	1.5459	1.6315
6700	0.54	3.8101	7.0558	6.3615	3.2456	0.5989	0.5102	1.1739	1.1739

For each module, it can be notice that the highest R_{load} /R_{teg} value is at the lowest heat flux through the module with the highest β value. A low heat flux through the module also means a small temperature gradient.

The actual ZT of Bi_2Te_3 modules has a smaller value at lower temperature, peaks at $\Delta T \simeq 100°C$ and decreases afterwards, as shown in *Figure 3-1*. Considering the research hypothesis that $R_{load}/R_{teg} = \sqrt{1+ZT}$, for the GM250-241-10-12 module at 30W and 130W heat flux, the ZT values would be 1.56 and 0.65 respectively. These results do not correspond to the general ZT trend shown in *Figure 3-1*. Moreover, the ZT value of the commercial modules does not exceed unity. Using the constant heat parameter characterization from Chapter 5 and (6-11), the ZT was calculated and plotted in Figure 6-12. The ZT values of the GM250-241-10-12 module are in the range of 0.39-0.45. The results for the hypothetical $R_{load}/R_{teg} = \sqrt{1+ZT}$ were plotted against the R_{load} /R_{teg} values calculated based on the experimental results carried on in this thesis and shown in Figure 6-16.

$$ZT = \frac{\alpha_{teg}^2 T}{R_{teg} K_{teg}} \qquad (6\text{-}11)$$

Where α_{teg} is the Seebeck coefficient of the module, R_{teg} the internal resistance, K_{teg} the thermal conductance and T the average temperature across the module.

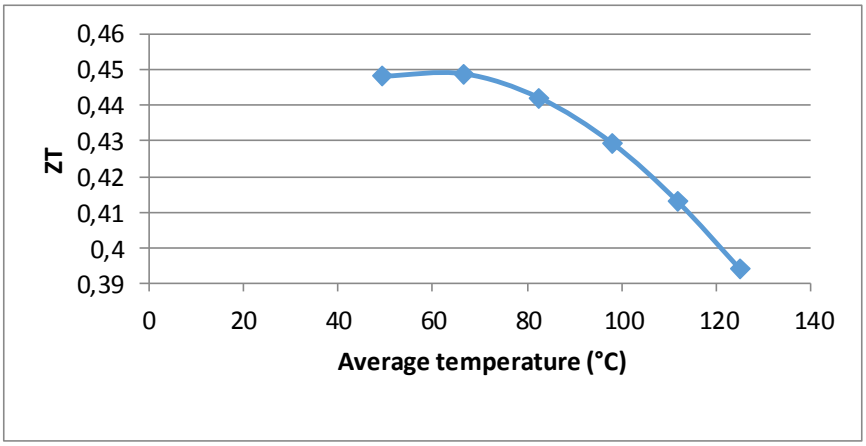

Figure 6-15 Calculated ZT values for the GM250-241-10-12 module based on the constant heat parameter characterization

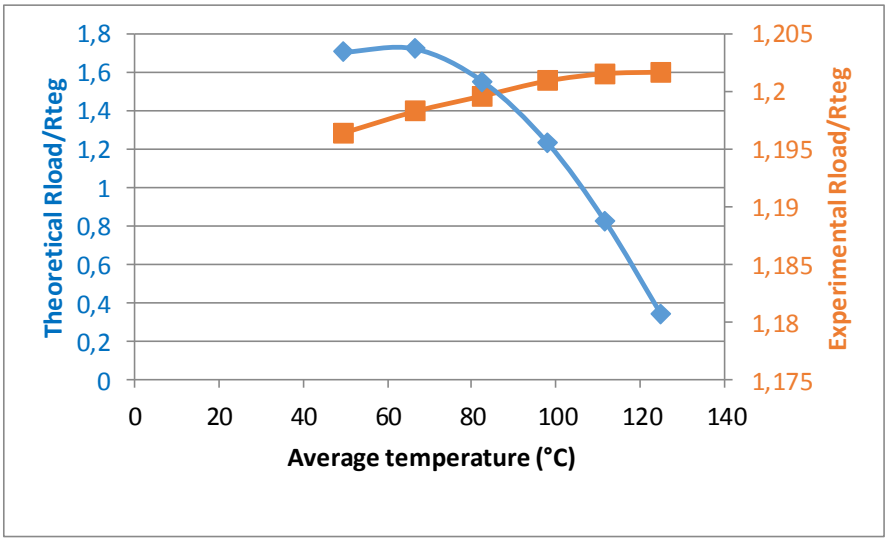

Figure 6-16 Theoretical $R_{load}/R_{teg} = \sqrt{1+ZT}$ *plotted against the experimentally obtained* R_{load}/R_{teg} *values calculated for GM250-241-10-12 module.*

It can be clearly seen that the two results are not equal or similar and follow opposite trends. Therefore, it can be concluded that the present research condition for maximum power $R_{load}/R_{teg} = \sqrt{1+ZT}$ does not hold for the case of constant heat characterization of TEGs. Much work still needs to be done to deeply understand the Peltier effect over the TEG systems when attempting to use it to maximizing the power output.

6.7. CONCLUSIONS

It is generally know that the performance of TE modules integrated into application is always less than the predicted performance based on one-module characterization. This TEG performance decrease is mainly due to the difference between the controllable test apparatus and the uncontrollable environmental factors that affect the actual systems. This chapter describes in detail the design of a hot gas test rig developed at the University of Glasgow with the purpose of validating TEG integration at the system level. Not only that the system is equivalent to a real TEG application (*i.e.*, car exhaust pipe) but it is also partially-controlled to allow one or multiple TE device testing.

The main effect of the TEG thermal conductivity manipulation by means of changing the operation voltage/current is its potential operation at a higher MPP than the theoretical one predicted by the *maximum power transfer theorem*. The hot gas system was used to test this concept which was first validated in Chapter 5 using a simple one-module test apparatus.

The test results achieved using the GM250-127-28-10 module on the hot has system clearly show the existence of the real MPP when the set voltage is different than half of the V_{OC}. The value of β identified for MPP operation varied in the range 0.54 – 0.62, depending on the module size and the heat flow through it. The work by (49) predicts peak system power will occur at the maximum power point of the system defined by $R_{load}/R_{teg} = \sqrt{1+ZT}$ and experiments conducted in this chapter show that this hypothesis does not hold for constant heat operation. Since *ZT* is TEG-specific and varies with absolute temperature, the implications for MPPT algorithms are profound: existing methods do not adequately accommodate the long thermal settling times varying β requires to reach equilibrium.

The test results on the hot gas system show how even 1°C change in the TEG cold-side temperature can cause a variation of up to 3% in the power generated by the module. The increased sensitivity is expected due to the lower temperature effect on the Carnot efficiency. Therefore, in a TEG system, one design consideration to maximize the power generated by the TEG is the cold-side heat exchanger. Not only should the materials used for the heat sinks have high thermal conductivity to allow the heat to be removed from the TEG, but also in case of liquid-cooled heat-exchangers, the temperature of the liquid should be kept as low as possible. In the case of air-cooled heat exchangers, the control of the air temperature is mostly restricted by the ambient environment.

An important matter tackled in this chapter and relevant not only to TEG systems but systems in general was the power losses associated with wiring interconnects. This topic is often ignored in research but can have a high impact on the power generated by TEGs especially those that produce high current levels. Choosing the correct wires and reducing the length as much as possible can prevent false readings and reduce wiring losses. Use of 4-wire measurement techniques can reduce the observed error but cannot compensate for ohmic losses in the conductors. For vehicular applications where the mass of the system is a primary consideration, heavy cables are contrary to the design objectives and hence the system designer needs to carefully assess the tradeoff between power loss in wiring vs. the use of many TEGs in series to increase the operating voltage of the array, but at the expense of lost power in the array due to temperature mismatch.

Nevertheless, the main topic of this chapter focused on demonstrating the existence of a new MPP higher than that predicted by the *maximum power transfer theorem*

conditions. This was shown and has been validated experimentally. The obvious finding is that design engineers should pay attention to the interconnected electrical and thermal features of TEG system and how they can be designed to operate at MPP. Clearly, the classical MPPT algorithms developed for PV systems and currently used in TEG systems are not sufficient for MPP operation. Demonstrating an increase in power output of nearly 10% whilst simultaneously reducing the heat flux reaching the cold side is a highly significant finding. There remains much work to do in designing autonomous algorithms that can effectively exploit this finding.

CHAPTER 7. GENERAL CONCLUSIONS

In this chapter the general conclusions of the thesis are summarized and suggestions for possible future work are given.

7.1. CONCLUSIONS

Overall, this thesis investigates possible methods to predict the potential efficiency of TEG integrated applications and offers information to be considered during the design, construction and testing of TEG systems for output power maximization.

Chapter 4 introduced an approach to design and model a TEG emulator for MPPT efficiency analysis. Dynamic MPPT efficiency is difficult to accurately calculate due to lack of TEG simulators. The TEG emulator was constructed using a programmable power supply (PV simulator) controlled to operate as a TEG using MATLAB based on the constant temperature parametric characterization of an oxide module. The performance of the TEG emulator was shown using the P&O algorithm and various test case scenarios: 1) three trapezoidal temperature profiles constructed based on literature research, 2) variable MPPT frequencies and 3) two resolution options (low/high) of the simulator.

The advantages of using a TEG emulator were addressed, however, improvements are necessary to be able to accurately predict the potential of TEG systems. On the other hand, it is a simple and accurate solution to test the operation and performance of the power electronics used in the TEG system.

It is later shown in **Chapter 5** that constant temperature characterization does not comply with existing conditions of TEG applications. Therefore, it is indicated that this method to be avoided in the future as it is partly the cause for false prediction of the TEG system potential.

Until the present, the *maximum power transfer theorem* was universally used to define the optimum operating point of a TE module where it would deliver the maximum possible power output. However this condition clearly disregards the thermal interactions that happen in a TEG system due to any electrical changes and the potential that the Peltier effect has in increasing the power output of a TEG. In **Chapter 5** and **Chapter 6** it was experimentally shown that manipulating the Peltier effect can be beneficial to the system efficiency and it makes the system operate at a higher MPP than the one defined by the *maximum power transfer*

theorem. This can only happen by understanding the valuable thermal influence on the electrical operation of a TEG.

The initial power increase range predicted in **Chapter 5** using a test fixture for one-module parametric characterization was 1.91% – 5.31% compared to the theoretical value. The test apparatus was customized to accommodate accurate measurements for one module, including heat loss characterization and controllable features (*i.e.* hot and cold site temperatures, clamping pressure). However, this is not the case in TEG applications where multiple modules are integrated and the system is not controlled. For this reason, a proper characterization of the concept that the Peltier effect can maximize the power generated by the TEG system was necessary. This was performed using the hot gas system described in **Chapter 6** and specifically built to resemble a realistic TEG application. Several differences were seen and discussed between the test fixture and the hot gas system, but the surprising results were the power increase percentages.

As mentioned, it is typical when using a customized test setup to overestimate the results compared to the ones of a real TEG system. In this case, the power increase range using the hot gas system was 2.5% – 8.3% which shows that these results are in good agreement with the ones presented using the test fixture in **Chapter 5.** Accurate performance predictions are possible when the modules are tested using the actual existing conditions in applications (*i.e.* constant heat operation). Strong suggestions for future considerations are given to both industry and research to consider this matter. Moreover, MPPT algorithms that comply with the specific thermal-electrical interactions in a TEG system should be developed instead of the "borrowed" ones from PV systems.

7.2. FUTURE WORK

Possible future work can be derived from the topics disused and analysed throughout this thesis. The main research directions are as follows:

Characterization of TE modules for applications:

- The use of cascaded module such as Bi_2Te_3 with oxide can cover a wider range of TEG application temperatures.

TEG emulator

- Implementation of the TEG emulator to operate in constant heat. This means that the Peltier should be considered in the MATLAB program that controls the SAS.

- Addition of the thermal interactions of all the system components. As research shows, never the power generated by a TEG system reaches the values predicted from one-module testing.

TEG system control

- Temperature mismatch for large surface multiple module integration is a fact. The DPP concept was originally developed for PV, but it should be considered and investigated for TEG systems too.
- The standard MPPT PV algorithms can no longer be used if the TEG system is to be operated at its real MPP. Constant heat MPPT methods for TEG systems are necessary that account for the slow thermal variations caused due to electrical variations.

Constant heat parametric characterization

- Inconsistencies were observed when attempting to correlate the maximum power or efficiency point of TEG systems in constant heat to the current research theory. Thorough experimental investigations are necessary to understand the thermal and electrical interactions caused by the manipulation of the Peltier effect to benefit the output power generation. Moreover, the actual correlation between ZT and the parameters of the module in constant heat needs to be investigated.

LITERATURE LIST

(1) Luan W, Tu S. Recent developments of thermoelectric power generation. Chinese Science Bulletin 2004;49(12):1212-1219.

(2) Hendricks T, Choate WT. Engineering scoping study of thermoelectric generator systems for industrial waste heat recovery. U.S. Department of Energy, 2006.

(3) Hsu C, Huang G, Chu H, Yu B, Yao D. Experiments and simulations on low-temperature waste heat harvesting system by thermoelectric power generators. Applied Energy 2011;88:1291-1297.

(4) Cao D, Peng FZ. Multiphase multilevel modular DC-DC converter for high current high gain TEG application. Energy Conversion Congress and Exposition (ECCE), 2010 IEEE 2010.

(5) Schock H, Brereton G, Case E, D'Angelo J, Hogan T, Lyle M, et al. Prospects for implementation of thermoelectric generators as waste heat recovery systems in class 8 truck applications. Journal of Energy Resources Technology 2013;135(2):022001.

(6) Tian Z, Lee S, Chen G. A comprehensive review of heat transfer in thermoelectric materials and devices. Annual Review of Heat Transfer 2014;17.

(7) Yang J, Caillat T. Thermoelectric materials for space and automotive power generation. Mrs Bulletin 2006;31:224-229.

(8) Markides CN. Low-concentration solar-power systems based on organic Rankine cycles for distributed-scale applications: overview and further developments. Frontiers in Energy Research 2015;3:47.

(9) LeBlanc S, Yee SK, Scullin ML, Dames C, Goodsom KE. Material and manufacturing cost considerations for thermoelectrics. Renewable and Sustainable Energy Reviews 2014;32:313-327.

(10) ObservatoryNANO. Briefing No. 17 - Thermoelectricity for energy harvesting. Seventh Framework Programme June 2011.

(11) Velez F, Segovia JJ, Martin C, Antolin G, Chejne F, Quijano A. A technical, economical and market review of organic Rankine cycles for the conversion of low-grade heat for power generation. Renewable and Sustainable Energy Reviews 2012;16(6):4175-4189.

(12) Mullen P, Siviter J, Montecucco A, Knox AR. A thermoelectric energy harvesterwith a cold start of 0.6 °C. Materials Today: Proceedings 12th European Conference on Thermoelectrics 2015;2(2):823-832.

(13) Kim RY, Lai JS. A seamless mode transfer maximum power point tracking controller for thermoelectric generator applications. IEEE Transactions on Power Electronics 2008;23(5):2310-2318.

(14) Laird I, Lovatt H, Savvides N, Lu D, Agelidis VG. Comparative study of maximum power point tracking algorithms for thermoelectric generators. Power Engineering Conference, 2008 AUPEC '08 Australasian Universities 2008:1-6.

(15) Kim S, Cho S, Kim N, Park J. A maximum power point tracking circuit of thermoelectric generators without digital controllers. IEICE Electronics Express 2010;7(20):1539-1545.

(16) Ni LX, Sun K, Zhang L, Xing Y. A power conditioning system for thermoelectric generator based on interleaved boost converter with MPPT control. 2011 International Conference on Electrical Machines and Systems (ICEMS) 2011:1-6.

(17) Ko Ko W, Souvik D, Panda SK. An optimized MPPT circuit for thermoelectric energy harvester for low power applications. 8th International Conference on Power Electronics - ECCE 2011:1579-1584.

(18) Laird I, Lu DDC. High step-up DC/DC topology and MPPT algorithm for use with a thermoelectric generator. IEEE Transactions on Power Electronics 2012;28(7):3147 - 3157.

(19) Yamada H, Kimura K, Hanamoto T, Ishiyama T, Sakaguchi T, Takahashi T. A novel MPPT control method of thermoelectric power generation with single sensor. Applied Sciences 2013;3:545-558.

(20) Nagayoshi H, Kajikawa T, Sugiyama T. Comparison of maximum power point control methods for thermoelectric power generator. Proceedings ICT '02 Twenty-First International Conference on Thermoelectrics 2002:450-453.

(21) Eakburanawat J, Boonyaroonate I. Development of a thermoelectric battery-chargerwith microcontroller-based maximum powerpoint tracking technique. Applied Energy 2006;83(7):687-704.

(22) Hejtmánek J, Knížek K, Švejda V, Horna P, Sikora M. Test system for thermoelectric modules and materials. Journal of Electronic Materials 2014;43(10):3726-3732.

(23) Wang H, McCarty R, Salvador JR, Yamamoto A, König J. Determination of thermoelectric module efficiency: a survey. Journal of Electronic Materials 2014;43(6):2274-2286.

(24) Tahhan M, Bazzi AM. A uniform temperature test rig for thermoelectric generator characterization and testing. Power and Energy Conference at Illinois (PECI) 2014:1-5.

(25) Bell LE. Cooling, heating, generating power and recovering waste heat with thermoelectric systems. Science 2008;321(5895):1457-1461.

(26) Beeby S, White NM editors. Energy harvesting for autonomous systems, Chapter 5 - Thermoelectric energy harvesting, by Gao Min. ; 2014.

(27) Tritt TM editor. Recent trends in thermoelectric materials research I, Chapter I Introduction, by Goldsmith, H.J. ; 2001.

(28) Lasance JM. The Seebeck coefficient. Electronics cooling magazine 2006.

(29) Chen J, Yan Z, Wu L. Influence of Thomson effect on the maximum power output and maximum efficiency of a thermoelectric generator. Journal of Applied Physics 1996;79:8823.

(30) Sandoz-Rosado EJ, Weinstein SJ, Stevens RJ. On the Thomson effect in thermoelectric power devices. International Journal of Thermal Sciences 2013;66:1-7.

(31) Min G, Rowe DM, Kontostavlakis K. Thermoelectric figure-of-merit under large temperature differences. Journal of Physiscs D:Applied Physiscs 2004;37:1301-1304.

(32) Apertet Y, Ouerdane H, Goupil C, Lecœur P. Internal convection in thermoelectric generator models. Journal of Physics: Conference Series 395 2012.

(33) Tilley R. Understanding solids: the science of materials, Chapter 15 Thermal properties. ; 2004.

(34) Snyder GJ, Toberer ES. Complex thermoelectric materials. Nature Materials 2008;7:105-115.

(35) MacDonald DKC. Thermoelectricity: An introduction to the principles. : Dover Publications, inc.; 2006.

(36) Szczech J, Higgins JM, Jin S. Enhancement of the thermoelectric properties in nanoscale and nanostructured materials. Journal of Materials Chemistry 2011;21(12):4037-4055.

(37) Goupil C, Seifert W, Zabrocki K, Muller E, Snyder GJ. Thermodynamics of thermoelectric phenomena and applications. Entropy 2011;13(8):1481-1517.

(38) Tritt TM, Subramanian MA. Thermoelectric materials, phenomena, and applications: a bird's eye view. Mrs Bulletin 2006;31:188-229.

(39) Snyder GJ. Small thermoelectric generators. Interface 2008:54.

(40) Harman TC, Walsh MP, Laforge BE, Turner GW. Nanostructured thermoelectric materials. Journal of Electronic Materials 2005;34(5).

(41) Zhao D, Tan G. A review of thermoelectric cooling: materials, modelling and applications. Applied Thermal Engineering 2014;66:15-24.

(42) Ohta H, Sugiura K, Koumoto K. Recent progress in oxide thermoelectric materials: p-type Ca3Co4O9 and n-type SrTiO3. CREST, Japan Science and Technology Agency 2008.

(43) Ohtaki M. Oxide thermoelectric materials for heat-to-electricity direct energy conversion. Kyushu University Global COE Program Novel Carbon Resources Sciences Newsletter 2010;3((Special Issue)).

(44) Zhang Q, Agbossou A. Phase change material and the thermoelectric effect for solar energy harvesting and storage. Proceedings of the ASME/JSME 2011 8th Thermal Engineering Joint Conference AJTEC 2011 2011:1-6.

(45) Vasquez J, Sanz-Bobi MA, Palacious R, Arenas A. State of the art of thermoelectric generators based on heat recovered from the exhaust gases of automobiles. Proceedings, 7th European Workshop on Thermoelectrics 2002:Paper 17.

(46) Oetringer K, Kober M, Altstedde MK. Upgrading hybrid-vehicles with a thermoelectric generator. Ecological Vehicles and Renewable Energies (EVER), 2014 Ninth International Conference on 2014:1-5.

(47) LeBlanc S. Thermoelectric generators: Linking material properties and systemsengineering for waste heat recovery applications. Sustainable Materials and Technologies 2014;1-2:26-35.

(48) Montecucco A, Siviter J, Knox AR. The effect of temperature mismatch on thermoelectric generators electrically connected in series and parallel. Applied Energy 2014;123:47-54.

(49) McCarty R. Thermoelectric power generation design for maximum poiwer: It's all about ZT. Journal of Electronic Materials 2013;42(7):1504-1508.

(50) Baranowski LL, Snyder GJ, Toberer ES. The misconception of maximum power and power factor in thermoelectrics. Journal of Applied Physics 2014;126102.

(51) Montecucco A, Knox AR. Maximum power point tracking converter based on the open-circuit voltage method for thermoelectric generators. IEEE Transactions on Power Electronics 2015;30(2):828-839.

(52) Schönecker A, Pichon PY, König J, Jägle M, den Heijer M, Kraaijveld B. Novel process for metal silicide nanostructures regarding cheap and large-scale material synthesis. Proceedings of the 11th European Conference on Thermoelectrics 2014:43-51.

(53) Liu L, Sun S, Zhang Q, Zhai P. The mechanical properties of skutterudite CoAs3by molecular dynamics (MD) simulation. Journal of Wuhan University of Technology-Mater Sci Ed 2008;23(3):415-418.

(54) Hu LP, Zhu TJ, Wang YG, Xie HH, Xu ZJ, Zhao XB. Shifting up the optimum figure of merit of p -type bismuth telluride-based thermoelectric materials for power generation by suppressing intrinsic conduction. NPG Asia Materials 2014;6(e88):1-8.

(55) Lee KH, Choi SM, Roh JW, Hwang S, Kim SI, Shin WH, et al. Enhanced thermoelectric performance of p-type Bi-Sb-Te alloys by codoping with Ga and Ag. Journal of Electronic Materials 2015;44(6):1531-1535.

(56) Lee GE, Eum AY, Song KM, Kim IH, Lim YS, Seo WS, et al. Preparation and thermoelectric properties of n-type Bi2Te2.7Se0.3:Dm. Journal of Electronic Materials 2015;44(6):1579-1584.

(57) Zou P, Xu G, Wang S. Thermoelectric properties of nanocrystalline Bi2(Te1xSex)3 prepared by high-pressure sintering. Journal of Electronic Materials 2015;44(6):1592-1598.

(58) Killander A, Bass JC. A stove-top generator for cold areas. Thermoelectrics, 1996 , Fifteenth International Conference on 1996:390-393.

(59) Nuwayhid RY, Rowe DM, Min G. Low cost stove-top thermoelectric generator for regions with unreliable electricity supply. Renewable Energy 2003 2;28(2):205-222.

(60) Champier D, Bédécarrats JP, Kousksou K, Rivaletto M, Strub F, Pignolet P. Study of a TE (thermoelectric) generator incorporated in a multifunction wood stove. Energy 2011;36:1518-1526.

(61) Champier D, Favarel C, Bédécarrats JP, Kousksou T, Rozis JF. Prototype combined heater/thermoelectric power generator for remote applications. Journal of Electronic Materials 2013;42(7):1888-1899.

(62) Bannar-Martin L, Manthanwar A, Patel B, Barker D, Morrison A. Portable power generation - GlobalTech energy challenge 2013. 2013.

(63) O'Shaughnessy SM, Deasy MJ, Kinsella CE, Doyle JV, Robinson AJ. Small scale electricity generation from a portable biomass cookstove: Prototype design and preliminary results. Applied Energy 2013;102:374–385.

(64) Montecucco A, Siviter J, Knox AR. A combined heat and power system for solid-fuel stoves using thermoelectric generators. Energy Procedia 2015;75:597-602.

(65) Wang H, Porter WD, Bottner H, Konig J, Chen L, Bai S, et al. Transport properties of bulk thermoelectrics — An international round-robin study, Part I: Seebeck coefficient and electrical resistivity. Journal of Electronic Materials 2013;42(4):654-664.

(66) Wang H, Porter WD, Bottner H, Konig J, Chen L, Bai S, et al. Transport properties of bulk thermoelectrics: An international round-robin study, Part II: Thermal diffusivity, specific heat, and thermal conductivity. Journal of Electronic Materials 2013;42(6):1073-1084.

(67) Holgate TC. Increasing the efficiency of the multi-mission radioisotope thermoelectric generator. Journal of Electronic Materials 2015;44(6):1814-1821.

(68) Luo Q, Li P, Cai L, Zhou P, Tang D, Zhai P, et al. A thermoelectric waste-heat-recovery system for Portland cement rotary kilns. Journal of Electronic Materials 2015;44(6):1750-1762.

(69) Baranowski LL, Snyder GJ, Toberer ES. Effective thermal conductivity in thermoelectric material. Journal of Applied Physics 2013;113:204904.

(70) Brazdil M, Pospisil J. Thermoelectric power generation utilizing the waste heat from a biomass boiler. Journal of Electronic Materials 2013;42(7):2198-2202.

(71) Juanico LE, Rinalde FN, Taglialavore E, Molina M. Development of a portable thermogenerator for uncontrolled heat sources. Journal of Electronic Materials 2013;42(7):1846-1854.

(72) Karim AM, Federici JA, Vlachos DG. Portable power production from methanol in an integrated thermoeletric/microreactor system. Journal of Power Sources 2008;179:113-120.

(73) Nuwayhid RY, Shihadeh A, Ghaddar N. Development and testing of a domestic woodstove thermoelectric generator with natural convection cooling. Energy Conversion and Management 2005;43:1631-1643.

(74) Kaasjager ADJ, Moeys GPG. A hot plate solar cooker with electricity generation - combining a parabolic trough mirror with a Sidney tube and heat pipe. Global Humanitarian Technology Conference (GHTC), 2012 IEEE 2012:6-11.

(75) Adavbiele AS. Generation of electricity from gasoline engine waste heat. International Journal od Energy Technology and Policy 2013;3(5):16-33.

(76) Hatzikraniotis E. On the recovery of wasted heat using a commercial thermoelectric device. Proceedings of the International Congress on Advances in Applied Physics and Materials Scienc 2011.

(77) Anatychuk LI, Luste OJ, Kuz RV. Theoretical and experimental study of thermoelectric generators for vehicles. Journal of Electronic Materials 2011;40(5):1326-1331.

(78) Rauscher L, Fujimoto S, Kaibe HT, Sano S. Efficiency determination and general characterization of thermoelectric generators using an absolute measurement of the heat flow. Measurement Science and Technology 2005;16:1054.

(79) Takazawa H, Obara H, Okada Y, Kobayashi K, Onishi T, Kajikawa T. Efficiency measurement of thermoelectric modules operating in the temperature difference of up to 550K. Proceedings of the 25th International Conference on Thermoelectrics, 2006 ICT '06 2006:189-192.

(80) Sandoz-Rosado E, Stevens RJ. Experimental characterization of thermoelectric modules and comparison with theoretical models for power generation. Journal of Electronic Materials 2009;38:1239-1244.

(81) Anatychuk LI, Havrylyuk MV. Procedure and equipment for measuring parameters of thermoelectric generator modules. Journal of Electronic Materials 2011;42(1292-1297).

(82) PANCO GmbH. TEGeta — Measurement of Efficiency and Specifications of Thermoelectric Power Generators, Manual. 2013.

(83) Montecucco A, Buckle J, Siviter J, Knox AR. A new test rig for accurate nonparametric measurement and characterization of thermoelectric generators. Journal of Electronic Materials 2014;42:1966-1973.

(84) Pierce RD, Stevens RJ. Experimental comparison of thermoelectric module characterization methods. Journal of Electronic Materials 2015;44(6):1796-1802.

(85) Su CQ, Wang WS, Liu X, Deng YD. Simulation and experimental study on thermal optimization of the heat exchanger for automotive exhaust-based thermoelectric generators. Case Studies in Thermal Engineering 2014;4:85-91.

(86) Sharp J, Bierschenk J. The prevalence of standard large modules in thermoelectric applications. Journal of Electronic Materials 2015;44(6):1763-1767.

(87) Vadstrup C, Schaltz E, Chen M. Individual module maximum power point tracking for thermoelectric generator systems. Journal of Electronic Materials 2013;42(7):2203-2208.

(88) Wu H, Sun K, Chen M, Chen Z, Xing Y. Hybrid centralized-distributed power conditioning aystem for thermoelectric generator with high energy efficiency. Energy Conversion Congress and Exposition (ECCE), 2013 IEEE 2013:4659-4664.

(89) Chen M. Adaptive removal and revival of underheated thermoelectric generation modules. IEEE Transactions on Industrial Electronics 2014;61(11):6100-6107.

(90) Shenoy PS, Kim KA, Johnson BB, Krein PT. Differential power processing architecture for increased energy production and reliability of photovoltaic systems. IEEE Transactions on Power Electronics 2012;28(6):2968-2979.

(91) Qin S, Cady ST, Dominguez-Garcia AD, Pilawa-Podgurski RCN. A distributed approach to MPPT for PV sub-module differential power processing. Energy Conversion Congress and Expozition (ECCE), 2013 IEEE 2013:2778-2785.

(92) Qiu Z, Sun K, Wu H, Huang J, Xing Y. A high efficiency cascaded thermoelectricgeneration system with power balancing mechanism. 2015 IEEE Applied Power Electronics Conference and Exposition (APEC) 2015:647 - 653.

(93) Montecucco A, Siviter J, Knox AR. Simple, fast and accurate maximum power point tracking converter for thermoelectric generators. 2012 IEEE Energy Conversion Congress and Exposition (ECCE) 2012:2777-2783.

(94) Kim B, Bun L, Goupil C, Dagues B, Maussion P. Modeling and tuning of MPPT controllers for a thermoelectric generator. First International Conference on Green Energy ICGE 2014 2014:220-225.

(95) Nagayoshi H, Maiwa H, Kajikawa T. Power conditioner with variable switching control for thermoelectric generator systems. Journal of Electronic Materials 2013;42(7):2282-2286.

(96) Phillip N, Maganga O, Burnham KJ, Ellis MA, Robinson S, Dunn J, et al. Investigation of maximum power point tracking for thermoelectric generators. Journal of Electronic Materials 2013;42(7):1900-1906.

(97) Maganga O, Phillip N, Burnham KJ, Montecucco A, Siviter J, Knox AR, et al. Hardware implementation of maximum power point tracking for thermoelectric generators. Journal of Electronic Materials 2014;43(6):2293-2300.

(98) Man EA, Sera D, Mathe L, Schaltz E:,L. Dynamic performance of maximum power point trackers in TEG systems under rapidly changing temperature conditions. Journal of Electronic Materials 2015.

(99) Kim RY, Lai JS. Aggregated modeling and control of a boost-buck cascade converter for maximum power point tracking of a thermoelectric generator. Applied Power Electronics Conference and Exposition, 2008 APEC 2008 Twenty-Third Annual IEEE 2008:1754-1760.

(100) Kim S, Cho S, Kim N, Baatar N, Kwon J. A digital coreless maximum power point tracking circuit for thermoelectric generators. Journal of Electronic Materials 2011;40(5):867-872.

(101) Park J, Kim S. Maximum power point tracking controller for thermoelectric generators with peak gain control of boost DC–DC converters. Journal of Electronic Materials 2012;41(6):1242-1246.

(102) Wu H, Sun K, Zhang J, Xing Y. A TEG efficiency booster with buck–boost conversion. Journal of Electronic Materials 2013;42(7):1737-1744.

(103) Park H, Sim M, Kim S. Achieving maximum power from thermoelectric generators with maximum-power-point-tracking circuits composed of a boost-cascaded-with-buck converter. Journal of Electronic Materials 2015;44(6):1948-1956.

(104) Kim RY, Lai JS, York B, Koran A. Analysis and design of maximum power point tracking scheme for thermoelectric battery energy storage system. IEEE Transactions on Industrial Electronics 2009;56(9):3709-3716.

(105) Gao J, Sun K, Ni L, Chen M, Kang Z, Zhan L, et al. A thermoelectric generation system and its power electronics stage. Journal of Electronic Materials 2012;41(6):1043-1050.

(106) Desai NV, Ramadass YK, Chandrakasan AP. A bipolar ±40 mV self-starting boost converter with transformer reuse for thermoelectric energy harvesting. Low Power Electronics and Design (ISLPED), 2014 IEEE/ACM International Symposium on 2014:221-226.

(107) Meli M, Dillersberger H. Efficiently harvesting energy from temperature differences in order to power wireless systems. Wireless Congress 2014 2014.

(108) Pilawa-Podgurski RCN, Pallo NA, Chan WR, Perreault DJ, Celanovic IL. Low-power maximum power point tracker with digital control for thermophotovoltaic generators. Applied Power Electronics Conference and Exposition (APEC), 2010 Twenty-Fifth Annual IEEE 2010:961- 967.

(109) Sera D, Mathe L, Kerekes T, Spataru SV, Teodorescu R. On the Perturb-and-Observe and Incremental Conductance MPPT methods for PV systems. IEEE Journal of Photovoltaics 2013;3(3):1070-1078.

(110) Esram T, Chapman PL. Comparison of Photovoltaic Array Maximum Power Point Tracking Techniques. IEEE Transactions on Energy Conversion 2007;22(2):439-449.

(111) Laird I, Lu DDC. Steady state reliability of maximum power point tracking algorithms used with a thermoelectric generator. Circuits and Systems (ISCAS), 2013 IEEE International Symposium on 2013:1316 - 1319.

(112) Koutroulis E, Kalaitzakis K. Novel battery charging regulation system forphotovoltaic applications. IEE Proceedings - Electric Power Applications 2004;151(2):191 - 197.

(113) Man EA, Schaltz E, Rosendahl L, Rezaniakolaei A, Platzek D. A high temperature experimental characterization procedure for oxide-based thermoelectric generator modules under transient conditions. Energies 2015;8(11):12839-12847.

(114) Keysight Technologies. Testing terrestrial solar-powered inverters using solar array simulation techniques - Application note. 2009.

(115) Hussein KH, Muta I, Hoshino T, Osakada M. Maximum photovoltaic power tracking: an algorithm for rapidly changing atmospheric conditions. Generation, Transmission and Distribution, IEE Proceedings 1995;142(1):59-64.

(116) CENELEC. European Standard DS/EN 50530 - Overall efficiency of grid connected photovoltaic inverters. 2010.

(117) Montecucco A, Siviter J, Knox AR. Constant heat characterisation and geometrical optimisation of thermoelectric generators. Applied Energy 2015;149:248–258.

(118) Oku M, Sakoda T, Hayashi N, Tashima D. Basic characteristics of a heat and electricity combined generation system using biomass fuel. Renewable Energy Research and Application (ICRERA), 2014 International Conference on 2014:222-228.

(119) Anatychuk LI, Luste OJ, Kuz RV. Theoretical and experimental study of thermoelectric generators for vehicles. Journal of Electronic Materials 2011;40(5):1326-1331.

(120) Altstedde MK, Rinderknecht F, Friedrich H. Integrating phase-change materials into automotive thermoelectric generators. Journal of Electronic Materials 2014;43(6):2134-2140.

(121) Min G. Principle of determining thermoelectric properties based on I–V curves. Measurement Science and Technology 2014;25(8):085009 (6pp).

APPENDICES

Appendix A. 1

Appendix A.

The following equations describe an exponential solar cell model and are used by the Solar Array Simulator in SAS mode to establish the *I-V* output characteristics.

$$V = \frac{\frac{V_{OC} \cdot ln\left[2 - \left(\frac{I}{I_{SC}}\right)^{N}\right]}{ln(2)} - R_S \cdot (I - I_{SC})}{1 + \frac{R_S \cdot I_{SC}}{V_{OC}}} \qquad \textit{(A-7-1)}$$

$$R_S = \frac{V_{OC} V_{MPP}}{I_{MPP}} \qquad \textit{(A-7-2)}$$

$$N = \frac{ln\left(2 - 2^{a}\right)}{ln\left(\frac{I_{MPP}}{I_{SC}}\right)} \qquad \textit{(A-7-3)}$$

$$a = \frac{V_{MPP} \cdot \left(1 + \frac{R_S \cdot I_{SC}}{V_{OC}}\right) + R_S \cdot (I_{MPP} - I_{SC})}{V_{OC}} \qquad \textit{(A-7-4)}$$

Where N is a parameter related to the array shunt resistance and R_S is the output resistance of the solar array.

The relationship between N, R_S, I_{MPP} and V_{MPP} is shown in Figure- A-1.

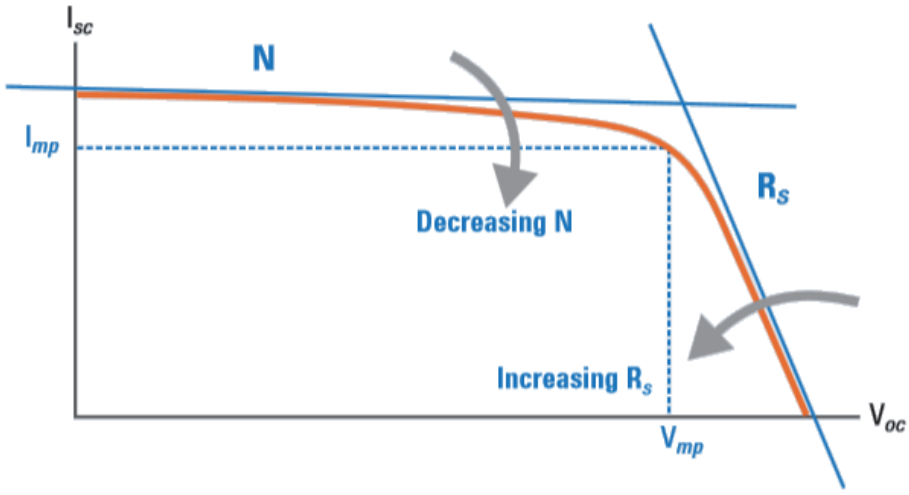

Figure- A-1 The I-V characteristic of a solar cell and the relationship between N, R_S, I_{MPP} and V_{MPP}.

ISSN (online) – 2246-1248
ISBN (online) - 978-87-7112-766-9

AALBORG UNIVERSITY PRESS